Electrically actuated microfluidic methods of sample preparation for isothermal amplification assays

By

Ali Shahid

B.Sc., M.S.

A Thesis

Submitted to the School of Graduate Studies

in Partial Fulfillment of the Requirements

for the Degree

Doctor of Philosophy

McMaster University

Electrically actuated microfluidic methods of sample preparation for isothermal amplification assays

DOCTOR OF PHILOSOPHY (2018)

McMaster University

Hamilton, Ontario, Canada

(Mechanical Engineering)

TITLE: Electrically actuated microfluidic methods of sample preparation for isothermal amplification assays

AUTHOR: ALI SHAHID

B.Sc., Mechanical Engineering, University of Engineering & Technology (U.E.T), Lahore, Pakistan

M.S., Mechanical Engineering, Korea Advanced Institute of Science & Technology (KAIST), South Korea

SUPERVISOR: Professor\Ponnambalam (Ravi) Selvaganapathy

Department of Mechanical Engineering

NUMBER OF PAGES: xxv, 153

Abstract

Waterborne or foodborne diseases are caused by consuming contaminated fluids or foods. The presence of pathogenic microorganisms can contaminate food or drinking water. These microorganisms can cause sickness even if they are present in minimal concentrations. The World Health Organization (WHO) has defined the standards for clean drinking water as the absence of *E. coli* in a 100 mL collected volume. Contaminated water or food can cause many diseases, and diarrhea is one of a prominent disease. Early detection of contamination in food or drinking water is critical. Conventional culture-based methods are time-consuming, labour intensive, and not suitable for on-site testing. Nucleic acid-based tests are sensitive and can rapidly detect pathogens. Microfluidic technology can play a significant role to develop low-cost, rapid, integrated, and portable nucleic acid-based detection devices. Microfluidic systems for isothermal amplification assays can be classified into two groups such as droplet-based and chamber-based systems. In this thesis, both droplet-based and chamber-based approaches were used to build the microfluidic methods for isothermal amplification assays.

First, a simple electromechanical probe (tweezers) was developed that can manipulate a small aqueous droplet in a bi-layer oil phase. The tweezer consisted of two needles positioned close to each other and used polarization of the aqueous droplet in an applied electrical field to confine the droplet between the needles with minimal solid contact. AC electric potential was applied to the two metal electrodes. Droplet acquired a charge from the high voltage electrode and consequently performed an oscillatory motion with the same electrode. This droplet motion was controlled using two parameters of electric potential and frequency of the applied signal. Initially, electrically actuated droplet (0.3 µL) motion was investigated for a range of applied potential (400-960 Volts) and frequencies (0.1-1000 Hz). The droplet motion with high voltage electrode was characterized into three modes such as detachment, oscillation, and attachment.

Mechanical motion of tweezer was used to transport droplet to various positions. Consequently, operations such as transportation, extraction, and merging were demonstrated. First, droplet (5 µL) transportation was characterized under the applied potential of 2000 Volts at various frequencies (5 to 1000 Hz). The droplet was successfully transported to the speed of 15 mm/s at higher frequencies (100 or 1000 Hz). Droplets of various volumes (12-80 µL) were extracted by increasing applied electric potential, from 0 to 6000 Volts at 5 Hz. Then, the operation of droplets merging was demonstrated using operational conditions for electrical tweezer.

Finally, electrical tweezer was used to prepare samples for isothermal amplification assays. Two droplets consisted of various reagents of isothermal amplification assays, were transported and merged using the electrical tweezer. Then, a merged droplet (25 µL) was transported and immobilized in the amplification zone. The temperature of the amplification zone (~65°C) was maintained using an in-situ heater. DNA amplification was verified by measuring the off-chip end-point fluorescence intensity of isothermal assays.

Second, an integrated microfluidic device has been developed to prepare a sample for isothermal amplification assays. And in-situ real-time amplification assays were performed to detect bacteria. The device consisted of two chambers (lysis and amplification) connected through a microchannel. A low-cost fabrication method was introduced to embed two resistive wire heaters around both chambers. Initially, bacteria cells were thermally lysed in the lysis chamber at 92°C for 5 min. Then, DNA was electrophoretically transported from lysis to the amplification chamber. The electric potential of 10 Volts was applied for 10 min for DNA transportation. Next, transported DNA was amplified at 65°C and DNA amplification was detected by measuring in-situ fluorescence intensity in the real-time format. The operation of the integrated microfluidic device was demonstrated in three steps. 1) Operation of individual components. 2) Operation of two components in a coupled format. 3) Integrated operation of three components with measurement of fluorescent intensity in a real-time format. The bacteria samples with the concentration of 100 CFU/mL were detected in less than one hour.

Acknowledgements

First, I would like to take this opportunity to express my sincere gratitude to my supervisor Dr. Ponnambalam (Ravi) Selvaganapathy for the opportunity he has provided me to pursue Ph.D. under his supervision. He provided me with continuous support, guidance, and mentorship throughout the challenging journey of the Ph.D. program at McMaster University. This doctorate studies were a treasurable learning opportunity and will have an excellent impact on my whole life. I am also very grateful to the members of the supervisory committee, Dr. Jamal Deen and Dr. Herb E. Schellhorn for their guidance, valuable comments, and suggestions during the study. I would also like to thank Dr. Chan Ching for his inputs in all the meetings that enhance my understanding and critical thinking.

Second, I am very thankful to Dr. James Mahoney who educated me in understanding the biological aspect of my research and provided me with access to his laboratory facilities and biological resources. I am also thankful to Sylvia Chong for giving me training on handling the biological samples. I appreciate the help and assistance provided by Dr. Marta Prinz during my experiment at the Bio-Interfaces Institute. I am grateful to the technical staff, Ron Lodewykes, Joe Verhaegheat, Mark Mackenzie, Michael Lee, John Colenbrander, and Dan Wright of the Mechanical Engineering Department Machine Shop Facilities for their immense assistance and support for the fabrication and development of the various devices and experimental setups. I want to say thank to Dr. Z. Peng and Mrs. Doris V. Stevanovic at the Center of Emerging Device Technology for providing me with training and support for using the clean room facilities and mask fabrication.

I am also thankful to my colleagues at CAMEF, Dr. Wen-I Wu, Dr. Pouya Rezai, Siawash Shinwary, Shehad Islam, Bo. Dang, Peter. Lee, Chah Zhu, Dr. Leo Hsu, Dr. Md. K Kamrul Russel, Dr. Reza Ghaemi, Dr. Rana Attalla, Jun Yang, Harpreet Matharoo, Sondos Ayyash, Aditya, Juncong Liu, Mohammadhossein Dabaghi, Ali Akbar, Pankaj

Saini, Michael Zlatin, Shayan Liaghat, Melizeth Bolanos, Asma and Celine Ling for the continuous support, helping hands and for their great sense of humour.

I would like to appreciate the everlasting love and support received from my parents, Mr. Mian Shahid Javed and Ms. Mussrat Shahid, especially for believing in me and allowing me to continue studies in Canada. I want to extend my gratitude to my siblings, Adila Shahid and Ambreen Shahid; lovely brothers, M. Atif, Sami Khan, Dr. Umar Latif, Adeel Habib; my family members, Tahira Latif, Naheed Tariq, Asad Chaudhary; my friends, M. Qmar Rafique, Syed Adeel Ahmad and Syed Ahmed Raza. Finally, special thanks to my wife who gave me emotional support during the most challenging time of my life subsequently, helped me in achieving my dream. A special thanks to my daughter Aairah Ali Shahid who bring happiness to my life.

Table of Contents

List of figures

List of abbreviations

a	Acceleration
A	Ampere
ABS	Acrylonitrile-Butadiene-Styrene
AC	Alternating current
APVD	Atmospheric pressure vapor deposition
A. U.	Arbitrary unit
B3	Backward outer primer
BIP	Backward inner primer
BSA	Bovine serum albumin
CAMEF	Centre for Advanced Micro-Electro-Fluidics
CCD	Charged couple device
CFU	Colony-forming unit
CNC	Computer numerical control
COC	Cyclic olefin copolymer
DAQ	Data acquisition
DC	Direct current
ddH_2O	Doubly distilled water
DI	Deionized
DMF	Digital microfluidics
DNA	Deoxyribonucleic acid
dNTPs	Deoxyribonucleic acid triphosphates
E	Electric field
EPON SU-8	A polymeric solid epoxy novolac resign
ESEQuant	A commercial fluorescence device
EWOD	Electro-wetting on dielectric
F3	Forward outer primer
F_d	Drag force

F_{def}	Dielectrophoretic force
F_e	Electrophoretic force
F_i	Inertia force
FIP	Forward inner primer
FP	Forward outer primer
FTA	Flinders technology associates
GAPDH	Glyceraldehyde 3-phosphate dehydrogenase
GDWQ	Guidelines for drinking-water quality
GFP	Green fluorescent protein
GND	Grounded electrode
HBV	Hepatitis B virus
HDA	Helicase-dependent amplification
HIPORA	A three-layer microporous silicon coating structure
HIV	Human immunodeficiency virus
HlyA	L. monocytogenes
HNB	Hydroxynaphthol blue
HVE	High voltage electrode
ICP	Inductively coupled plasma
InvA	Salmonella
ITP	Isotachophoresis
KS	Kaposi's sarcoma
LAMP	Loop-mediated isothermal amplification
LB	Backward loop primer
LED	Light emitting diode
LF	Forward loop primer
LPCVD	Low-pressure chemical vapour deposition
m	Mass
MB	Magnetic beads
MEMS	Micro-Electro-Mechanical system

min	Minute
mL	milliliter
MRSA	Methicillin-resistant Staphylococcus aureus
NAIL	Nucleic acid detection using isotachophoresis and loop-mediated isothermal amplification
NASBA	Nucleic acid sequence-based amplification
nd	No dye
PAA	Polyacrylamide
PBS	Phosphate buffer saline
PC	Polycarbonate
PCR	Polymerase chain reaction
PDMS	Polydimethylsiloxane
pGEF	Vector for expressing GFP in bacteria
PID	Proportional–integral–derivative
PMMA	Poly (methyl methacrylate)
PRV	Pseudorabies virus
Pt	Platinum
q	Electric charge
r	Radius
PTFE	Polytetrafluoroethylene
RCA	Rolling circle amplification
RIE	Reactive ion etching
RPA	Recombinase polymerase amplification
RUO	Research use only
SDA	Strand displacement amplification
SEBS	Styrene ethylene butylene styrene
SEM	Scanning electron microscope
SPE	Solid phase extraction
STEC	Shiga toxin-producing Escherichia coli

TB	Mycobacterium tuberculosis
TEC	Thermoelectric cooler
UV	Ultraviolet
V	Volts
v	Speed
W	Watts
WGS	Wire guided system
WHO	World Health Organization
µL	microliter
°C	Degree centigrade
η	Viscosity
σ	Conductivity
∇E^2	Square of electric field gradient
ε	Emissivity

Chapter: 1 Motivation and organization

1.1 Motivation

Presence of pathogenic microorganisms even at small concentrations in food and drinking water can cause severe illnesses to human beings. These microorganisms include *Salmonella*, *Shigella*, *Yersinia*, and *Escherichia coli* (*E. coli*). These pathogenic microorganisms cause various diseases such as pneumonia, urinary tract infections, diarrhea, typhoid fever, food poisoning, gastroenteritis, enteric fever, and enterocolitis. *E. coli* is a bacterium which is mostly harmless but, some of the strains can cause severe foodborne or waterborne illnesses. According to guidelines for drinking-water quality (GDWQ) provided by the World Health Organization (WHO), *E. coli* should be absent in any collected sample of size of 100 mL [1]. According to WHO each year 4 billion people are affected by diarrhea worldwide and 2.2 million people died in the year 1998 [2]. However, infants and young children are at higher risk upon exposure to diarrhea with 1.7 billion children affected each year and 525,000 deaths among them [3]. In the year 2000, *E. coli* contaminated the municipal water supply of a small town of Walkerton, Ontario. Subsequently, 27 people hospitalized, and five people died [4].

Early detection of pathogens is critical to saving human life from the adverse effect of contaminated food. Pathogens are conventionally detected using the culture-based methods. Culture-based methods are oldest, well established and widely used methods to monitor the quality of food and drinking water. These detection methods rely on the specific culture medium and distinguish the bacterial species and numbers. These detection methods consisted of various steps such as pre-enrichment, selective enrichment, selective plating, biochemical screening, and serological confirmation. Subsequently, these steps make these detection methods as time-consuming and labour intensive. For instance, culture-based detection methods can detect *Escherichia coli* (*E. coli*) in 21 to 48 hours [5] and can take up to 14 to 16 days [6] to detect *Campylobacter.*

Nucleic acid amplification that is based on the molecular biomarkers rather than culture is more rapid, sensitive and quantitative for the detection of pathogens. There are two approaches used for DNA amplification such as non-isothermal and isothermal amplification. Polymerase chain reaction (PCR) is a non-isothermal amplification method in which DNA molecules are amplified by exposing them to the repetitive temperature cycling. Isothermal amplification methods amplify DNA molecules using the enzyme activity at a constant temperature. Microfluidics systems can be used to overcome the limitations of the existing conventional detection systems. Microfluidic systems have many advantages such as low-cost, small volumes, rapid processing, and portability.

The primary objective of this thesis is the development of microfluidic devices which can prepare samples and perform isothermal amplification. First, electrical tweezer has been developed that can handle microdroplets using the time-varying electrical potential. Electrical tweezer was designed to perform the various droplet-based microfluidic operations such as transportation, extraction, and merging. The operations of transportation and merging were used to perform DNA amplification using the isothermal amplification assays. Second, a well-based microfluidic device was developed to amplify DNA using the isothermal amplification assays. The DNA amplification module of the microfluidic device was integrated with the sample preparation component. Subsequently, sequential steps of lysis, transportation, and amplification were performed on-chip. The DNA amplification was detected by measuring the in-situ fluorescence intensity in a real-time format.

1.2 Organization of chapters

Chapter 2: Introduction

This chapter describes the background and literature survey. Initially, various nucleic acid amplification methods are discussed in detail. These amplification methods included the polymerase chain reaction (PCR) and loop-mediated isothermal amplification (LAMP). Then, microfluidic technology-based devices using the PCR method are

discussed. These devices are categorized into (1) stationary chamber-based devices, (2) flow through-based devices, (3) convective flow-based devices, and (4) droplet-based devices. In the second section of the chapter, microfluidic devices that use the isothermal assays for DNA amplification are discussed. (1) Chamber-based microfluidic devices including single chamber and multi-chamber-based amplification devices. Multi-chamber-based devices are further categorized into devices with the arrays of straight channels or arrays of wells. Then, droplet-based microfluidic systems are discussed. (2) Heating and detection systems used for LAMP assays are presented. Various detection systems are discussed including the gel electrophoresis, naked eye detection, real-time turbidity measurement, electrochemical detection, and fluorescence-based detection system. (3) Microfluidic systems are introduced with or without the integrated on-chip sample preparation module.

Chapter 3: Design and fundamentals of electrical tweezers

This chapter describes the fundamental design of an electrical tweezer device to manipulate the droplets. Then, materials and methods of electrical tweezer are discussed that included fabrication, materials, and experimental setup. Later, the oscillatory droplet motion that was actuated by the electric potential in the bi-layer oil medium is discussed. Furthermore, numerical simulations were performed to explain the oscillatory droplet motion. Finally, the oscillatory droplet motion is categorized for various parameters of frequency, electric potential, and droplet volume.

Chapter 4: Applications of electrical tweezer

In this chapter, the application of electrical tweezer for various droplet-based microfluidic operations has been discussed. First, experimental setups required to perform the droplet-based application are presented. The experimental setup consisted of a droplet transportation unit and droplet extraction unit. Then, the droplet-based microfluidic operations such as transportation, extraction, and merging are described. Next, in the second section of the chapter, application of electrical tweezer for the loop-mediated

isothermal amplification (LAMP) assays is demonstrated. The experimental setups required to perform LAMP assays are discussed. Finally, the amplification LAMP assays using the electrical tweezer has been shown. The DNA is amplified using various droplet-based operations. These operations included transportation, merging and finally, heating the droplet at ~ 65˚C.

Chapter 5. A low-cost heater integrated microfluidic device to perform integrated sample processing and detection of bacteria

This chapter describes the integrated microfluidic device that has been developed to perform sample processing and amplification of bacterial samples. First, the conceptual design of the device is presented that includes the operation of the device and effect of various parameters on the device performance. Then, experimental setups, sample preparation, and loading, device fabrication is discussed. Next, the operation of the device is demonstrated in three different steps. Initially, the operation of individual components of lysis, transportation, and amplification are discussed. Then, the operation of two components is presented in the integrated format, for instance, the integrated operation of lysis and transportation. Finally, the on-chip integrated operation of all three components of a microfluidic device is presented.

Chapter 6. Conclusions and future work

This chapter highlights the findings and the contribution of both types of devices. Future work is presented at the end of the chapter.

1.3 Contributions

A simple electromechanical probe (tweezers) is presented that can manipulate a small aqueous droplet in a bi-layer oil phase. Mechanical motion of the tweezer can be used to perform various droplet-based microfluidic operations such as aliquoting, merging, and transportation. Finally, the droplet-based operations were used to perform DNA

amplification using the LAMP assays. This electromechanical tweezer is of interest in low-throughput, small-volume biological and chemical assays where the investigator requires direct and open access to the samples.

Publication

1. **Ali Shahid**, Sylvia Chong, James Mahony, M. Jamal Deen and P. Ravi Selvaganapathy, (2017), "*Electrical tweezer for droplet transportation, extraction, merging and DNA analysis*", Micromachines November 30, 2017, (**Published**).

Conference presentation and poster

2. **Ali Shahid,** Sylvia Chong, James Mahony, Jamal Deen, P. R. Selvaganapathy, (2018), "*Electrical tweezer for DNA analysis by loop-mediated isothermal amplification (LAMP)*, Proceedings of the 5th European Conference on Microfluidics μFlu18 3rd European Conference on Non-Equilibrium Gas Flows, NEGF18, February 28-March 2, 2018, Strasbourg, France.

3. **Ali Shahid**, P. R. Selvaganapathy (2016), "*Electrical tweezers for the droplet transportation"*, Ontario-on-a-chip, May 26, 2016, University of Toronto, ON (**Poster**).

4. **Ali Shahid**, P. Ravi Selvaganapathy, (2015), "*Electrical tweezers for droplet transportation and extraction"*, Cage Club Student Conference on High Voltage Engineering and Applied Electrostatics, August 20, 2015, University of Western Ontario, ON (**Presentation**).

5. **Ali Shahid**, P. Ravi Selvaganapathy (2014), **"***Electrical tweezers for transport of water droplets"*, Cage Club Student Conference on High Voltage Engineering and Applied Electrostatics, August 15, 2014, McMaster University, Hamilton, ON (**Presentation**).

6. **Ali Shahid**, P. Ravi Selvaganapathy, (2011), "*Movement of water droplet in oil under the influence of electric field*," Cage Club Student Conference on High

Voltage Engineering and Applied Electrostatics, August 16, 2011, University of Waterloo, Waterloo, ON (**Presentation**).

A low-cost heater was integrated on-chip to create the localized heating zones in a microfluidic device to perform DNA amplification using the isothermal amplification assays. Then, the amplification module was integrated with on-chip sample preparation and post-amplification components. These on-chip components were operated to detect the bacteria samples in a simple fashion using the power supply.

Publication

1. **Ali Shahid**, Sylvia Chong, Athanasios Paschos, James Mahony, M. Jamal Deen, Herb E. Schellhorn, and P. Ravi Selvaganapathy, "*A low-cost heater integrated microfluidic device to perform integrated sample processing and detection of bacteria". (***Manuscript in preparation***).

Conference presentation and poster

2. P. R. Selvaganapathy, **A. Shahid**, J. Mahony, M.J. Deen, (2018), "*Electrical methods for simple sample preparation",* 101st Canadian Chemistry Conference and Exhibition, May 27-31, 2018, CSC, Edmonton, AB

3. **Ali Shahid**, Sylvia Chong, Athanasios Paschos, James Mahony, M. Jamal Deen, Herb E. Schellhorn, P. R. Selvaganapathy, (2016), "*Microfluidic integrated devices for water quality monitoring"*, MacWater, July 21, 2016, Challenges in water monitoring (MacWater), Hamilton, ON (**Poster**).

Chapter: 2 Introduction

2.1 Background

2.1.1 Nucleic acid-based amplification methods

Many nucleic acid amplification methods have been developed over the past 40 years. These amplification methods can be classified into two categories of non-isothermal amplification and isothermal amplification methods. Polymerase chain reaction (PCR) is a non-isothermal amplification method that is most commonly used. Isothermal amplification methods can be classified as strand displacement amplification (SDA) [7], helicase-dependent amplification (HDA) [8], nucleic acid sequence-based amplification (NASBA) [9], rolling circle amplification (RCA) [10], [11], recombinase polymerase amplification (RPA) [12] and loop-mediated isothermal amplification (LAMP) [13]. This chapter provides an overview of the DNA amplification techniques and discusses the operating principles of the polymerase chain reaction (PCR) and loop-mediated isothermal amplification (LAMP) methods. In the next phase, microfluidic technology-based devices to perform amplification assays such as polymerase chain reaction (PCR) and loop-mediated isothermal amplification (LAMP) are discussed.

2.1.1.1 Polymerase chain reaction

Polymerase chain reaction (PCR) was the first DNA amplification method that was developed in the early 1980s [14]. PCR is a well-known and widely used DNA amplification technology due to its simple operation. PCR exponentially amplifies DNA molecules, from a single copy to several millions of copies of DNA with a few repetitive temperature cycles. Every temperature cycle of PCR consists of the three steps, denaturation, annealing and extension as shown in Figure 2.1.

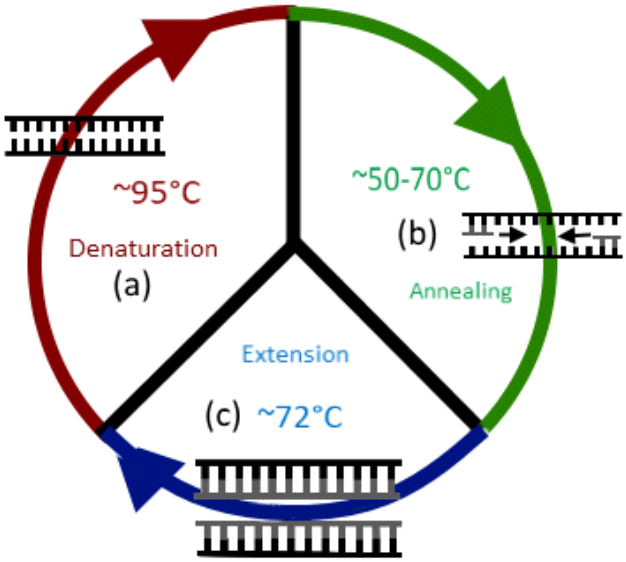

Figure 2.1 Reaction sequence of polymerase chain reaction (PCR). (a) Denaturation (95˚C). (b) Annealing (50-70˚C). (c) Extension (~ 72˚C).

A double strand of DNA is split to form two single-stranded DNA molecules at the elevated temperature of ~ 95°C (Figure 2.1a) during the denaturation step. Then, the annealing step (Figure 2.1b) is performed at the lowered temperature (~50-70°C). During the annealing process, small complementary synthetic single-stranded DNA molecule known as primers are attached to the specific defined site of the single-stranded DNA molecule. Finally, in the extension step (Figure 2.1c) which occurs at 72˚C, the polymerase enzyme copies the single-stranded DNA in between the two primer locations. DNA molecules exponentially increase when exposed to this temperature cycle repeatedly. Conventional PCR process is straightforward, but it requires significant instrumentation to acquire, monitor, and control different temperatures in each stage. Also, it takes a longer time to complete the amplification reaction. The microfluidic technology was used to establish PCR systems to overcome limitations of conventional PCR systems.

2.1.1.2 Isothermal amplification of nucleic acid

Isothermal DNA amplification assays were developed later to simplify the amplification process further and eliminate thermocycling. These isothermal assays depend

on the enzyme activities at the constant temperature. A number of methods such as strand displacement amplification (SDA) [7], helicase-dependent amplification (HDA) [8], nucleic acid sequence-based amplification (NASBA) [9], rolling circle amplification (RCA) [10], [11], recombinase polymerase amplification (RPA) [12], loop-mediated isothermal DNA amplification (LAMP) [13] were developed.

2.1.1.2.1 Loop-mediated isothermal amplification (LAMP)

Among the many isothermal methods that have been developed, LAMP has been the most widely used method primarily due to its simple operation, high specificity, and high amplification efficiency. LAMP assays amplify targeted DNA at the constant temperature (60-65°C) using four to six specifically designed sets of primers and with the strand displacement activity of polymerase *Bacillus stearothermophilus (Bst)* [13]. The DNA can be amplified from a few copies to 10^9 copies in less than an hour using the LAMP assays. The reaction sequence of the LAMP is demonstrated in Figure 2.2.

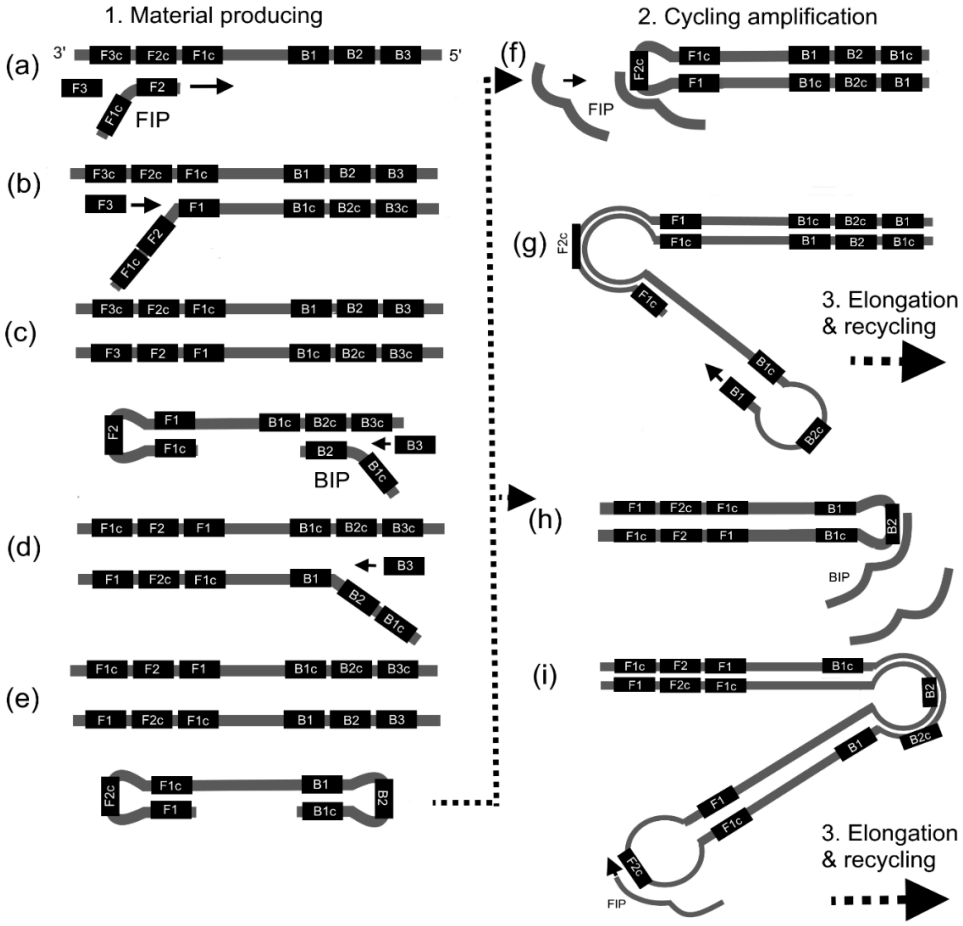

Figure 2.2 Reaction sequence of loop-mediated isothermal amplification (LAMP).

The sets of primers required for LAMP assays were categorized as forward and backward primers. Specifically, it was classified as forward inner primers (FIP), backward inner primers (BIP), forward outer primers (FP), and backward outer primers (BP). During the initial phase of the reaction, four primers were used while only inner primers were used later in the cycling phase. The F2 segment of FIP attached to its complementary segment (F2c) of targeted DNA and started strand synthesis (Figure 2.2).

The outer primer was small and less in concentration. Then, the outer primer F3 was attached to the complementary segment (F3c) of targeted DNA and started strand displacement synthesis (Figure 2.2b). Subsequently, this strand displacement activity synthesized the double strand DNA and looped out structure was formed at one end due to

the presence of a complementary segment (Figure 2.2c). And BIP was attached to complementary segment B2c. The BIP performed synthesis, and outer primer (B3) initiated the strand displacement activity (Figure 2.2d). Subsequently, the dumb-bell structure was formed at the end (Figure 2.2e). This dumb-bell like structure was immediately converted to the stem-loop structure which helped to initiate the cycling process. During the cycling step, the FIP was attached to the loop structure and performed the strand displacement synthesis. Subsequently, two inserted stem-loop structures were formed (Figure 2.2g). Afterwards, BIP assisted in finishing the cycling stage (Figure 2.2i). During the LAMP amplification, the targeted DNA was amplified 3-fold every half cycle. Final LAMP product was the mixture of various structures that included stem-loop structures and cauliflower. These structures were of various stem lengths and multiple loops.

2.2 Literature survey

2.2.1 Miniaturized systems for polymerase chain reaction (PCR)

PCR amplify DNA molecules based on the temperature cycling subsequently, made heating and cooling time as a critical factor for the rapid operation of the system. The small sample volumes used in miniaturized systems made them time efficient as the surface to volume ratio increased for miniaturized systems. Microfluidic devices to perform PCR assays has been reviewed extensively in the literature.[15]–[21]. A variety of miniaturized PCR systems have been designed, and they can be broadly classified into (1) chamber-based, (1) flow-through devices, (3) droplet-based devices, and (4) convection flow. Some of the technologies that were developed initially for micro PCR amplification has then been adapted for LAMP amplification which is the central focus of this thesis. Therefore, it is worthwhile to review microscale devices for PCR amplification.

2.2.1.1 Stationary chamber-based devices

The conceptual design of stationary chamber-based devices is similar to the conventional macroscale PCR devices. The sample is injected in the stationary reaction chamber, and subsequently, the chamber is heated and cooled during the repetitive temperature cycles. Microfluidic systems have a high surface to volume ratio that consequently reduce the heating and cooling time. This feature enables microscale devices to achieve a faster reaction time as compared to macroscale counterparts. Devices with either single chamber [22]–[27], or multi-chambers [28]–[36] were developed to perform PCR in this format.

2.2.1.1.1 Single chamber-based devices

Microfluidic devices with single chambers were filled with the sample and exposed to the temperature cycle to perform PCR. This format was easy to fabricate and therefore has been widely adopted by several research groups. The chamber size for these devices ranged from 200 nL [37] to 50 µL [38]. Precise temperature control was the main challenge for the successful operation of stationary single chamber-based PCR devices. Many temperature control strategies were used for stationary chamber PCR devices by various research groups. Various heating systems including thin layer heaters [39]–[46], thermoelectric cooler (TEC) on single side [24], [25], [38], [47], [48], thermoelectric cooler (TEC) on both sides [24], double cartage heater [49], infrared heating [26], [50], [51], and microwave heating [52]. Heating rates of 2 [49] to 65 [52] °C/s were achieved. Similarly, various cooling method were used such as convective air cooling [26], [41], [44], [49], [53]–[55], compressed air cooling [50], [56], thermoelectric cooling [24], [25], [48], air impingent cooling [52] and liquid [57], [58]. Cooling rates ranged from 1.2 [49] to 45 [33] °C/s were achieved. PCR samples were amplified by exposing them to repetitive temperature cycles ranged from 25 [26] to 50 [59]. A few examples of stationary single chamber-based microfluidic PCR devices have been compiled in Figure 2.3.

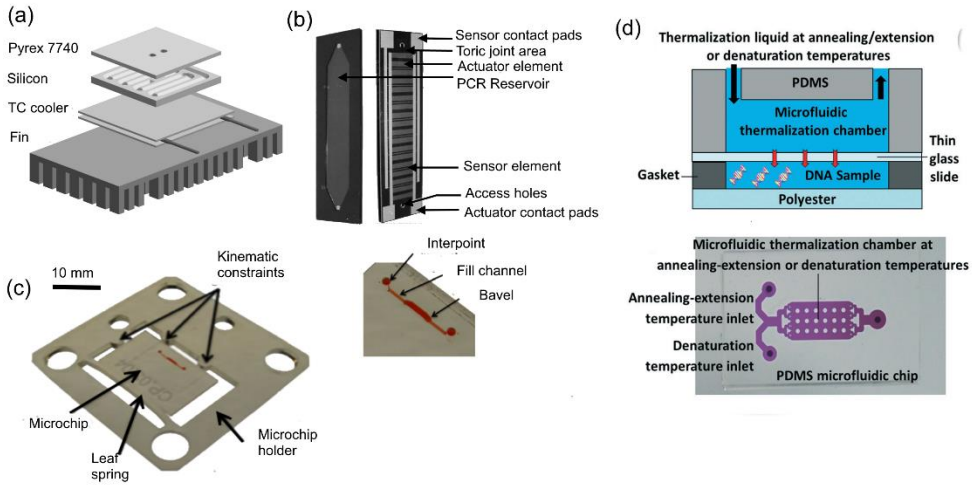

Figure 2.3 . (a) Microchip with thermal module [38]. (b) Microchip with the front and rare view [42]. (c) Photograph of a plug and play polymer microchip [26]. (d) Schematics and top view of a microfluidic device [58].

Several examples can be cited for microfluidic devices with a single chamber design those have been developed for the rapid DNA amplification. For instance, a single chambered microfluidic device has been developed to amplify the *hepatitis C virus* in 30 min [38] as shown in Figure 2.3a. This device consisted of single-chamber to handle the 50 µL of sample volume. This sample volume was relatively higher than the typical sample volume (25 µL) used in the macroscale PCR devices. This device was fabricated with the glass-silicon materials using the microfabrication techniques such as photolithography, electrochemical etching, wet etching, and anodic bonding. The thermoelectric cooler (TEC) controlled by the PID controller was used to maintain heating and cooling temperature cycles. Heating and cooling temperature cycles were maintained with the thermoelectric cooler (TEC) that was controlled by the PID controller. Heating and cooling rates of 4 and 2.2 ˚C/s were achieved to execute 30 temperature cycles.

Another fast device has been developed to achieve the amplification in 20 min [42] as shown in Figure 2.3b. This device with the single chamber was fabricated to handle the small sample volume of 25 µL. The device was fabricated with silicon and glass materials using microfabrication methods. The fabrication process consists of various techniques that

include the dry thermal oxidation, low-pressure chemical vapor deposition (LPCVD), reactive ion etching (RIE), atmospheric pressure vapor deposition (APVD), photolithography, wet chemical etching, and anodic bonding. Fast heating and cooling rates of 10-15 ˚C/s were achieved to complete 40-45 cycles.

Then, the DNA amplification time was further reduced to 10 min using the microfluidic device [26] as shown in Figure 2.3c. The device consisted of a stationary chamber designed to handle a smaller volume of 820 nL. This microfluidic device was fabricated using Polymethylmethacrylate (PMMA) as the substrate material, and microchambers were fabricated using CNC machining. The thin layer of the polymer film was attached to the bottom of the chip using the thermal bonding. The transparent biocompatible tape was used to seal the top of the chip. PCR samples were amplified using 25 repetitive temperature cycles.

Finally, DNA amplification was achieved in 2 min using the ultrafast microfluidic device [58] as shown in Figure 2.3d. This chip was a single chambered device and was fabricated to handle a volume of 25 µL. The polyester, gasket, thin glass slide and polydimethylsiloxane (PDMS) were used to fabricate the device. The liquid heating and cooling methods were used to maintain the temperatures required for Denaturation, Annealing, and Extension. The commercial coolant liquid Koolance (Koolance, WA, USA) was used as a heat exchange fluid. The convective heat transfer coefficient for liquids is higher than air consequently rapid temperature cycling was achieved despite a large sample size. The 30 repetitive temperature cycles were used to amplify DNA.

2.2.1.1.2 Multi chamber-based devices

Microfluidic PCR devices have also been designed with multi-chambers to perform DNA amplification using PCR. These multi-chambered devices are usually used for high throughout operation by performing amplification reactions of multiple targeted genes in parallel. Due to parallel processing, the amplification process is more time and cost

effective. A few examples of multi chamber-based PCR devices are demonstrated in Figure 2.4.

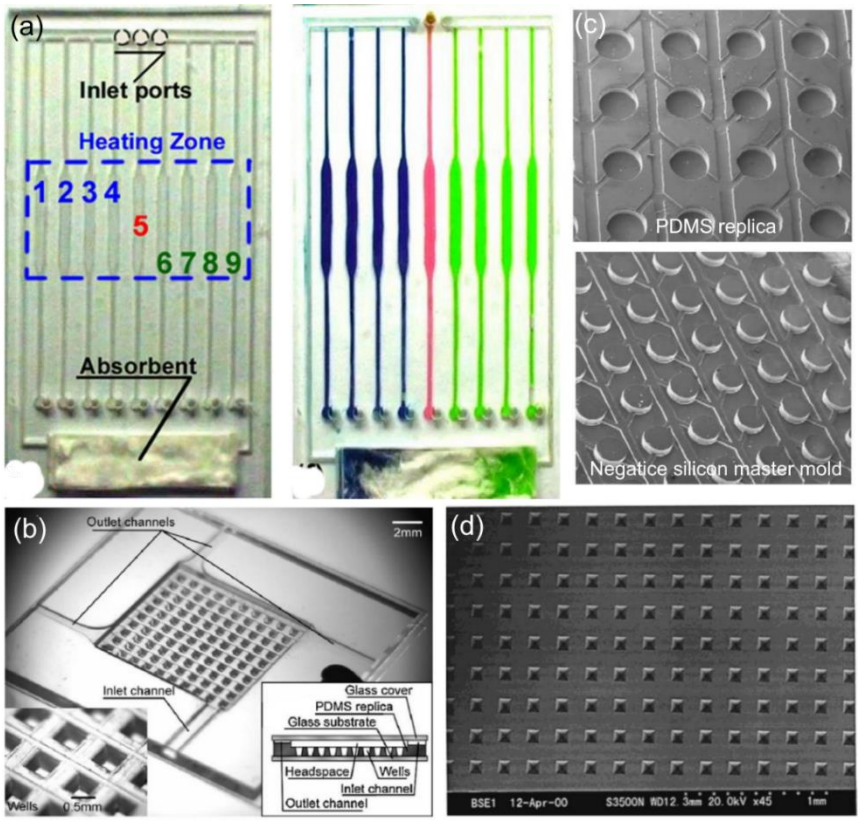

Figure 2.4 Multi chamber-based devices for PCR. (a) A microfluidic device to perform PCR with arrays, a heating zone, inlet ports and filling of chambers and channels [60]. (b) PDMS matrix of 100 wells [30]. (c) SEM images of silicon master mold and PDMS replica [28]. (d) SEM images of microchambers [61].

Microfluidic devices of various chamber sizes have been developed that ranged from 450 pL [62] to 20 µL [63]. The surface to volume ratio increases with the decrease in the sample volume. Consequently, the heat transfer rapidly increases with the reduction in sample size as heat transfer depends upon the surface area. Additionally, amplification devices of the various arrangement of microarrays that ranged from 4 reaction chambers [64] to the 1064 chamber [28] per device, were used to perform amplification reactions in parallel. The sample loading step is the primary challenge involved in the operation of multi chamber-based PCR devices. Various approaches such as the capillary force-based filling

[65], pressure driven filling [28], vacuum assisted filling [30], surface treated [61] were successfully used to load a sample in microfluidic devices. A few examples of which are explained in detail.

Microfluidic devices were developed with multi-chambers for the rapid amplification of PCR assays. The amplification chamber size was significantly reduced to handle the smaller reaction volumes. For instance, a multi-chambered microfluidic device was developed where the size of each chamber was ~ 5 µL [60] as shown in Figure 2.4a. The device consisted of an array of 9 reaction chambers in parallel. Four different pathogens were simultaneously identified in these straight chambers using the amplification assays. This device was fabricated using glass and PDMS materials. Initially, microchambers and microchannels both were treated with the Triton X-100 to make them hydrophilic. Then, primers were pre-loaded and dried in reaction chambers. The capillary-based flow was used to load the reaction mixture in arrays of microchambers. The absorbent pad automatically absorbed the excess volume at the end. A Peltier element was used to create localized heating zones for the temperature cycling. Each temperature cycle consisted of three steps of denaturation (30s), annealing (30s), and extension (120s). The 40 repetitive temperature cycles were used to amplify the targeted DNA.

Another multichambered-based PCR amplification device has been developed to handle smaller reaction volumes of 120 nL [30] as shown in Figure 2.4b. This device consisted of 100 wells matrix to detect the ten different targeted gene of cDNA. The device consisted of three layers of glass and PDMS materials. The PDMS layer was sandwiched between two glass layers and contained microchambers. The primers were pre-suspended and dried in the microchambers. The vacuum aided setup was used to load the reaction mixture into 100 wells within 0.2s and subsequently the device was sealed. The thermoelectric cooler (TEC) with a controller was used to implement temperature cycle. The 40 repetitive temperature cycles were applied to amplify the targeted DNA. The use of a vacuum pumping system makes it less suitable to use it in the point-of-care setting.

Then, the chamber size was further reduced to handle the sample volume of 25 nL in the multichambered microfluidic device [28] as shown in Figure 2.4c. The device consisted of 1064 column chambers that were fabricated using the PDMS material. The silicon master mold made the PDMS replica. The deep etching technique coupled with the inductively coupled plasma (ICP) was used to fabricate the 3-D master mold. The PDMS channels and chambers were made hydrophilic by plasma treatment at the time of PDMS-PDMS bonding. The sample was loaded using the syringe pressure and capillary force immediately after the bonding. The commercial thermocycler was used to apply 30 temperature cycles (94, 65, and 72˚C). The samples were exposed to each temperature for the 30s in each temperature cycle. This plasma treatment makes the PDMS surface temporarily hydrophilic which limit the use of a device. Additionally, the fabrication of 3-D silicon master mold is a complicated and expensive process.

Finally, chamber size was reduced to 85 pL in the multichambered based microfluidic device [61] as shown in Figure 2.4d. This device consisted of 100 × 100 arrays of microchambers. The device was fabricated using the silicon wafer with the semiconductor technology. The fabrication processes such as photolithography, anisotropic etching, and thermal oxidation were used. The water was retained in microchambers for more than 3h by making inner walls hydrophilic while the outer surface was hydrophobic. The surface was treated with BSA solution to reduce the absorption. The cross-over contamination was avoided using the HIPORA membrane. HPORA is a waterproof and breathable membrane consisted of three layers, so water cannot pass through it, but moisture can go out. The membrane sandwiched between layers of silicon and glass. The commercial PCR amplification instrument was used to implement temperature cycling for the microfluidic device with heating/cooling rates of 1˚C/s. Finally, pGFP fragments were amplified in ~2.5h using the 40 temperature cycles. Flow-through systems

In flow-through systems, the PCR sample was pumped in the microchannel with three temperature zones required to perform nucleic acid amplification reaction. Microchannels of various formats were successfully employed such as serpentine channel

[66]–[71], radial/circular channel [72], [73], and straight channel [74]–[77]. Flow-through PCR devices have small thermal mass and subsequently, analysis time was reduced. However, due to the large surface to volume ratio of microchannels the sample absorption on channel walls was unavoidable.

2.2.1.2 Flow-through based devices

2.2.1.2.1 Serpentine channel-based flow-through devices

Serpentine-shaped microchannels are most commonly used format for the flow-through PCR devices. Generally, a syringe pump was used to precisely control the fluid flow in the serpentine-shaped channel. Mostly, devices were fabricated using silicon, glass, polydimethylsiloxane (PDMS) [66], [67], [78]–[90], polycarbonate (PC) [91], [92], steel capillary [82], or copper (Cu)-clad [93].

Syringe pumps pushed samples through microchannels of flow-through devices. Typical flow rates used were ranged from 0.5 µL/min [90] to 30 µL/min [79]. Various amplification reaction times were achieved from 5 min [93] to 45 min [94]. Some illustrative examples of microfluidic devices with the serpentine-shaped microchannel are presented in Figure 2.5

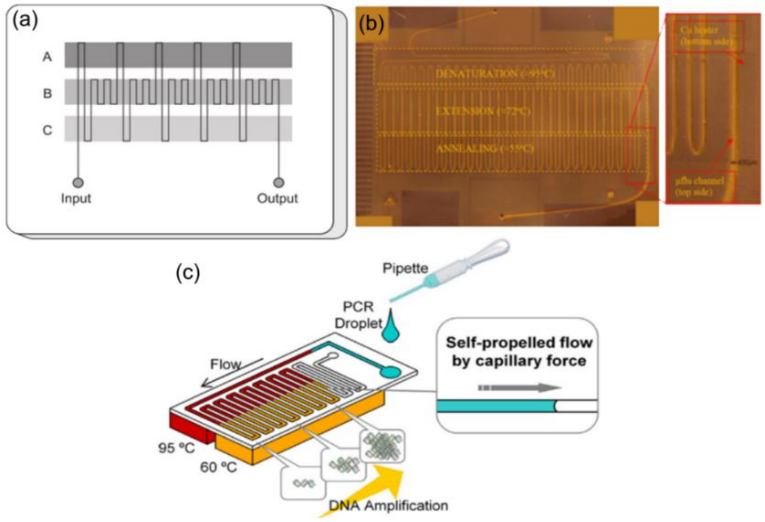

Figure 2.5 Flow-through microfluidic devices for PCR with serpentine shaped microchannels. (a) A microfluidic device to perform PCR [83]. (b) Polymer-based microfluidic device [93]. (c) Capillary flow-based microfluidic device [95].

The first flow through amplification device was developed by Kopp et al. (Figure 2.5a) [83]. Microchannels in this device were 40 µm (deep) 90 µm (wide) and were etched and bonded with the cover with access holes (400 µm). The syringe pump was used to push the 25 µm PCR sample of gyrase gene of Neisseria gonorrhoeae with 176 bp, at various flow rates (5.8 - 72.9 nL/s). The sample was pushed through temperature zones (95, 77, and 60°C) repeatedly through the serpentine-shaped microfluidic channel. The 20 amplification cycles were completed in the 90s to 18.7 min by pushing samples at various flow rates.

Another flow through-device has been developed to perform PCR reaction in 5 min [93] as shown in Figure 2.5b. The device was fabricated using the thin polymeric substrate with on-chip integrated heaters. The serpentine-shaped microchannel of 145 cm was fabricated in the top polyimide (PI) layer. The serpentine-shaped microchannel was designed with the different widths for different temperature zones such as the width of 400 µm was selected for extension zone, and the width of 200 µm was chosen for the denaturation and annealing sections. The resistive microheaters were fabricated in the bottom layer of the commercially available Cu-clad PI (Copper layer) substrate. The PCR

sample consisted of 92-bp DNA fragment from the mouse housekeeping glyceraldehyde 3-phosphate dehydrogenase (GAPDH) gene, was used to validate the performance of a microfluidic device. The syringe pump was used to push the PCR sample at various flow rates of 1.8 to 7.8 μL/min through three temperature zones (95, 72 and 55 °C) for 30 cycles.

Another pumpless flow-through device has been developed with the self-propelled sample mechanism using the capillary-driven flow [95] as shown in Figure 2.5c. The microchannel with the dimensions of 150 μm (width), 150 μm (depth), and 1600 mm (length) was fabricated in the silicon substrate. Microchannels were made hydrophilic by removing the oxide layer. Finally, the glass cover was bonded with the silicon substrate. Two cartridge heaters in the aluminum block were used to establish the three different temperature zones. The PCR sample was moved through temperature zones, and the assay was completed in less than 14 min. The use of capillary self-driven flow eliminated the need for using external pumps. The device fabrication was involved with the expensive fabrication processes that make it less suitable to develop the low-cost device.

2.2.1.2.2 Radial/Circular channel-based flow-through devices

In this class of devices, PCR samples were pushed in microchannels through three temperature zones. Microchannels were designed in such format that either sample was pushed in a circular direction or radial direction. The single heating source can be used in this format to create the localized heated zone of ~ 92˚C in the middle area while the low-temperature zones could be created subsequently on the peripheral zones. Microfluidic devices were fabricated using silicon [96] and polymer materials [97]–[99]. Mostly, syringe pumps were used to push the PCR sample in microchannels. Two examples of devices with the radial/circular designed microfluidic channels are shown in Figure 2.6.

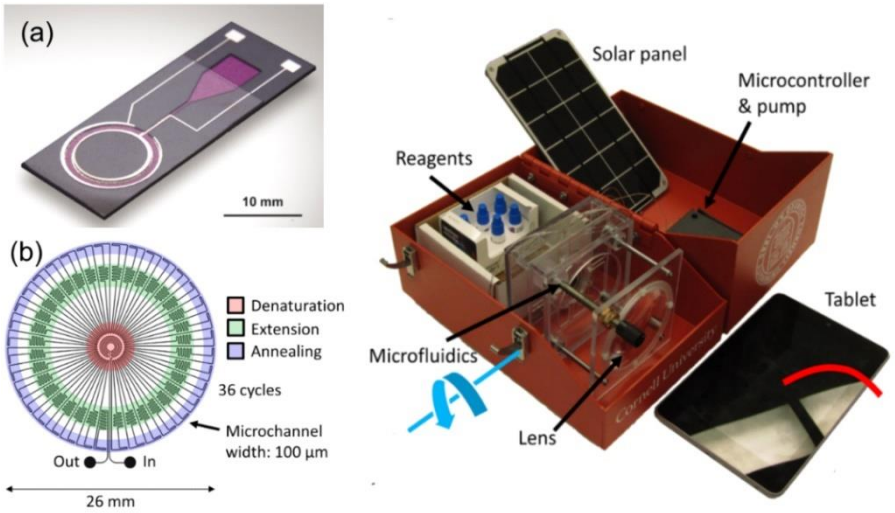

Figure 2.6 Flow-through microfluidic devices with a circular/radial-shaped microchannel for PCR. (a) Microfluidic device based on the magnetohydrodynamic principle with circular-shaped microchannel [96]. (b) Solar power-based microfluidic device with radial-shaped microchannel [99].

For instance, the microfluidic device has been developed with the microchannel in the circular format [96] as shown in Figure 2.6a. The microchannel was etched in the silicon by bulk micromachining (depth: 150 µm, width 1160 µm, and an internal radius of 4.42 mm) or by rapid prototyping using EPON SU-8 (depth = 180 µm, width = 1000 µm and inner radius = 4.5 mm). The fabricated microreactor was sealed with a film that was laminated to it. The 20 amplification cycles were performed by pushing the PCR sample in the microchannel using the magnetohydrodynamic actuated flow. Temperature zones were established using the thermoelectric cooler (TEC) device.

Another solar power based integrated microfluidic system has been developed for the diagnosis of Kaposi's sarcoma (KS) [99] as shown in Figure 2.6b. The system consisted of an Android tablet, solar panel, microfluidic chip, lens, and fixture, peristaltic pump, and microcontroller. The solar energy-based heating system was used to develop the temperature zones. The light was focused on to the middle of the device creating a high-temperature zone while the temperature was lower outside the zone. The sample was

pushed in the radial directions of microchannels (width: 100 µm) to perform an amplification reaction in 30 min.

2.2.1.2.3 Straight channel-based flow-through devices

In this class of devices, the PCR samples were shuttled back and forth between heating zones in straight microchannels of a microfluidic device. Two illustrative examples have been shown in Figure 2.7.

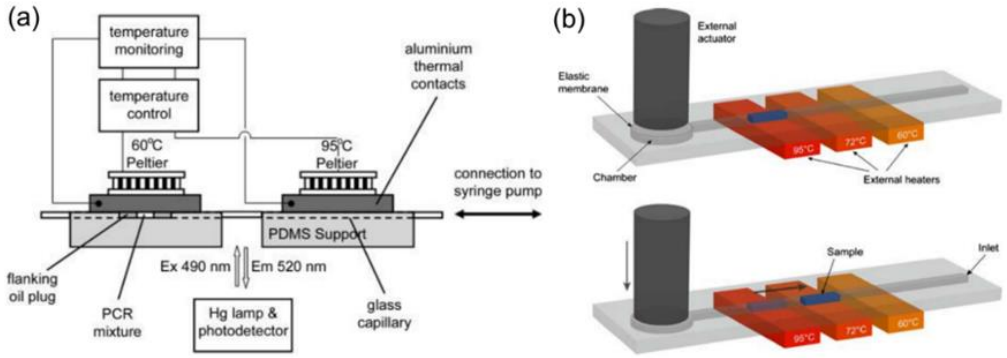

Figure 2.7 Flow-through microfluidic devices with a straight microchannel for PCR. (a) Schematic of a microfluidic device with a bi-directional flow of samples [100]. (b) The principle of PCR with the sample shuttling in the straight channel-based microfluidic device [101].

Microfluidic device with the straight channel has been developed to perform PCR reaction in 43 min [100] as shown in Figure 2.7a. The device consisted of glass capillary with the inner diameter of 1 mm. Two Peltier heating elements were used to establish elevated temperature zones for PCR. The sample volume of 2 µL was shuttled between the heating zones. Consequently, samples were amplified using 40 repetitive temperature cycles.

Another microfluidic flow-through device with the straight channel has been developed to accomplish the amplification reaction in less than 5 min [101] as shown in Figure 2.7b. The straight microchannel was integrated with the flexible membrane-based pumping system. This system was developed to precisely control the bi-directional

movement of the sample between the temperature zones. External heaters were attached at the bottom of the device to establish the temperature zones. The sample volume of ~ 100 nL was amplified in less than 5 min by completing 20 amplification cycles.

2.2.1.3 Convective flow-based PCR devices

In this class of devices, the principle of the buoyancy-driven flow was used to move the sample through a temperature gradient. Mainly three approaches were followed to fabricate the convective-flow based devices including closed cell-shaped [102]–[105], ring-shaped [103], [106], [107] and toroid-shaped [108]–[110]. Illustrative examples of the convective flow-based microfluidic devices are presented in Figure 2.8.

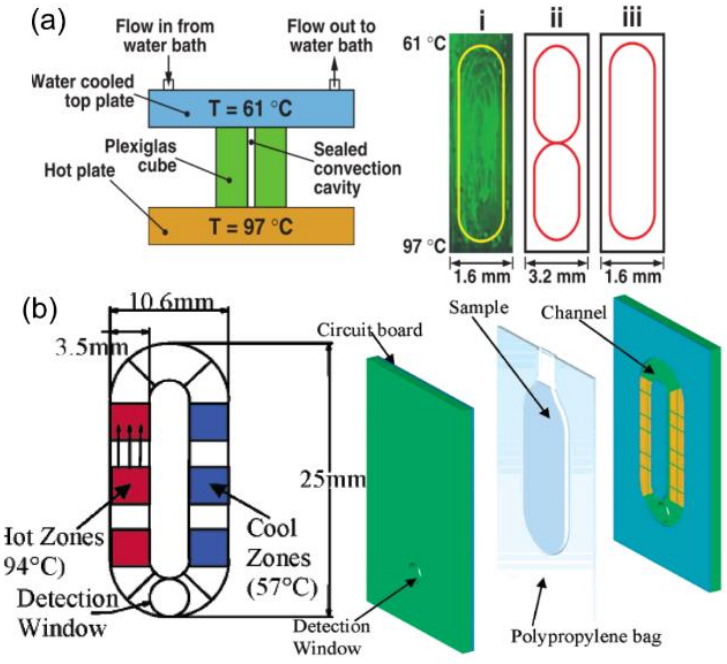

Figure 2.8 Convective flow-based microfluidic devices for PCR. (a) Rayleigh-Bernard convection-driven microfluidic device [102]. (b) Schematics of O-shaped convection driven microfluidic device [106].

The buoyancy-driven flow based microfluidic device first time has been developed by the Krishnan et al. [102] as shown in Figure 2.8a. The sample volume of 35 µL was circulated in the closed cavity of Plexiglas cubes between hot (bottom) and cold (top)

plates. Flow visualization technique was used to optimize the geometry of the cell for DNA amplification.

Another buoyancy-driven flow based device with the glass capillary and a single heating element has been developed [104]. The glass capillary with the dimensions of 51 mm (length), 2.3 mm (inner diameter) and 3.2 mm (outer diameter) was used. The temperature gradient was established in the capillary tube by placing it on the single heating element (digital dry bath incubator). Consequently, the PCR sample with the ~ 30 copies per reaction was amplified in 30 min.

Another instrument free with a single cavity microfluidic device has been developed. The buoyancy-driven flow was used to circulate the sample through the temperature gradient [105]. Chemical heating source of exothermic chemical reaction has been used to establish the temperature gradient. The device was fabricated using the polycarbonate (PC) material. The sample volume of 40 µL was circulated in the cavity due to convective flow. Consequently, the DNA was amplified in less than 35 min and visually detected using the integrated lateral flow strip.

The device with the ring-shaped cavity has been used to implement the convective flow for DNA amplification [106] as shown in Figure 2.8b. One side of the ring was kept at the higher temperature (~ 94°C) while, the second side was maintained at the low temperature (~ 57°C). Initially, the PCR sample was loaded in the polypropylene bags. The sample was circulated in the O-ring shaped cavity due to the buoyancy-driven flow. Consequently, PCR samples were amplified in less than 30 min.

Another device with different ring-shaped that was U-shaped has been developed [111]. The U-shaped capillary tube with an inner diameter of 1.6 mm was used. The isothermal heating element was placed at the bottom of the capillary. The PCR sample was circulated in the capillary due to buoyancy-driven flow. Consequently, DNA was amplified in 25 min and amplification was detected using the charged couple device (CCD). Another triangular-shaped device has been developed in which the DNA amplification process was

integrated with the sample preparation [112]. The DNA amplification was detected using the fluorescence-based detection system. Initially, the magnetic beads (MB) assays have been used for photothermal lysis of the bacteria cells. Then, the PCR sample was circulated in the closed cavity. The triangular shaped device was fabricated using the polytetrafluoroethylene (PTFE) capillary tube, and the temperature gradient had been developed across it. The real-time fluorescence detection was performed using the wireless camera-based system. The sample with the concentration up to the limit of 1 copy/µL was detected in less than 25 min.

2.2.1.4 Droplet-based PCR devices

Droplets have been used to perform PCR amplification in the microfluidic format. These devices can be categorized into the two groups: 1) Systems in which droplets flowed continuously in a microchannel and 2) Devices in which the discrete droplets were handled. Droplet-based microfluidic systems for PCR have several advantages over the continuous flow-based devices. In the case of droplets, the thermal mass of droplets is smaller than those devices in which the sample volumes flow in the continuous format. The temperature uniformity can be higher in the droplets enabling faster cycling time. The cross-contamination is significantly reduced as the droplet did not contact the channel walls. Additionally, the surface absorption of PCR reagents on the walls of microchannels can be minimized. Finally, the system can be made cost effective as the smaller reagents volumes are used.

2.2.1.4.1 Continuous flow of droplet-based devices

In this class of devices, droplets were generated at a T-junction or cross junction due to the shear force at the oil-water interface due to different flow rates of two immiscible fluids. Then, generated droplets were pushed in a carrier medium through the temperature zones. Various architecture of microfluidic channels were utilized including straight channel [113], serpentine channel [114], spherical channel [115], [116], circular/radial

[117], [118]. A few examples of devices used to perform PCR in continuous flow-based droplets format are shown in Figure 2.9.

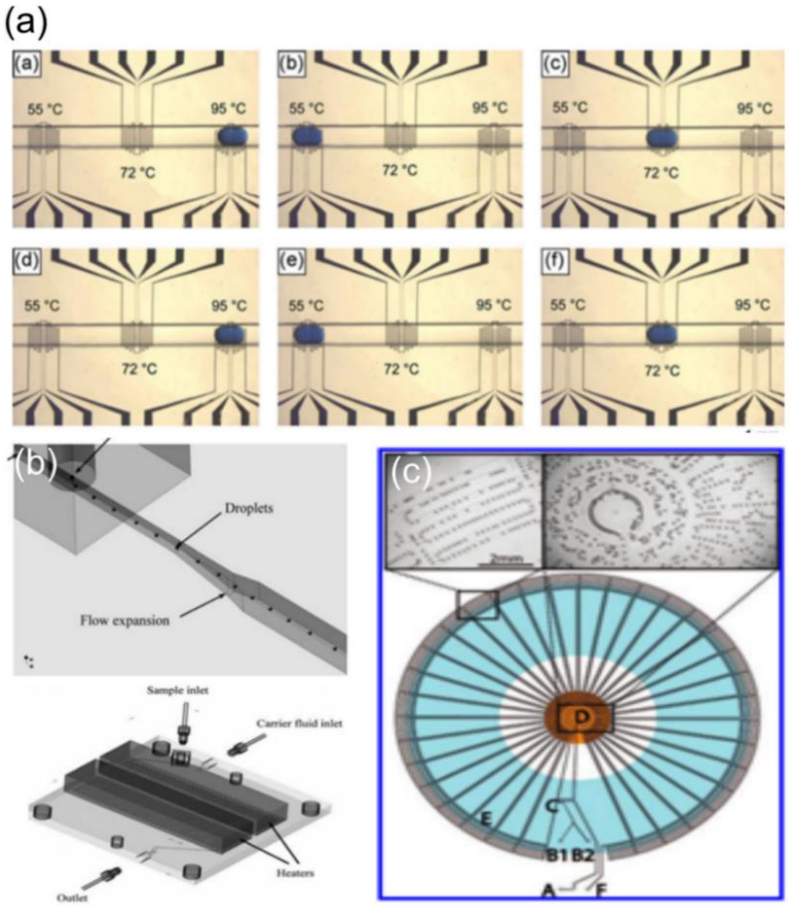

Figure 2.9 The continuous flow of droplet-based microfluidic devices. (a) Optical image of a microfluidic device with a straight channel format. Droplet (1 µL) is shuttling between various temperature zones [113]. (b) Schematics of the device with a serpentine channel with inlet and outlets. The region of extrusion of droplets in oil medium through an orifice (50 µm) [114]. (c) Top view of the droplet-based microfluidic device to move droplets in the radial direction [118].

The droplet-based microfluidic device has been developed to perform PCR in the straight channel [113] as shown in Figure 2.9a. The device was fabricated using glass and PDMS materials. The heater was fabricated using the conventional microfabrication technology. The droplet was shuttled between three temperature zones (95, 72, and 55˚C) in the oil medium. Three temperature zones were established having a certain distance

between them. Two syringe pumps were used to move the droplet (1 µL) back and forth in the oil medium through temperature zones. PCR sample was amplified using 35 repetitive temperature cycles in less than 50 min.

Another device with the serpentine-shaped channel has been developed to perform PCR in droplet format [114] as shown in Figure 2.9b. The ~ 63 mm long microchannel was machined in polycarbonate (PC) sheets. An acetate foil was used to seal the microchannels. The UV curable epoxy was used to attach acetate foil with the polycarbonate. The droplets were generated due to the high shear by passing the sample through an orifice (50 µm) into the oil medium. The droplet size was controlled by varying the flow rate. For instance, droplets with the diameter of 100-155 µm were generated using the flow rate of 4 µL/min. These droplets were pushed through the various temperature zones to complete 32 amplification cycles.

Finally, a microfluidic device with the circular/radial-shaped microchannel has been developed [118] as shown in Figure 2.9c. Microchannels were fabricated with the dimensions of 75 µm deep and 200-500 µm wide. The droplets were generated at the T-junction and transported with the flow rate of ~ 160 µL/h. The temperature gradient was established using the annular shaped Peltier module (15 W), thermoelectric heat pumps and fan-cooled heat exchangers. DNA was amplified in 17 min by pushing the droplets through temperature zones to complete 34 temperature cycles.

2.2.1.4.2 Discrete droplet-based PCR devices

Another class of devices that handle individual (discrete) droplets to perform the PCR has been investigated. Two methods were used for discrete droplet-based systems. These methods include digital microfluidics (DMF) and wire-guided system (WGS).

2.2.1.4.2.1 Digital microfluidics-based PCR devices

Digital microfluidics (DMF) is one of the most established technology to handle the discrete droplets [119]. This technology is based on the principle of electrowetting on

dielectric (EWOD) [120], [121]. In this method, the local contact angle of an aqueous droplet was changed due to the application of the potential on an electrode underneath a dielectric material. Subsequently, the discrete droplets were manipulated on the hydrophobic substrate due to spatial control of the contact angle through electric potentials. A few examples of PCR amplification performed using digital microfluidic technology is shown in Figure 2.10.

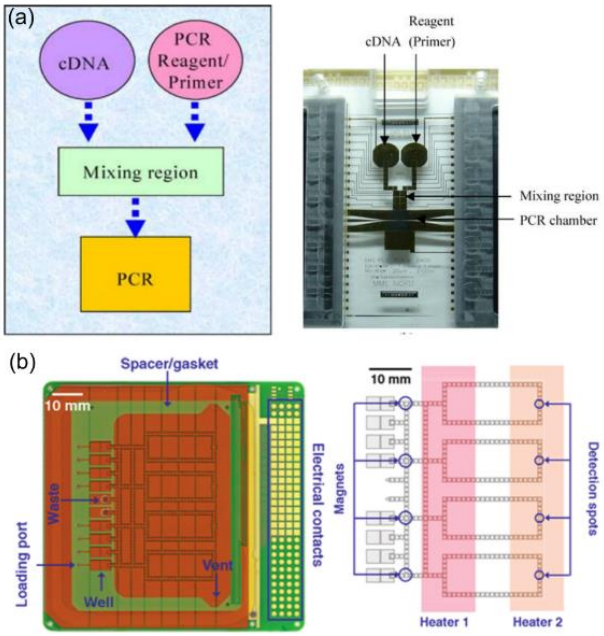

Figure 2.10 Digital microfluidic-based microfluidic devices for PCR. (a) Schematics and a photograph of a digital microfluidic-based chip for PCR [122]. (b) Schematics of a self-contained digital microfluidic system for PCR [123].

The digital microfluidics or electrowetting technology was utilized for the first time to perform PCR assays by Chang et al. [122] as shown in Figure 2.10a. The device was fabricated using the standard microfabrication technology. An applied voltage of 12 V_{RMS} at the frequency of 3 kHz was applied to perform various droplet-based microfluidic operations. Two droplets (~730 nL) containing reagents and cDNA were extracted from the separate reservoirs. Then, droplets were mixed in the mixing region and subsequently, the merged droplet was transported to the amplification zone. The voltage of 9 Volts was applied to establish the temperature cycle. The heating and the cooling rates of 38˚C/s and

7.9˚C/s were achieved respectively. The sample volume of 15 µL was amplified in 55 min by 25 repetitive temperature cycles. The conventional PCR machines amplified the sample volume of 50 µL in 110 min.

Then, multiplex PCR assays were amplified in the microfluidic device based on the electrowetting principle [123] as shown in Figure 2.10b. The whole PCR system consisted of heaters, magnetic, controllers and detectors. The PCR cartridge was fabricated using a PCB substrate and glass. Then, this cartridge was loaded in the instrument. Samples were loaded on the cartridge and stored in the reservoirs. First, the two droplets of the volume of 330-660 nL consisted of master mix and DNA sample were extracted from the two different reservoirs. Then, the droplets were mixed to prepare the PCR reaction mixture. Afterwards, droplets were transported between temperature zones to complete 40 repetitive temperature cycles.

2.2.1.4.2.2 Wire-guided system-based PCR devices

The wire-guided system is an alternate technology to manipulate discrete aqueous droplets. The droplet was placed either on the superhydrophobic surface or suspended in the immiscible oil medium. Afterwards, the metal wire was contacted with the droplet. Subsequently, the droplet was attached to the metal wire. The water droplet had a stronger adhesive attraction to the wire as compared to the oil medium or substrate.

Consequently, the droplet followed the metal wire upon the movement of the metal wire. The wire-guided system was used to perform PCR in the discrete droplet format. The wire guided-based systems for PCR [124]–[126] are demonstrated in Figure 2.11.

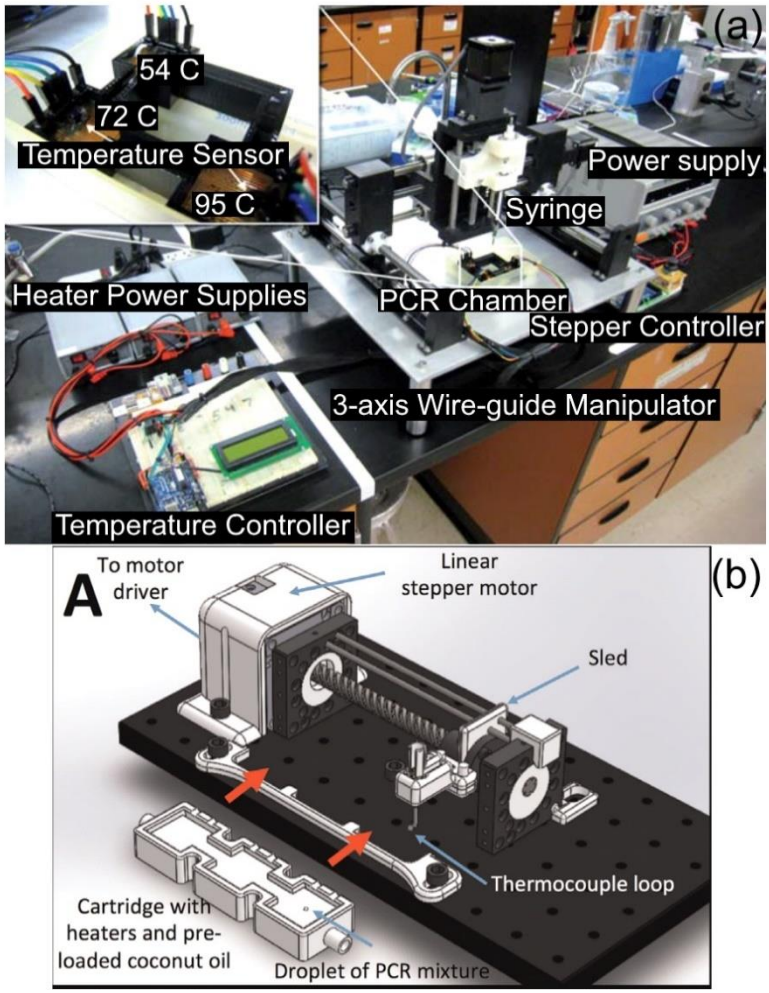

Figure 2.11 Wire-guided systems for discrete droplet-based PCR. (a) Experimental setup to perform droplet-based PCR using 2-dimensional system [124]. (b) Schematics of a wire-guided system for PCR in a linear configuration [126].

A two-dimensional wire-guided system has been developed to move the discrete water droplet in the oil medium through different temperature zones [124] as shown in Figure 2.11a. The device was fabricated using the acrylonitrile butadiene styrene (ABS) polymer with the rapid prototyping. It consisted of three square shape chambers those were connected with the channels to form a closed loop. These chambers and connecting channels were filled with the silicone oil. The three temperature zones were established in the three different chambers. The wire-guided system rapidly transported the droplet of the

volume of 10 µL at the speed of 20 mm/s. DNA samples were amplified by performing 30 repetitive temperature cycles in 6 min 30 s.

Another wire-guided system based device integrated with the detection system has been developed [126] as shown in Figure 2.11b. The detection system was developed based on the end-point fluorescence detection using the smartphone. The device was fabricated using the acrylonitrile butadiene styrene (ABS) polymer by rapid prototyping. The compact system has been developed by connecting the three rectangular chambers in the linear configuration. The device was filled with the silicon or coconut oil. The coconut oil was used to make the system portable as this oil is in the solid state at room temperature. The droplet of the volume of 10 µL was transported through the three temperature zones. Additionally, a wire thermocouple was used to acquire the accurate temperature feedback along with the droplet transportation. The DNA was amplified in 19 min using this system.

2.2.2 Microfluidic systems for isothermal-based amplification

DNA is amplified at the constant temperature using enzymes activity for isothermal amplification. The feature of using constant temperature has a benefit to building low-cost systems with simple instrumentations. The microfluidic device to perform loop-mediated isothermal amplification assays has been reviewed extensively in the literature [127]–[132].

2.2.2.1 Chamber-based microfluidic devices

Since the isothermal amplification methods such as LAMP assays require only a single steady temperature to perform the amplification assays, chamber-based microfluidic systems are ideally suited for them, and several such systems have been developed. These systems can be categorized into two types, single chamber-based systems [133]–[139] and multichambered-based systems [140]–[151].

2.2.2.1.1 Single chamber-based LAMP devices

These devices consist of a single chamber to accomplish the LAMP assays in a microfluidic format. First, the LAMP mixture was loaded in the single chamber of a microfluidic device. Then, the isothermal temperature ranged from 60-65°C was established in the amplification chamber. A variety of devices have been developed to handle a range of sample volumes from 10 µL [135] to 25 µL [133]. The LAMP assays were amplified in a time range from 17 min [152] to 65 min [153] dependent on the amount of DNA present in samples. These devices were fabricated using the materials such as glass-PDMS [152], [153], polymethyl methacrylate (PMMA) [133], [134], [136] and polycarbonate (PC) [135], [137]. A few examples of single chamber-based microfluidic devices are shown in Figure 2.12.

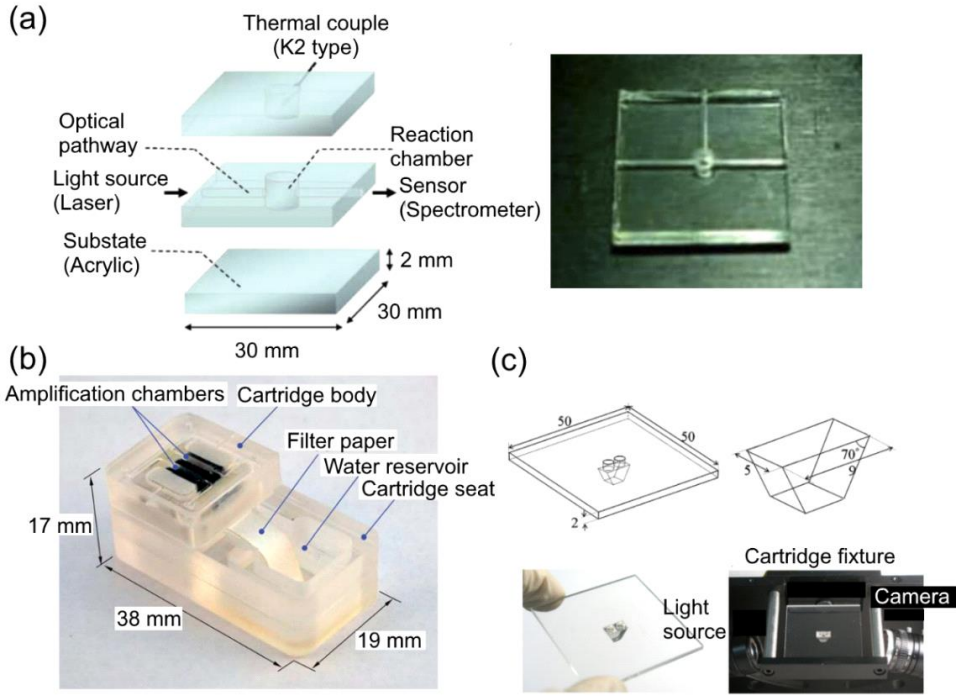

Figure 2.12 Single chamber-based microfluidic devices to perform LAMP assays. (a) Exploded view and the photograph of a single chamber-based device fabricated using the three layers of PMMA [133]. (b) A photograph of an instrument free self-heating device [136]. (c) Photograph of a prism and base apparatus of a disposable SPRLAMP sensing cartridge [135].

For instance, the microfluidic device with a single chamber was developed to handle the sample volume of 25 µL [133] as shown in Figure 2.12a. Three sheets of PMMA material were used to fabricate the microfluidic device. The *hepatitis B virus (HBV)* was used as a test model for these experiments. The lowest sample concentration of 50 copies/tube was detected by treating the sample at 65˚C for 60 min. Another microfluidic device capable of processing smaller samples of 15.6 µL has been developed [136] as shown in Figure 2.12b. The device was fabricated using the PMMA material. The Mg–Fe alloy was reacted with water to generate heat that was required for LAMP assays. The amplification chamber reached the temperature of ~ 60˚C in 10 min. The amplification temperature was maintained for 60 min. The *Escherichia coli* (*E. coli*) DNA was detected with the detection limit of 10 molecules per reaction.

Similarly, another device with a single chamber to handle a smaller volume of 10 µL has been developed [135] as shown in Figure 2.12c. The device was fabricated using the PMMA sheet with a trapezoidal shaped cavity to place the trapezoidal shaped prism fabricated by polycarbonate (PC). A thin-film heater was controlled by the PID controller used to maintain the temperature of 65˚C for LAMP assays. The *hepatitis B virus* (*HBV*) template with the minimum sample concentration of 2 fg/mL was detected using the surface plasmon resonance (SPR) system in 17 min.

2.2.2.1.2 Multi chamber-based LAMP devices

The multi chamber-based microfluidic devices are mainly divided into two categories, straight channels-based arrays [125], [126] and well-based arrays [140], [142], [145], [146], [148]–[151]. The multichambered-based design offers the advantage to perform the amplification reaction of multi-target genes in parallel.

2.2.2.1.2.1 Straight channel arrays for LAMP-based devices

Microfluidic devices have been developed to amplify multiple targeted genes in the straight channel format. The microfluidic device with the eight channels parallel to each other has been developed [141] as shown in Figure 2.13a.

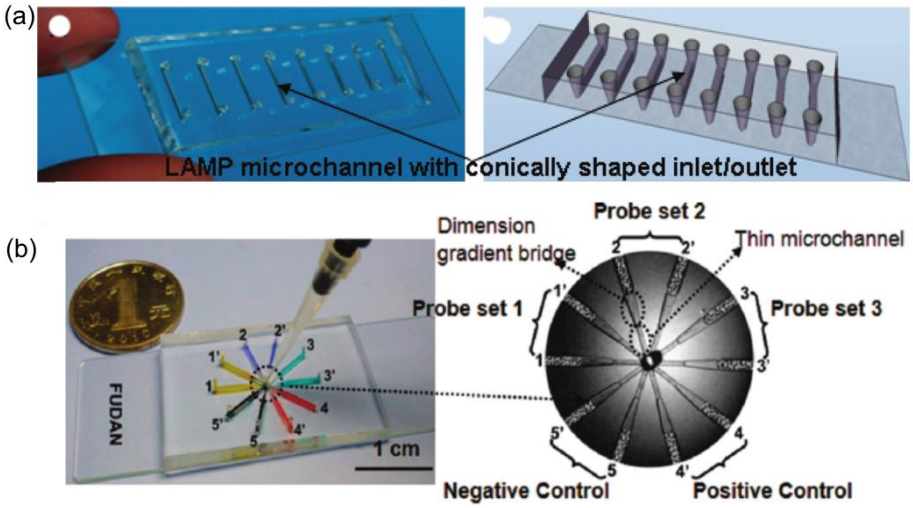

Figure 2.13 Straight channel-based LAMP systems. (a) Schematic view and a photograph of a microfluidic device with 8 microchannels [141]. (b) Photograph and structure of a microfluidic device with 10 microchambers in octopus shape [144].

The device was fabricated using glass-PDMS materials. Each channel was designed to accommodate a volume of ~ 5 µL. Inlets and outlets were designed in conical shape to avoid the trapping of gas. Samples were filled in the microchannels with the aid of capillary force. Afterwards, the uncured PDMS was poured and cured to seal the device. The laboratory water bath was used to maintain the temperature of 63˚C. The *Pseudorabies virus* (*PRV)* was detected with the detection limit of 10 fg/µL in less than 60 min.

Another microfluidic device with a higher number of microchannels (10) has been developed [144] as shown in Figure 2.13b. Microchannels were designed to make a structure like an octopus. This device was fabricated using glass-PDMS materials. The sample was loaded from the central hole, and the capillary force filled all microchannels. The device was loaded in the water bath at 63˚C for amplification. The three substrains of human influenza A and eight swine viruses were identified in 30 min with the detection limit of 10 DNA copies/µL.

2.2.2.1.2.2 Well-based arrays for LAMP-based devices

Microfluidic devices have been developed consisting the multi-chambers in the well-based arrays format. A few illustrative examples are presented in Figure 2.14.

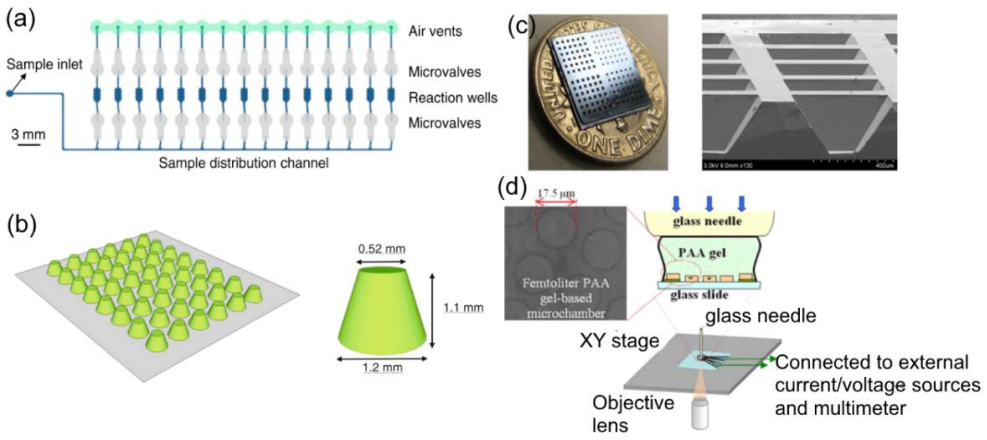

Figure 2.14 Microfluidic devices with well-based arrays for LAMP assays. (a) Schematics of a microfluidic device with 15 arrays of chambers [146]. (b) Schematics of gel-based arrays of chambers [151]. (c) Silicon-based device with well-based arrays of microchambers [142]. (d) Femtoliter sized multi chambers of PAA gel-based device [140].

The microfluidic device consisted of an array of 15 chambers has been developed [146] as shown in Figure 2.14a. Each microchamber was designed with the volume of 1 µL. Subsequently, these chambers constituted the 15 µL that was a total volume that the microfluidic system could handle simultaneously. The device was fabricated using the cyclic olefin polymer (COP) and adhesive films. This device consisted of three layers that included the lower layer having the microstructures fabricated by hot embossing. Adhesive layers made the middle and top layers. These adhesive layers contained the patterns that were made by the knife plotter. Sample was loaded from the inlet port using a pipette. The PID controller-based temperature controlling system was used to establish the amplification temperature. Several virulence and marker genes including *Salmonella, Campylobacter jejuni, Shigella, and Vibrio cholerae* were detected with the concentration up to the 10-100 DNA/ µL in 20 min.

Another microfluidic device with the higher number of chambers (48) in the format of 6×8 arrays has been developed [151] as shown in Figure 2.14b. Each microchamber consisted of a semisolid polyacrylamide gel-post. The gel-post structure was made in the conical shape with the flat top. The glass mold was prepared by drilling the holes (0.67 µL/chamber) in the glass (1.1 mm). Then, the drilled glass was bonded with another glass plate. The acrylamide gel reagents were mixed with the LAMP reaction mixture. The mixture was loaded in the chambers and sealed with the glass. The UV lamp was used to polymerize the mixture filled in microchambers. Then, the microcontroller was used to control the Peltier element to maintain the amplification temperature. The 12 genes of *Mycobacterium tuberculosis (TB)* genomes per gel post (63 fg DNA) were detected in 75 min.

Another microfluidic device with 144 microchambers in the format of 4 arrays of 6×6 chambers has been developed [142] as shown in Figure 2.14c. Microchambers were capable of handling the sample volumes of 10-30 nL. The device was fabricated using the silicon wafer with the standard microfabrication technology. The primers were dried on the surface of the chambers, and then the sample was loaded. Then, microinjector was used to load both primers and samples. Afterwards, the sample was covered with the mineral oil. Multiplex operation of the device was demonstrated by amplifying the copies of genes including *L. monocytogenes (HlyA), Stx2 (E. coli O157), InvA (Salmonella)* in 60 min.

Microfluidic device with the microchambers of a small size of 0.38 pL (diameter=17.5µm and height =1.5µm) has been developed [140] as shown in Figure 2.14d. The device consisted of glass and polyacrylamide (PAA) gel-based microchambers. The λ-DNA was amplified with a single molecule per reaction chamber in 20 min.

2.2.2.2 Droplet-based microfluidic devices for LAMP assays

The droplet-based microfluidic systems have been used to perform LAMP assays. Two approaches (Figure 2.15) have been applied that included a continuous flow of droplets and discrete controlling of droplets by digital microfluidics (DMF).

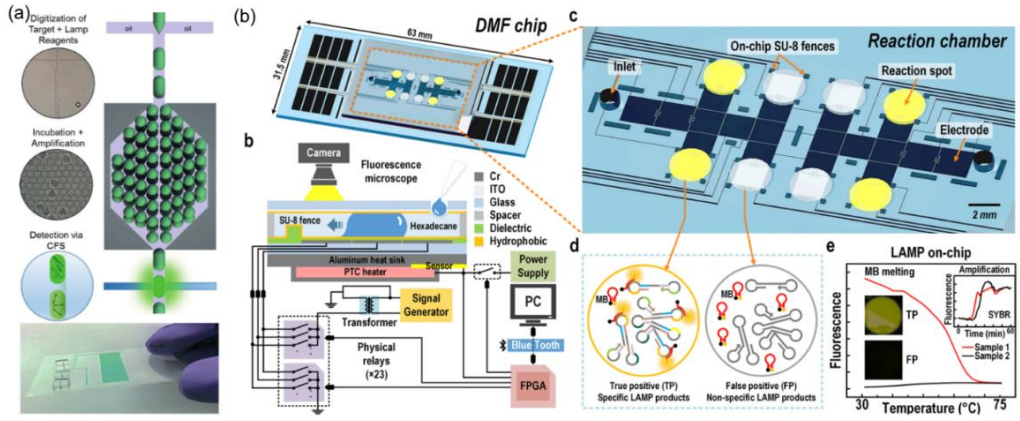

Figure 2.15 Droplet-based microfluidic systems for LAMP assays. (a) Schematics of a microfluidic device for continuous flow of the droplets-based system [154]. (b) Schematics of a digital microfluidics-based microfluidic system [155].

Microfluidics system based on the continuous flow of droplets has been developed [154] as shown in Figure 2.15a. The high-throughput droplets were generated to enhance the number of reactions those were performed at the same time. Various operations such as droplet generation, incubation, and detection were performed for LAMP assays. The device was fabricated using PDMS and glass materials. First, high-throughput droplets (10 pL) were generated at the rate of one million droplets in 110 min. Then, these droplets were transported through the incubation zone (63˚C). The Peltier heating element was used to maintain the amplification temperature in the incubation region. Afterwards, the fluorescence intensity was measured during the droplet transportation through the detection zone. The number of reactions with this design could be significantly higher but, it is difficult to integrate with the sample preparation steps. Furthermore, the use of syringe pumps makes such systems bulky.

Another approach was followed to handle the discrete droplets based for LAMP assays in the microfluidic format based on the electrowetting or digital microfluidics (DMF) [155] as shown in Figure 2.15b. The working principle of digital microfluidics is already explained in the previous section (2.2.1.4.2.1). The purified *Trypanosoma brucei* DNA was used the test model for the experiments. The reaction volume of 1 µL was used with the reduced consumption of reagents volumes (10×). On-chip unknown sample with

a concentration of 10 copies/reaction was detected. Furthermore, on-chip melting curve analysis was performed in less than 5 min which was three times faster if the melting curve analysis was conducted in the off-chip format.

2.2.3 Heating systems for LAMP assays in a microfluidic format

The LAMP assays required constant temperature for DNA amplification. Consequently, simple heating systems are needed compared to the PCR based amplification systems. The electrical and chemical methods have been used to produce the heat that required maintaining the amplification temperature.

Chemical methods of heating using the exothermic reactions to generate heat have also been used. For instance, Mg-Fe alloy which undergoes exothermic reaction on exposure to water has been used to providing heating for amplification of LAMP assays [136]. Additionally, calcium oxide (CaO) also undergoes an exothermic chemical reaction when brought in contact with the water [138] and has been used to perform an amplification reaction in PCR tubes. These exothermic chemical reactions have been used to maintain the amplification temperature of ~ 65˚C.

More often electrical heaters were used to generate heat that was required to maintain the amplification temperature (~ 65˚C). Electrical heaters convert the current that passes through the resistor element to heat. Microfluidic devices have been heated either using external heaters or on-chip integrated heater. On-chip integrated heaters were fabricated using the conventional microfabrication technologies. The various types of the external electrical heaters included the commercial flexible heaters [133]–[135], [137], [139], [145], [146], [156], heat block [152], [153], [157], water bath [141], [144], [147], thermo-electric cooler (TEC) [151], [158], [159], oven [143] and thermocycler [150]. Commercial heaters are ready-to-use heating systems, and microfluidic devices only need to be brought in contact with them. They are good to use in a lab-based setting where portability is not a concern.

Furthermore, it is difficult to get the customized size heaters and therefore creating the localized heating zone is challenging with this format of heaters. This issue was addressed by integrating the on-chip heater using the MEMS-based fabrication technology. Lam et al.[140] fabricated a microfabricated heater made of patterning a Titanium (Ti) film that was deposited on a glass substrate.

Another device capable of performing the sample preparation and DNA amplification has been developed [160], [161]. Microheaters and temperature sensors were fabricated on the glass substrate using the metals of Platinum (Pt) and Gold (Au). Metal deposition methods of e-beam and sputtering were used to fabricate the microheaters. These systems are expensive and require the sophisticated fabrication facilities. Consequently, these expansive fabrication methods make it difficult to build a low-cost system especially these fabrication facilities are difficult to build in low resource settings.

2.2.4 Detection system for microfluidic-based LAMP

DNA amplification of LAMP assays has been detected by various techniques including gel electrophoresis, naked eye detection, real-time turbidity, electrochemical detection, and fluorescence-based detection.

2.2.4.1 Gel electrophoresis

Gel electrophoresis is a technique which is used to separate DNA molecules according to their size. Negatively charged DNA stained with the dye, such as ethidium bromide, is loaded at one end of the gel. Next, an electric potential was applied, and subsequently, DNA is transported to the other side and in the process separated according to their size. Gel electrophoresis is the conventional method that was used to detect the DNA amplification. Consequently, many groups used this technique to validate their results [136], [139], [151]. Mainly, the gel electrophoresis method was used to detect the amplification assays in an off-chip format [138], [160], [161]. Electrophoretic analysis of DNA has also been integrated on-chip with the LAMP assays [162].

2.2.4.2 Naked eye detection

DNA amplification of LAMP assays has been visually detected with the naked eye without using any instruments. For instance, a chemical reaction between the deoxyribonucleotide triphosphates (dNTPs) and magnesium sulfate (Mg_2SO_4) produces magnesium pyrophosphate as a by-product. The white precipitates of magnesium pyrophosphate can be seen via naked eye. Thus, the results of an amplification reaction can be determined by either the presence or the absence of precipitate. This detection method is low-cost, and results could be determined without the use of any expensive instruments [144]. Alternatively, dyes that change color have used as an end-point detection method [159]. For instance, hydroxy naphthol blue (HNB) produces a purple colour in LAMP reaction mixture due to the presence of magnesium ions. As the amplification reaction proceeds, the concentration of magnesium ions is reduced due to the formation of magnesium pyrophosphate. Consequently, the colour of the reaction mixture is changed from purple to blue.

2.2.4.3 Real-time turbidity

Real-time turbidity measurement is one of the methods that was used to detect the DNA amplification of LAMP assays. As magnesium pyrophosphate is produced as a by-product during the LAMP amplification reaction, it increases the turbidity of the reaction mixture. There are various methods used to measure the turbidity. For instance, an optical sensor has been used to measure the real-time turbidity of LAMP assays [133], [134]. The optical sensor was also used to measure the turbidity of LAMP assays in the microchamber [141], [144].

2.2.4.4 Electrochemical detection

Electrochemical detection is another a low-cost detection method for DNA amplification. Three sets of electrodes named as working, reference, and counter electrodes were used to perform the electrochemical reaction. The electric potential was applied

between the working and reference electrode. And the current was measured between the working and counter electrode. The current was measured due to the redox reaction (reduction-oxidation) occurred between the working electrode and redox molecules. Hsieh et al. [153] have developed the single chamber-based microfluidic device for LAMP assays. The electrochemical detection method using the methylene blue (MB) was integrated for in-situ quantitative analysis of DNA amplification. Initially, more free MB molecules were available for redox reaction with the gold working electrode. Subsequently, the current was higher. DNA molecules were increased as the amplification reactions proceed later more MB molecules were intercalated with DNA.

Consequently, less number of molecules were available for redox reaction and the current was reduced that indicated the amplification of DNA. The samples were amplified with the minimum 16 copies of DNA in a reaction mixture in less than 50 min. Another redox molecule of Hoechst 33258 was used by Safavieh et al. [152].

The working and counter electrodes were fabricated using carbon. However, the reference electrode was fabricated using the Ag/AgCl. The working principle was similar as described earlier, the redox current was reduced with the increase in the number of DNA molecules as the amplification reaction proceeded. Consequently, more MB molecules were intercalated with the DNA molecules. Another microfluidic device has been developed with eight separate microchambers to perform amplification of multiplex LAMP assays [143]. The device consisted of eight working electrodes and a counter electrode, and both were fabricated using the ITO (Indium Tin Oxide) glass. A reference electrode was fabricated in the middle using the Ag/AgCl. The MB molecules were utilized as redox molecules for electrochemical detection.

2.2.4.5 Fluorescence-based detection

DNA amplification was detected in the microfluidic format by measuring the fluorescence intensity of intercalating dyes attached to double-stranded DNA. The intercalating dyes have a higher fluorescence intensity when they are intercalated within

double-stranded DNA rather than freely floating in the solution. The number of double-stranded DNA increases as the amplification reaction proceeds which intercalates with more of the dyes leading to a higher emitted intensity of light. Mainly, two approaches of end-point and real-time detection were followed for the fluorescence-based detection. Various techniques were developed to detect the end-point fluorescence level including fluorescence microscope [140], CCD camera-based system [157], and Cell phone-based system [163]. Similarly, the real-time fluorescence intensity of LAMP assays was measured using several technologies.

Fluorescence microscope was used to detect the DNA amplification by measuring the real-time in-situ fluorescence intensity of LAMP assays in the microfluidic format [142]. Other microfluidic systems have used smaller and more portable optical systems for fluorescence detection [137], [156], [164]. Recently, low-cost systems were developed using the charged-coupled device (CCD) [145], [146], [148], [151]. Finally, cell phone-based system [139] have been used that is useful in the low resource settings.

2.2.5 Integrated microfluidic devices for LAMP assays

2.2.5.1 Integrated LAMP-based devices with on-chip sample purification

Several of the sample preparation steps have also been integrated with DNA amplification in a microfabricated format. For instance, a microfluidic device has been developed to capture, concentrate and purify DNA present in the saliva samples using the membrane [156] as shown in Figure 2.16a.

The device consisted of a single chamber integrated with the Flinders Technology Associates (Whatman FTA) membrane. The purified DNA was amplified using LAMP assays in the microchamber. Initially, the saliva sample was mixed off-chip with the lysis buffer (100 µL) and loaded in the device. The membrane filtered the sample and subsequently, captured and concentrated the DNA. Then, buffer (Roche inhibitor removal)

was loaded to remove an inhibitor if it was present in the mixture. Afterwards, the washing buffer was used twice to wash the membrane. Then, LAMP reaction mixture (22 µL) was loaded in the chamber. The thin-film heater was used to maintain the amplification temperature of 60˚C in the amplification chamber. Finally, the real-time DNA amplification was performed using the LAMP assays. The in-situ DNA amplification was measured by monitoring the fluorescence intensity using the commercial optical detection system. The sample was amplified with the detection limit of 10 *human immunodeficiency virus (HIV)* particles per reaction in less than an hour. Although various samples preparation steps have been integrated on-chip, the multiple elution steps used that make this device unsuitable for the application in the point-of-care format.

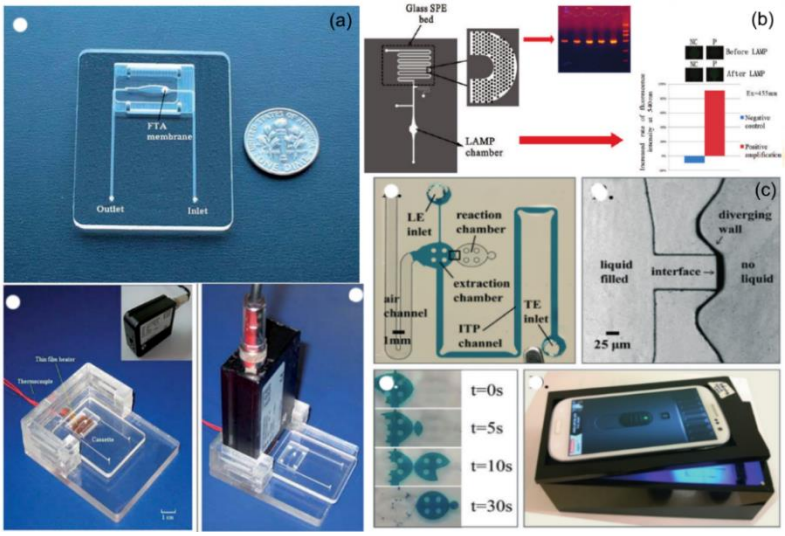

Figure 2.16 Microfluidic LAMP-based integrated device with on-chip sample purification. (a) Photographs and experimental setup for real-time detection of LAMP assays in a cassette-shaped microfluidic device [156]. (b) Schematics of glass-based (Micropillars) microdevice for DNA purification, amplification and online detection of LAMP assays [157]. (c) Photographs of a microfluidic device based on Isotachophoresis (NAIL) for extraction, amplification, and detection of DNA [163].

Next, a microfluidic device was developed for DNA extraction and online detection using the LAMP assays [157] as shown in Figure 2.16b. The device was fabricated using glass as the substrate material. It consisted of a serpentine channel with glass micropillars for solid phase extraction (SPE) of DNA. The operation of this device consisted of various

steps including the sample loading, washing, eluting, DNA amplification, and online detection. The sample was mixed off-chip with the lysis buffer, and then it was pushed (3 µL/min) into the microchannel. The micropillars were etched in microchannels to capture DNA. Microchannel was washed to remove any other contaminants after the accumulation. Then, the obtained DNA was eluted in the buffer and mixed with the LAMP reagents in the LAMP chamber. DNA was amplified by placing the device on the heat block at 65°C for 60 min.

In another instance, a microfluidic device named as NAIL (nucleic acid detection using Isotachophoresis and loop-mediated isothermal amplification) was developed [163] Figure 2.16c. The operation of a microfluidic device included the sequential steps of DNA extraction from the complex milk samples and amplification the *E. coli (O157: H7)* that was extracted using the NAIL. The device was fabricated by styrene-ethylene/butylene-styrene (SEBS) material. First, bacteria cells were lysed off-chip used the chemical method. Then, the sample and buffer were loaded in the device. The Isotachophoresis (ITP) technique was used to isolate and purify DNA. The concentrated DNA was moved into the DNA amplification chamber using a capillary valve. The LAMP reagents that were already dehydrated and stored in the amplification chamber mixes with the sample as it is pushed in. Then, the device was placed on the hot plate at 65˚C to perform an amplification reaction.

Finally, cell phone-based system was used to detect the DNA amplification by measuring the fluorescence intensity. The bacterial concentration of 10^3 CFU/mL was successfully detected in approximately an hour. Although DNA was extracted from the complex sample like milk, sample processing step of lysis was performed off-chip. Furthermore, the use of the capillary valve creates additional complication in the fabrication.

2.2.5.2 Integrated LAMP-based devices with on-chip sample preparation

Complete on-chip sample preparation combined with amplification has been implemented in a microfluidic format [161] as shown in Figure 2.17a. The sample preparation operations were performed on-chip in a single chamber using the magnetic microbead assays. This three-layered device was fabricated using the glass substrate and two PDMS layers. The glass substrate was patterned with metal for microheater and a temperature sensor. The device mainly consisted of three chambers including reagent chamber, washing buffer chamber, and cell lysis/DNA hybridization/LAMP reaction chamber. Bacterial sample along with the magnetic beads (MB) coated with specific nucleotide were loaded in the reaction chamber (Cell lysis/DNA hybridization/LAMP). Then, LAMP reagents and washing buffer were loaded in the reagent chamber and washing buffer. Initially, the reaction chamber was exposed to 95˚C for 10 min to lyse the MRSA cells. The released DNA from the cells were concentrated by hybridization with the target complementary DNA attached to the magnetic beads. A magnet was used to concentrate the beads and wash off the unwanted materials. Then, LAMP mixture was injected into the reaction chamber, and the temperature increased for amplification. A spectrometer was used to read the amplification results. The *methicillin-resistant Staphylococcus aureus (MRSA)* bacteria was detected in 60 min (Lysis: 10 min, Hybridization: 10 min, Amplification 40 min) with the detection limit of 10 fg/µL. Although the entire sample preparation was integrated, this device needed several washing steps which required storage of reagents, pumping devices as well as magnetic beads for concentration and accumulation which make it complicated to fabricate and use.

A similar design was used by another research group where they increased the throughput of the microfluidic device by performing sequential operations in the eight parallel chambers [164] as shown in Figure 2.17b. The microfluidic device was fabricated using cyclic olefin copolymer (COC) with eight chambers (10 µL/chambers). The washing buffer and LAMP reagents were loaded to the chip using the peristaltic micropump and

stepper motor. Initially, samples were mixed with the lysis buffer and magnetic beads and subsequently loaded to the microfluidic device. Then, external magnetic was placed underneath the device to hold the magnetic beads those were hybridized with the DNA. Afterwards, a washing buffer was pushed through the microchambers. Finally, LAMP reagents were loaded in the microchambers. Subsequently, isothermal amplification was performed at 65˚C for 40 min. The commercial device was used to detect the fluorescence level. The *Salmonella spp* bacteria was detected with the detection limit of 50 cells/chambers. Although parallel chambers were used to handle the samples of various concentrations simultaneously, microbeads-based assays and usage of pumps complicated the operation. Furthermore, the use of external heater and commercial detection systems make this system expensive.

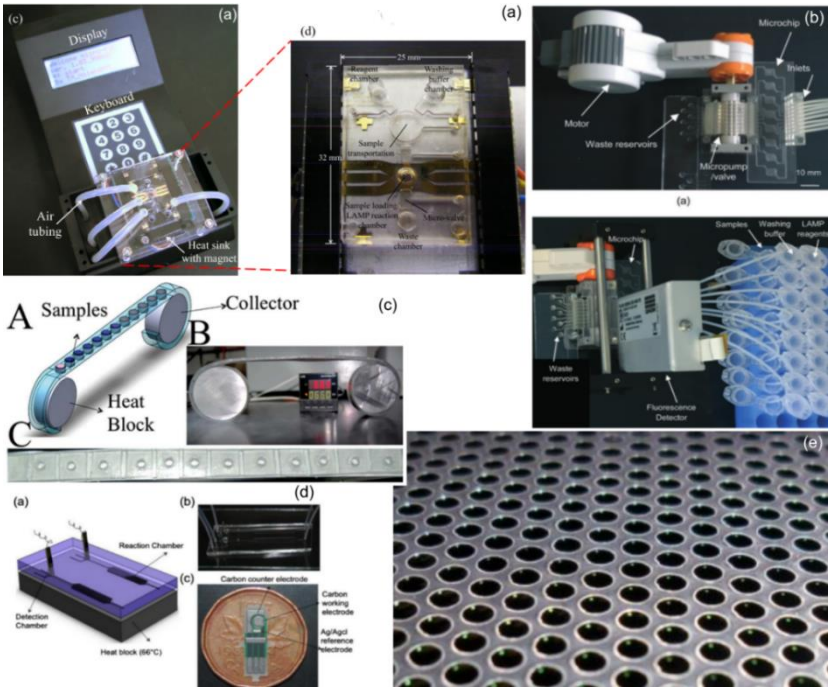

Figure 2.17 Microfluidic integrated LAMP-based devices with the sample preparation steps. (a) A photograph of the handheld microfluidic device to detect the *methicillin-resistant Staphylococcus aureus* using magnetic beads assays [161]. (b) Overview of an integrated microfluidic device with sample preparation and real-time detection [164]. (c) Schematics and photograph of a cassette-based microfluidic device with colorimetric detection [159]. (d) Schematics of a microfluidic device to detect *E. coli* using electrochemical detection [152]. (e) Photograph of a microfluidic device with arrays of microchambers to detect *E. coli* using fluorescence detection [165].

Another low-cost microfluidic device has been developed to detect bacteria using the instrument free optical detection method [159] for LAMP assays as shown in Figure 2.17c. The device was fabricated using three layers of flexible polyethylene strips. The chambers were punched in the middle piece with the volume of 35 µL each chamber. Flat flexible trips were attached on the top and bottom side using the double-sided tapes. The flexible strip was passed over the circular reels (collector) connected with the external electrical heater. Bacteria samples (5 µL) were loaded in chambers and stripped was rolled to collectors (Figure 2.17c). Samples were thermally lysed at 90˚C for 5 min. Afterwards, the chamber was rolled back from the collectors, and 20 µL of LAMP reaction mixture was added. The pipette was used to mix the reaction mixture manually and then chambers were sealed with the tape again. Then, the flexible strip was rolled back to the collector, and DNA amplification reaction was performed at 65˚C. The naked eye visually detected the DNA amplification due to the change in colour from yellow to green due to calcein. The *E. coli* and *S. aureus* bacteria were detected with the detection limit of 30 CFU/mL and 200 CFU/mL in less than one hour. The low-cost detection process was used in this format. Nonetheless, quantitative analysis was not possible due to the colorimetric based detection method. Furthermore, the opening of the chamber after the lysis is an additional step which could cause the cross-over contamination.

Microfluidic devices, as shown in Figure 2.17d, have been developed where the sample preparation was eliminated direct amplification at 66˚C was performed to combine lysis and amplification in one step [152]. The device consisted of a single chamber and fabricated with the glass and PDMS. The aluminum heat block was used to maintain the amplification temperature. The sample was loaded in the device with the syringe pump with the flow rate of 15 µL/min. Then, DNA amplification was detected using the electrochemical detection method. The *E. coli* sample was detected with the minimum sample concentration of 48 CFU/mL in 35 min.

In a different work, a microfluidic device with multi chambers was presented to detect bacteria samples only performing the amplification reaction (63˚C) [165] as shown

in Figure 2.17e. The thick polyester film was used to fabricate the device. The device consisted of an array of microchambers with the volume of 2 µL each. Bacteria cells were mixed with LAMP assays and directly loaded in the reaction chamber. A CCD camera-based system was used to detect the real-time fluorescence intensity of samples. Gram-negative (*E. coli*) and gram-positive *Enterococcus faecalis (E. faecalis*) bacteria were detected range from 10^5 to <10 CFU in about 20 min. These single chamber-based devices can detect bacteria in a single step. This method is limited in applicability to the bacteria with the stronger cell wall and requires a higher temperature for lysis.

2.2.6 Summary

This chapter provided an overview of the microfluidic technologies used for the DNA amplification. DNA amplification can be mainly divided into isothermal and non-isothermal methods both of which have been miniaturized. PCR is the non-isothermal amplification method that is most commonly used. Various microfluidic approaches were used to perform PCR amplification. These approaches included the fixed-chamber based systems, flow-through system, convective flow systems, and droplet-based systems. Loop-mediated isothermal amplification (LAMP) based systems have also been developed in the microscale as one of the isothermal amplification methods that simplify the instrumentation required. Various designs including, single and multichambered designs, droplet-based designs have been developed. A variety of heating methods and detection systems have been used which are discussed. Finally, the integrated microfluidic devices that combine cell lysis, DNA concentration, and isolation and combine it with amplification have also been developed. These devices are categorized mainly into two groups that include the devices with the off-chip sample preparation and device with the on-chip sample preparations. However, many microfluidic amplification devices have been developed with the integrated components of sample preparations. Nonetheless, more improved systems are needed to establish with least operational steps, fewer instrumentations, and low-cost customized heaters.

Chapter: 3 Electrical tweezers for control and transportation of droplets

This chapter introduces the electrical tweezer that was designed to perform various droplet-based microfluidic operations. First, design parameters of the electrical tweezer, fabrication, materials, and experimental setups are discussed. Then, the oscillatory droplet motion with the high voltage electrode of electrical tweezer, in the bi-layer oil medium, under the influence of alternating current (AC) electric field is presented. Next, the characterization of the droplet motion based on the parameters of frequency and electric potential is described. Finally, the effect of droplet volume on the oscillatory motion is studied.

3.1 Design of electrical tweezer

The electrical tweezer was designed to handle discrete water droplets mechanically. The droplet handling system mainly consisted of two components: the electrical tweezer and bi-layer oil medium. There were various parameters involved in the operation of the electrical tweezer such as dielectrophoretic force (F_{def}), electrophoretic force (F_e), drag force (F_d), inertial forces (F_i), viscosity (η) of the medium, density (ρ) of the medium, and temperature (T). Therefore, fundamental principles of electrostatics and fluid mechanics are critical in designing of the electrical tweezer system.

3.1.1 Dielectrophoretic force (F_{def})

Dielectrophoretic force (F_{def}) is exerted on polarizable particles when these particles are subjected to the non-uniform electric field during their presence in a medium which has a different conductivity compared to the particle. The dielectrophoretic force is described by the equation [166], [167].

$$F_{DEP} = 2\pi\varepsilon_m r^3 \frac{\sigma_p - \sigma_m}{\sigma_p + 2\sigma_m} \nabla E^2 \quad 3.1$$

Where ε_m is the permittivity of the medium in which droplet is suspended, r is the radius of the particle, σ_p, and σ_m are the conductivities of particles and medium. E shows the electric field strength and ∇E^2 represents the square of the electric field gradient.

Once droplet was dispensed between the electrodes in the oil medium, it experienced the dielectrophoretic force. Because water molecules were polarized, conductivities of the droplet and the medium were different ($\sigma_{droplet} > \sigma_{oil}$), and a non-uniform electric field was applied between electrodes.

3.1.2 Electrophoretic force (F_e)

The electrophoretic force is force experienced by the charged particle when particle encountered with the electric field. The electrophoretic force is given in the equation [168].

$$F_e = qE \quad 3.2$$

Where q is the charge of the particle, E is the electric field strength. The water droplet acquired a charge directly by contact with the high voltage electrodes. The droplet experienced the electrophoretic force after acquiring a charge.

The electric field strength was controlled using three parameters such as the shape of electrodes, the distance between electrodes, and the applied electric potential. First, the shape of electrodes was chosen from the two options of rod- or sheet-shaped electrodes. Although the sheet-shaped (Flat) electrodes provided a more uniform electric field between the electrodes, they made it challenging to visualize droplet and obstructed the view of the user. Additionally, sheet-shaped electrodes were challenging to manipulate especially in the confined space. Therefore, the rod-shaped electrodes were selected for use.

Second, the electric field depends upon the applied potential (Electric field=V/d) subsequently the high electric field strength can be achieved by applied the high electric

potential. The time-varying electric potential was used to keep the droplet in the confined space with the electrical tweezer.

Finally, the distance between electrodes was used to control the two parameters such as electric field strength and volume of the droplet to be handled. The small distance between the electrodes can help to generate the high electric field strength even with the low applied potential. Furthermore, electrical tweezer was used to handle the droplets of various sizes ranging from 0.2 to 25 µL. The distance of 4 to 10 mm between the electrodes was selected to handle these droplets. For instance, a fixed distance of ~ 4 mm was chosen to handle the smaller droplet volumes (0.3 µL). This spacing was sufficient for the droplet and its motions to be accommodated and analyzed at moderate applied electric potential. Bigger droplets (10-25 µL) were accommodated between the electrodes with a larger distance of 10 mm between the electrodes.

3.1.3 Drag force

This drag force was generated due to the contact between the surfaces of the moving droplet and the medium. The spherical object moving in a medium can be considered in a stroke's drag regime if Reynold's number $R_e \leq 1$. The drag force on the spherical object can be estimated using the formula [169].

$$F_d = 6\pi\eta r v \qquad 3.3$$

Where η is the viscosity, r is the radius of the object, v is the speed of a spherical object in motion. The droplet motion under the influence of the electric field had Reynold's number either Re <1 or in some instance it was Re ~1. So, stroke's drag equation can be used to estimate the drag force on the droplet. Furthermore, the viscosity of the medium can also affect the droplet motion in the oil medium. For instance, the drag force would be high if the oil medium with the high viscosity was be used.

3.1.4 Inertia force

Inertia force (F_i=ma) is significant in a situation where the droplet is accelerated from the state of rest. For instance, the droplet stopped completely when it contacted the high voltage electrode or when the droplet stopped and changed the direction of motion due to change polarity change.

3.1.5 Density of the medium

The droplet motion in the oil medium can be primarily affected by the density of the medium. For instance, the effect of gravity on the droplet motion cannot be ignored if the oil medium with the density lower than water is used. This problem was overcome by using the bi-layer of oil medium. The oil medium consisted of two oils including paraffin oil (800 kg/m^3) and fluorinert oil (1855 kg/m^3). The fluorinert oil settled at the bottom, and paraffin oil floated on the top. The water droplets (1000 kg/m^3) settled down at the interface of bi-layer oil medium.

3.1.6 Temperature of the medium

The electrical tweezer system was designed to operate either at room temperature (~25°C) or the elevated temperature (65°C). This temperature range will have a very minimal effect on the densities of both oils used as a medium. Consequently, despite small temperature effects on oil medium, the water droplet will stay at the interface of oil medium as the density of water will be in between the densities of both oils. Thus, temperature effects can be neglected for an electrical tweezer system.

3.2 Assembly of electrical tweezer

The assembly of electrical tweezer and oil medium both are shown in Figure 3.1. The electrical tweezer consisted of two parts, a holder (Component that held electrodes) and electrodes (Fingers of tweezer). The holder consisted of the bottom and top parts, and

both are shown in Figure 3.1 (a & c). These parts were fabricated with the ABS (Acrylonitrile-Butadiene-Styrene) material using the 3D printer (Dimension BST 768, Stratasys, MN, USA). The 3D printer built the components using the FDM (Fused deposition modeling) technology.

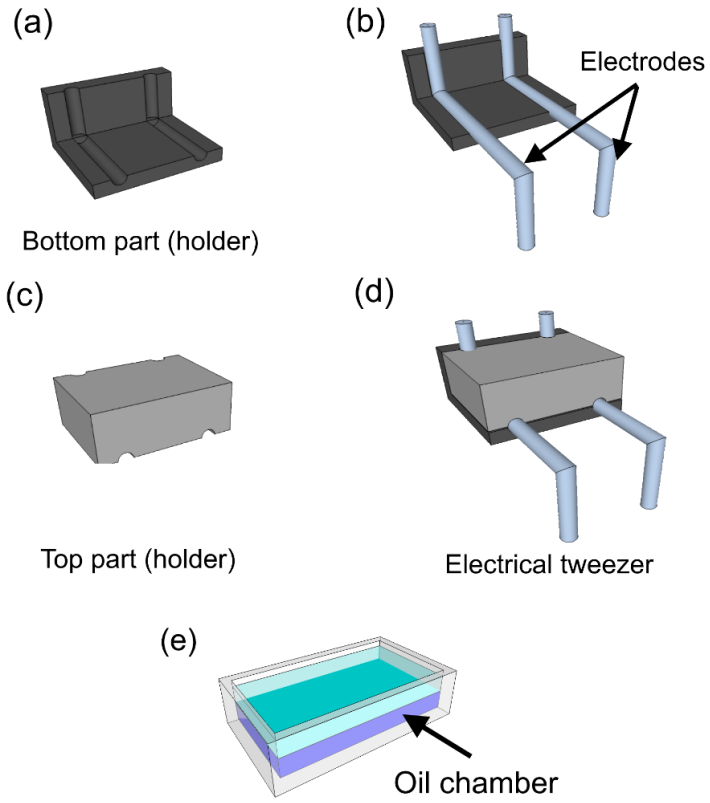

Figure 3.1 Assembly of electrical tweezers. (a) Bottom component of the electrical tweezer holder. (b) Placement of electrodes on the bottom component of the holder. (c) Top component of the electrical tweezer holder. (d) Placement of the top component and anchoring with the bottom component of a holder to complete the assembly. (e) The acrylic chamber filled with a bi-layer of oil (Paraffin and Fluorinert oil).

The stainless-steel rods were used to make the electrodes. The stainless-steel rods were mechanically bent and placed on the bottom component of the holder (Figure 3.1b). Then, the top component was placed on the lower half of the assembly (Figure 3.1d). Finally, the top component (holder) was anchored using a screw with the bottom component. Subsequently, electrodes were sandwiched between both components (Figure

3.1). The whole assembly is referred to as the "Electrical tweezer" in subsequent text. The droplet manipulation medium consisted of a bi-layer dielectric oil medium of paraffin and fluorinert oil (Figure 3.1e).

3.3 Materials and Methods

3.3.1 Experimental setup to study the droplet oscillatory motion

The experimental setup to study the oscillatory droplet motion is shown in Figure 3.2. It consisted of three primary components of the imaging system, signal generation system, and the electrical tweezer system.

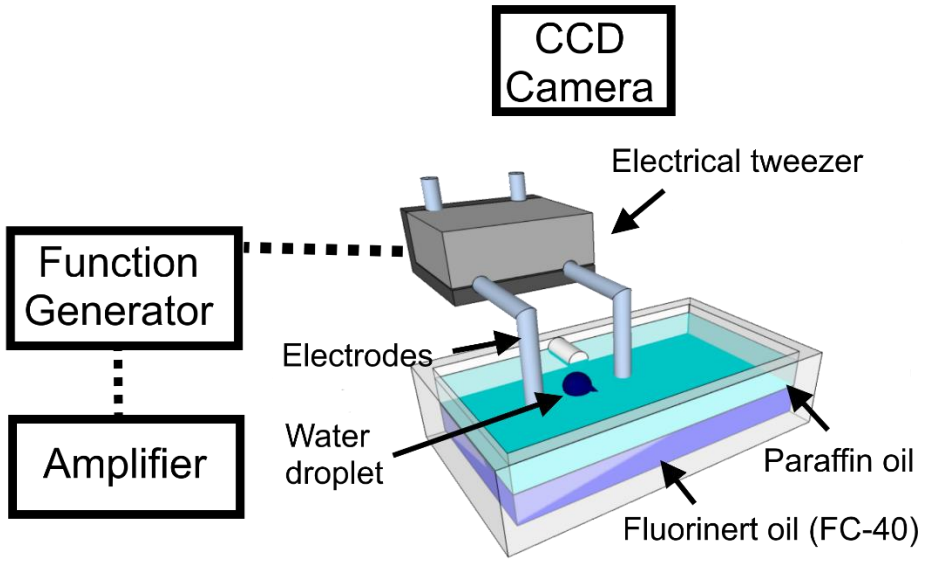

Figure 3.2 Electrical tweezer and bi-layer dielectric oil medium. Experimental setup to study the electrically influenced droplet oscillatory motion.

The imaging system was used to record the droplet motion consisted of a charge-coupled device (CCD) camera mounted on the microscope. The CCD camera (Coolpix P6000, Nikon, NY, USA) was used to record the droplet motion at a frame rate of 30 frames per second. The recorded images were analyzed by the software ImageJ (http://rsbweb.nih.gov/ij/). The signal generation unit consisted of a function generator

(AFG 3022B, Tektronix, Inc., OR, USA) and amplifier (Trek 10/10B-HS, Trek, Inc., NY, USA). The function generator generated the electrical signal for various applied electric potential at different frequencies. Then, the generated signal was amplified (Gain 1000V/V fixed) by the amplifier. One electrode of electrical tweezer was connected to the source terminal (High voltage), and the second electrode was attached to the ground terminal.

The transparent acrylic chamber was filled with the bi-layer dielectric oil medium. This oil filled chamber served as droplet handling medium. The bi-layer oil medium consisted of fluorinert oil (FC-40, 1855Kg/m^3, 3M, MN, USA) and paraffin oil (800Kg/m^3, Caledon Laboratories Ltd, ON, Canada). The fluorinert oil settled down at the bottom of the acrylic chamber, and paraffin oil floated on the top. An Eppendorf pipette was used to dispense the water droplets those quickly settled down at the interface of bi-layer of oils.

3.3.2 Image data analysis of droplet oscillatory motion

The electrically actuated droplet motion was studied by analyzing the recorded images. The CCD camera mounted on the microscope was used to record (Frame rate: 30 images per second) the oscillatory droplet motion. These recorded images were processed and analyzed by the software ImageJ. The ImageJ is a Java-based public domain software with an open architecture that was developed by the National Institute of Health (NIH). These recorded images were used to measure the droplet position with the high voltage electrode of the electrical tweezer. The droplet position in each frame was estimated by measuring the linear distance between the droplet edge and the high voltage electrode. Subsequently, the maximum distance to complete one oscillatory trip was also measured that was defined as the maximum oscillatory distance.

3.4 Droplet motion under alternating current (AC) electric field

The droplet motion in the bi-layer oil medium under the influence of ac electric field was studied. The droplet of DI water (0.3 µL) was dispensed between the probes (4

mm apart) at the interface of bi-layer oil medium. The sinusoidal electric potential (V=560 Volts, V_{Peak}/d= 140 V/mm) was applied with the frequency of 1Hz to the electrical tweezer. One electrode was connected to the source terminal (High voltage terminal). And the second electrode was grounded. The droplet motion with high voltage electrode was video graphed and presented in the image sequence format in Figure 3.3.

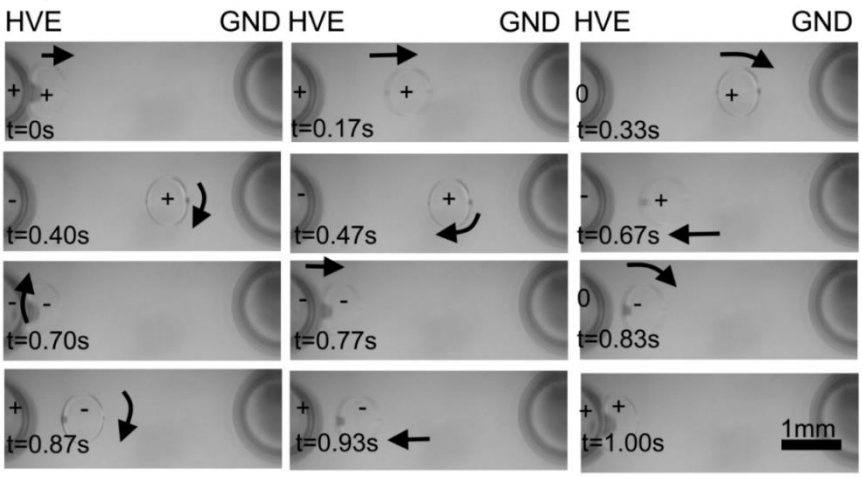

Figure 3.3 Sequential images of oscillatory droplet motion with the high voltage electrode of electrical tweezer (Electrodes 4 mm apart) for the ac applied potential of 560 Volts (V_{Peak}/d= 140 V/mm) at 1 Hz.

Initially, droplet travelled towards the high voltage electrode possibly because of one of the two mechanisms. First, the polarized molecules of water droplet experienced the dielectrophoretic force in the oil medium. Subsequently, the droplet moved slowly towards the high voltage electrode. Secondly, the droplet may acquire some charge from the pipette tips during the dispensing [170], and this charged droplet moved towards the high voltage electrode due to electrophoretic force.

The droplet performed an oscillatory motion with the high voltage electrode under the influence of ac electric field. The droplet completed two oscillatory trips for one frequency cycle of applied electric potential. These oscillatory trips were named as large oscillatory trip and short oscillatory trip in the subsequent text. Upon contact (At t = 0s), the droplet acquired a charge positive or negative depending on the polarity of the electrode

at that instance and subsequently, the charged droplet was accelerated away from the high voltage electrode (at t = 0.17s). The droplet was accelerated due to the electrophoretic force ($F_e = qE$) of repulsion between the similar charges.

Then, the droplet stopped (At t = 0.40s), and its motion was reversed (At t = 0.47s) towards the high voltage electrode without contacting the grounded electrode. This phenomenon occurred because the polarity was reversed. Then, the droplet moved back towards the high voltage electrode due to the electrophoretic force of attraction between the electrode and droplet. The droplet completed a large oscillatory trip by contacting the high voltage electrode (At t = 0.70s). Then, droplet once again accelerated away from the high voltage electrode (At t = 0.77s) to complete the shorter oscillatory trip. Upon contact, the droplet was discharged and acquired a charge similar to the high voltage electrode. Then, the droplet was accelerated due to the similar charges between the electrode and the droplet. Next, droplet stopped (At t = 0.87s) and accelerated (At t = 0.93s) back towards the high voltage electrode. Droplet completed the shorter oscillatory trip with the high voltage electrode (At t = 1s). The polarity of the high voltage electrode was switched, and the droplet was in the vicinity of high voltage electrode. The electrophoretic force of attraction accelerated the droplet back toward the high voltage electrode. Subsequently, droplet completed the short oscillatory trip with the electrode.

The droplet position in each frame was measured reference to the high voltage electrode and plotted for the one frequency cycle of the applied electric potential and shown in Figure 3.4a.

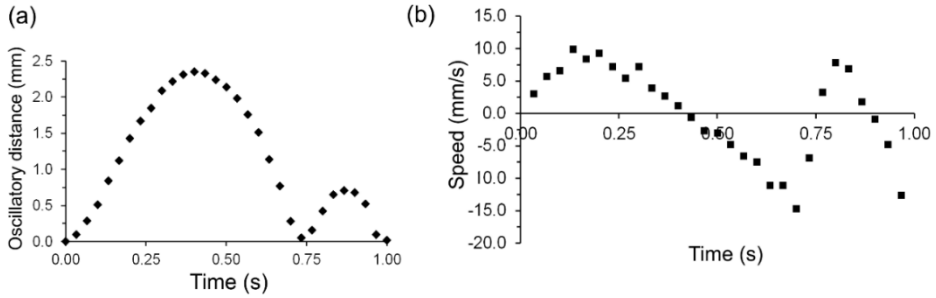

Figure 3.4 Droplet oscillatory motion with the high voltage electrode under the applied electric potential of V = 560 Volts (V_{peak}/d=140 V/mm) at 1Hz. (a) The distance of the droplet with a high voltage electrode. (b) Droplet speed during the oscillatory motion with the high voltage electrode.

The droplet completed two oscillatory trips, large and short oscillatory trips, with the high voltage electrode under the same electrical conditions as described before. The droplet maximum travelled distance was bigger for the large oscillatory trip compared to the short oscillation trip during the oscillatory motion with high voltage electrode. The droplet travelled the maximum distance of 2.35 mm and completed large oscillation trip in 0.73 s. And the maximum travelled distance and time were reduced to 0.71 mm and 0.27 s during the short oscillation trip.

The droplet speed during the oscillatory motion with the high voltage electrode was also plotted for the one frequency cycle (Figure 3.4b). The droplet moved rapidly (~15 mm/s) for small instance as it is approaching the high voltage electrode. The Reynolds number was highest at this moment under these operational conditions. Subsequently, the droplet experienced the high drag force. The droplet speed reduced as it moved away from the electrode consequently the drag force was reduced. The Reynolds number reduced with the decrease in speed (Re<1). Eventually, the drag force became zero (F_d=0) when the droplet stopped (v=0). Now, the electrical forces needed to overcome the inertia force to move droplet from the state of rest.

The numerical simulation was performed using COMSOL Multiphysics. These results were used to explain the phenomenon of the second short oscillatory trip with the high voltage. The temporal electric field was plotted between the two electrodes. The

results of the numerical simulation are shown in Appendix B. Then, the applied electric potential and the electric field strength corresponding to the droplet location at that instant was plotted over time on the same graph (Figure 3.5).

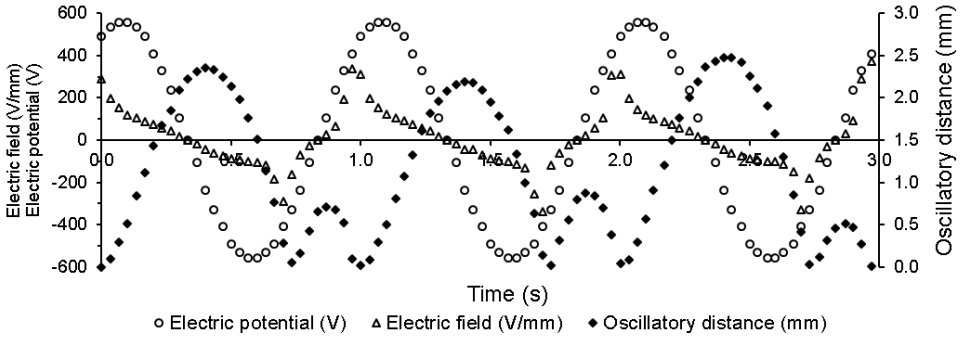

Figure 3.5 Droplet (0.3 µL) oscillatory motion with the high voltage electrode under the influence of a sinusoidal electric potential (V = 560 Volts, V_{Peak}/d=140 V/mm) at 1 Hz. The droplet oscillatory motion synchronized with the applied sinusoidal voltage and electric field (Results of a numerical simulation). Applied sinusoidal electric potential (○); sinusoidal electric field (Δ); and Oscillatory distance (◊).

The electric field strength at any particular location between the electrodes depends on the instantaneous applied electric potential and its location between the electrodes. For instance, at t = 0 s droplet is in contact with the high voltage electrode. The applied sinusoidal potential is ~ 490 Volts (peak), and the electric field strength is ~ 288 V/mm at that instance. It can be seen that the motion of the droplet closely tracks the electric field intensity and its direction at that particular location where it is present. The oscillatory droplet motion starts at the electrode surface where the electric field intensity is high and moves at high speed. As it moves away, the electric field intensity reduces both due to the change in the magnitude of the applied electric potential as well as due to the distribution of the field between the electrodes. Eventually, the electrical potential and the field change direction, which leads to a reversal in the direction of motion of the droplet. It arrives back at the electrode, makes contact, acquires charges once again and gets repelled from the electrode leading to the subsequent secondary oscillatory trip. The secondary motion also follows the direction and intensity of the electric field. The synchronous plotting of the

electric field and the position of the droplet demonstrates that the complex primary and a secondary oscillatory droplet motion is a result of temporal and spatial variation of the electric field encountered by the droplet.

3.4.1 Frequency dependent oscillatory trips

Experiments were conducted to study the number of oscillatory trips corresponding to the frequency of the applied signal. The droplet (0.3 µL) was dispensed between the electrodes (4 mm apart) at the interface of bi-layer oil medium. The applied electric potential of V = 560 Volts (V_{Peak}/d = 140 V/mm) with frequencies in the range of 1-5 Hz was used. The sequential images of droplet motion under these conditions show the frequency dependent number of oscillatory trips. (Appendix A). The number of oscillatory trips was found to increase with the increase in the frequency. The droplet completed one large and one short oscillatory trip for 1 Hz. The oscillatory trips were increased to five large and five short with the increase in frequency to 5 Hz. The effect of the frequency on the oscillatory droplet motion is shown in Figure 3.6.

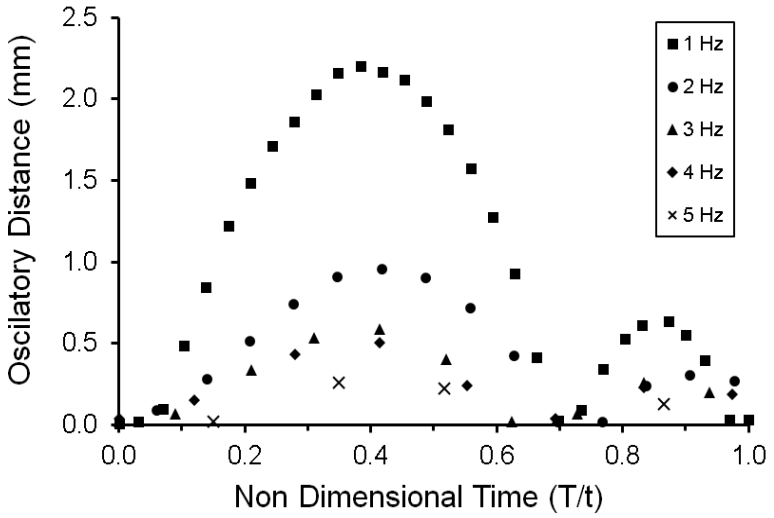

Figure 3.6 Effect of the non-dimensional time of the range of frequencies (1 to 5 Hz) of applied sinusoidal electric potential (V = 560 Volts: V_{Peak}/d = 140 V/mm) on the droplet (0.3 µL) oscillatory motion with the high voltage electrode.

The x-axis in this figure shows the non-dimensional time that was obtained by dividing the actual time (T) with the time period (t) of the applied signal. This non-dimensional time shows the effect of frequency alone on the droplet oscillatory motion. It can be seen that over the range of frequencies 1 to 5 Hz oscillatory motion of droplet was observed. The droplet followed the similar oscillatory behavior for all frequencies. Droplet completed two oscillatory trips (large and short) for each cycle of the applied electric potential.

3.4.2 Effect of electric potential and frequency on the droplet oscillatory motion

Here, the effect of electric potential and frequency on the droplet oscillatory motion was investigated. The droplet (0.3 µL) was dispensed in the bi-layer oil medium between the electrodes (4 mm apart). The droplet motion was tested for the range of frequencies 0.3-100 Hz and electric potentials (400-800 Volts, V_{peak}/d=100-200 V/mm). The effect of electric potential (480, 640, and 800 Volts, V_{peak}/d=120, 160, and 200 V/mm) on the droplet oscillatory motion at 2 Hz is demonstrated in the sequential images formant as shown in Figure 3.7. The forward motion of droplets during the large oscillation trip is only presented. These images qualitatively show that the maximum travelling distance was reduced with the decrease in applied electric potential from 800 to 400 Volts. (V_{Peak}/d=200 to 100 V/mm).

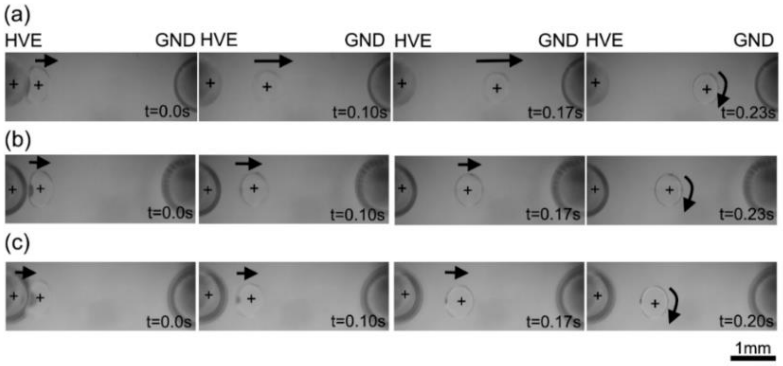

Figure 3.7 Sequential images show the effect of applied electric potential alone on the droplet (0.3 µL) oscillatory motion under the influence ac electric potential. (a) 800 Volts (V_{Peak}/d=200 V/mm), (b) 640 Volts (V_{Peak}/d=160 V/mm), and (c) 480 Volts (V_{Peak}/d=120 V/mm) at 2Hz.

Next, the effect of frequency on the droplet oscillatory motion was qualitatively investigated. The electric potential of 640 Volts (V_{Peak}/d=160 V/mm) at various frequencies (1, 3 and 5 Hz) was applied. The forward motion of droplet during the large oscillatory trip is presented in the sequential images format (Figure 3.8)**.** These images demonstrate that the maximum oscillatory distance was reduced with the increase in frequency from 1 to 5 Hz.

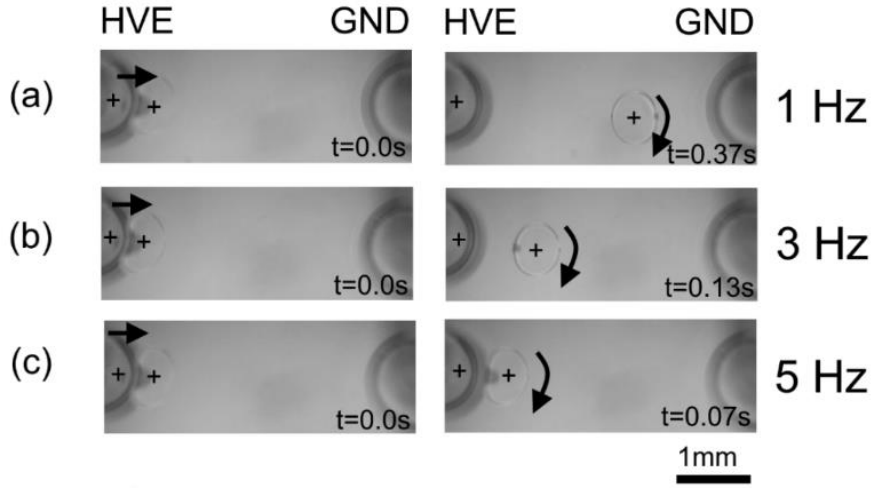

Figure 3.8 Sequential images show the effect of frequency (1 to 5 Hz) on the maximum oscillatory distance during the droplet (0.3 µL) motion with the high voltage electrode for the applied electric potential of 640 Volts (V_{Peak}/d=160 V/mm).

The maximum distance of the droplet was plotted for various applied electric potential and frequencies are shown in Figure 3.9.

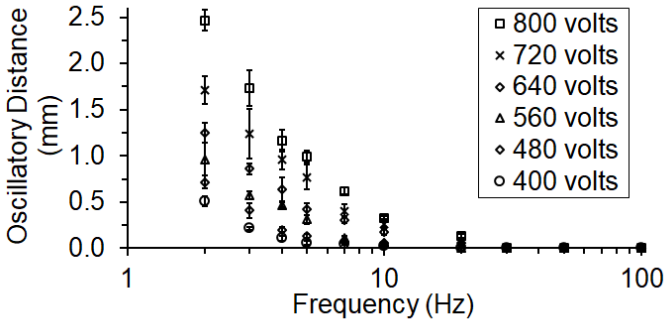

Figure 3.9 Characterization of the droplet (0.3 µL) motion with the high voltage electrode. The maximum oscillatory distance of water droplet with the high voltage electrode tested for the range of frequencies (2-100 Hz) and applied maximum sinusoidal electric potential (400-800 Volts, V_{peak}/d=100-200V/mm).

The maximum oscillatory distance was found to increase with the increase in the applied electric potential for the range of tested frequencies. For instance, when the applied electric potential was increased from 400 to 800 Volts (V_{Peak}/d = 100 to 200 V/mm) at a frequency of 2 Hz, the maximum oscillatory distance of droplet correspondingly increased from 0.51 mm to 2.47 mm. This oscillatory distance was increased because the electrophoretic force of repulsion ($F_e = qE$) between the electrode and droplet was higher for the high applied electric potential in comparison to low applied electric potential. This higher electrophoretic force of repulsion is the main reason for the extent of displacement of the droplet from the electrode.

However, for any applied electric potential, the maximum oscillatory distance of droplet was found to decrease with the increase in the frequency. For instance, when an electric potential of 800 Volts (V_{Peak}/d = 200 V/mm) was applied, and the frequency of the signal decreased from 2 to 10 Hz, the maximum oscillatory distance correspondingly decreases from 2.47 mm to 0.33 mm. This decrease in the distance is because the change of the polarity of the high voltage electrode occurs rapidly with the increase in the

frequency. This rapid change reduces the maximum travelling distance of the droplet in one cycle.

The maximum oscillatory distance did not change linearly with the change in the applied electric potential or frequency. The electric field strength was stronger near the high voltage electrode and weakened non-linearly away from the high voltage electrode. This non-linear distribution of the electric field between the electrodes resulted in the non-linear change in the oscillatory distance.

The droplet motion was grouped into the different modes based on its response to the applied electric potential and frequency. The droplet motion was tested for the range of applied electric potential from 400 to 960 Volts (V_{Peak}/d: 100 - 200 V/mm) for the range of frequency 0.1 to 50 Hz. The droplet motion was grouped into three modes: attachment; oscillation; and detachment. The sequential images of the three modes are shown in Figure 3.10.

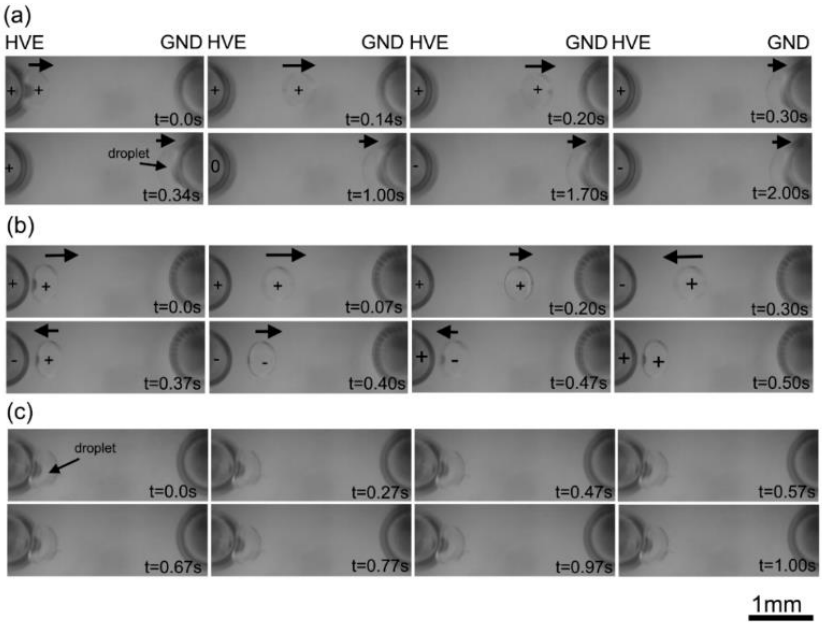

Figure 3.10 Sequential images exhibit the droplet (0.3 µL) mods under the influence of the tested range of electric potential (400-960 Volts, V_{Peak}/d=100-240 V/mm) and frequencies (0.1-1000 Hz). (a) Detachment: droplet failed to perform the oscillatory motion. (b) Oscillation droplet performed the oscillatory motion. (c) Attachment: droplet was immobilized with the high voltage electrode.

In the detachment mode, it was observed that the droplet did not return to the high voltage electrode after it was accelerated away from it (Figure 3.10a). For instance, when the droplet was exposed to 640 Volts (V_{Peak}/d: 160 V/mm) at 0.5 Hz. The droplet acquired a charge and accelerated away from the high voltage electrode. The droplet traversed the entire gap between the electrodes before the field was switched and contacted (At t = 0.3s) the grounded electrode where it was discharged. Subsequently, the droplet remained at the ground electrode or is left behind if the electrodes were in motion. For the successful operation of electrical tweezer, detachment mode needed to be avoided.

In the oscillatory mode, the droplet was found to perform periodic oscillations with the high voltage electrode after the initial contact with it. As shown in Figure 3.10b, the droplet contacted and directly acquired a charge (At t = 0.0s) from the high voltage electrode. The droplet accelerated away from the high voltage electrode (at t = 0.07s) and turned back towards the high voltage electrode upon the reversal of polarity (t = 0.30s). Then, droplet contacted the high voltage electrode (At t ~ 0.37s) and similarly completed a short oscillatory trip with the high voltage electrode (at t = 0.50s). In the attachment mode, the droplet was immobilized with the high voltage electrode after it contacted with it (Figure 3.10c). The electric potential of 640 Volts (V_{Peak}/d: 160 V/mm) at 50 Hz frequency was applied. The modes of droplet motion were plotted on an operating space diagram using the applied electric potential and frequency (Figure 3.11).

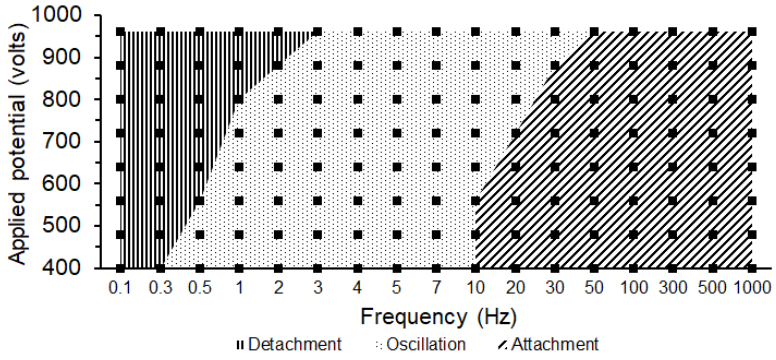

Figure 3.11 Characterization of the droplet (0.3 µL) oscillatory motion with the high voltage electrode under the tested range of frequencies (0.1-1000 Hz) and applied maximum sinusoidal electric potential (400-960 Volts, V_{Peak}/d: 100-240 V/mm).

The droplet motion was in the detachment mode at low frequencies. For instance, when an electric potential of 560 Volts (V_{peak}/d=140 V/mm) at 0.3 Hz was applied the droplet subsequently was in the detachment mode. Where it quickly attached itself to the ground electrode and discharged any charge it had acquired. Consequently, the droplet did not perform the oscillatory motion.

The detachment mode can be avoided by increasing the frequency at any applied potential. For instance, the droplet was in the oscillation mode when the frequency was increased from 0.3 to 1 Hz. And the droplet performed oscillatory motion successfully in the oscillation mode. Second, if the applied potential is increased at any frequency droplet can be again in the detachment mode. For instance, as the applied potential was increased from 560 to 960 Volts (V_{peak}/d=140 to 240 V/mm) at 1Hz subsequently droplet was in the detachment mode.

In the detachment mode, the polarity switched on the high voltage electrode very rapidly that, droplet did not get time to leave the electrode. And the droplet mechanically failed to respond to the high voltage electrode. Consequently, the droplet was immobilized with the electrode. For instance, when the frequency was increased from 1 to 10 Hz at the applied potential of 560 Volts (V_{peak}/d=140 V/mm) the droplet was in the attachment mode. The droplet could be in the oscillation mode when the electric potential was increased at any frequency. For instance, the droplet was in the oscillation mode when the applied potential was increased from 560 to 960 Volts (V_{peak}/d=140-240 V/mm) at 10 Hz. The droplet was in the attachment mode for all applied potentials beyond the 50 Hz. The detachment mode was useful for droplet transportation.

3.4.3 Effect of volume on the droplet oscillatory motion

The droplet volume is also an essential factor to characterize and optimize the operational conditions for electrical tweezer. The droplets of various volumes (0.2, 2, 10 and 20 µL) were tested for the applied electric potential of 1600 Volts (V_{Peak}/d = 160 V/mm)

at 2 Hz. The electrical tweezer with the electrodes ~ 10 mm apart were used in this study. The sequential images of droplet motion of various volumes are presented in Figure 3.12.

It can be observed that the shape of large droplet changed in response to the electric field strength. The droplet elongated towards the high voltage electrode where the electric field strength was high. While the droplet maintained circular shape in the middle section between the electrodes as the electric field strength was low in that region, the spherical shape of a droplet (10 µL) in the middle section between the electrodes at t = 0.20 s subsequently, elongated as it was near the high voltage electrode (at t = 0.33 s) as shown in Figure 3.12c. In contrast, the smaller droplets (0.2 & 2 µL) maintained their shape even in the zone with the stronger electric field.

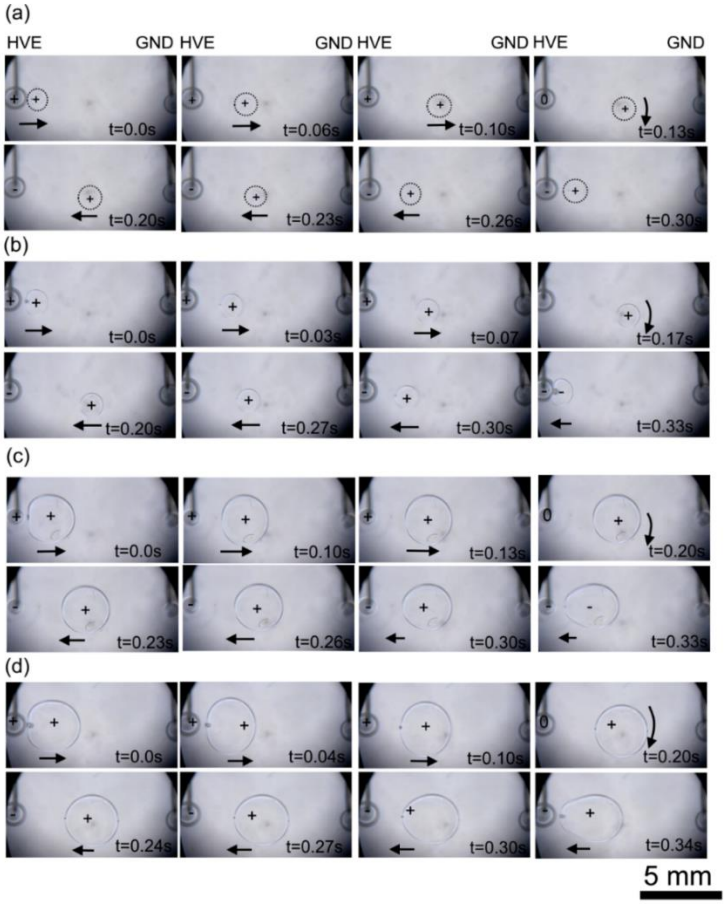

Figure 3.12 Sequential images of droplet oscillatory motion for 1600 Volts (V_{Peak}/d = 160 V/mm) at 2 Hz for the various droplet volumes. (a) 0.2 µL, (b) 2.0 µL, (c) 10 µL and, (d) 20 µL.

These results were quantified and plotted in Figure 3.13**.** The smaller droplets travelled larger distance compare to the large droplets. For instance, the droplet (2 µL) travelled the average distance of 3.87 mm while the droplet (20 µL) travelled the average distance of 2.27 mm. The forces such as drag force and inertia forces are important to explain the effect of volume on the oscillatory droplet motion. The drag force increased with the radius of the droplet. For instance, the droplet of 20 µL experienced the large drag force during the motion compared to the droplet of 2 µL.

Furthermore, inertial forces were significant the moment droplet was accelerated from the state of rest. The droplet of large volume requires a large force to accelerate it from the state of rest. Subsequently, the large droplet travelled the small distance. The smaller droplet travelled the large distance mainly due to the smaller inertial mass. Thus, droplet size has an essential role in determining the effective operation of electrical tweezer in all modes.

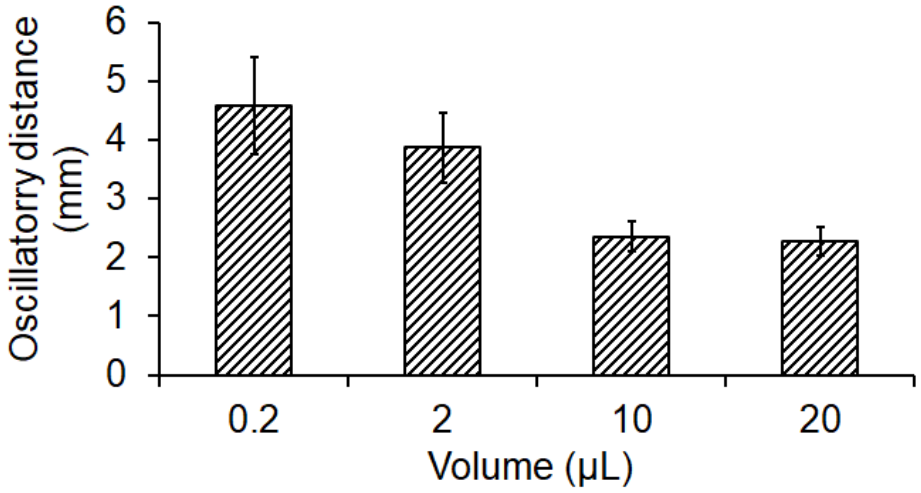

Figure 3.13 Effect of droplet volumes (0.2, 2, 10, 20 µL) on the maximum oscillatory distance during the droplet motion under the electric potential of 1600 Volts (V_{Peak}/d = 160 V/mm) at 2 Hz.

3.5 Summary

In this chapter, the fundamental physics behind the oscillatory droplet motion was analyzed. Initially, the design, fabrication, and assembly of electrical tweezer were presented. The droplet performed the oscillatory motion with the high voltage electrode of electrical tweezer under the influence of electric potential (AC). The droplet motion was characterized for the applied electric potential and frequency. Subsequently, droplet motion was characterized into the three modes of detachment, oscillation, and attachment. Finally, the effect of droplet volume on the oscillatory motion was studied.

Chapter: 4 Applications of electrical tweezer

This chapter describes the applications of the electrical tweezer technology that was developed in the previous chapter. Initially, the electrical tweezer was used to exhibit droplet-based basic microfluidic operations. Subsequently, some of these operations were combined to perform an isothermal amplification assay. In the first section, the use of electrical tweezer to perform the basic droplet-based microfluidic operations such as transportation, extraction, and merging is demonstrated. In the beginning, the experimental setup for droplet-based unit operation is discussed. Then, each unit operation is qualitatively discussed using the sequential images. Next, the unit operations of transportation and extraction are characterized. In the second section, the application of the electrical tweezer for the loop-mediated isothermal amplification (LAMP) assays is presented. First, the experimental setup and LAMP assays used are presented. Finally, the amplification of LAMP assays is demonstrated using the electrical tweezer.

4.1 Electrical tweezer for droplet-based microfluidic unit operations

4.1.1 Experimental setup for droplet-based unit operations

The experimental setup (Figure 4.1) that was used to demonstrate the droplet-based microfluidic unit operations mainly consisted of three units; (1) Droplet oscillatory unit; (2) Droplet transportation unit; and (3) Droplet extraction unit.

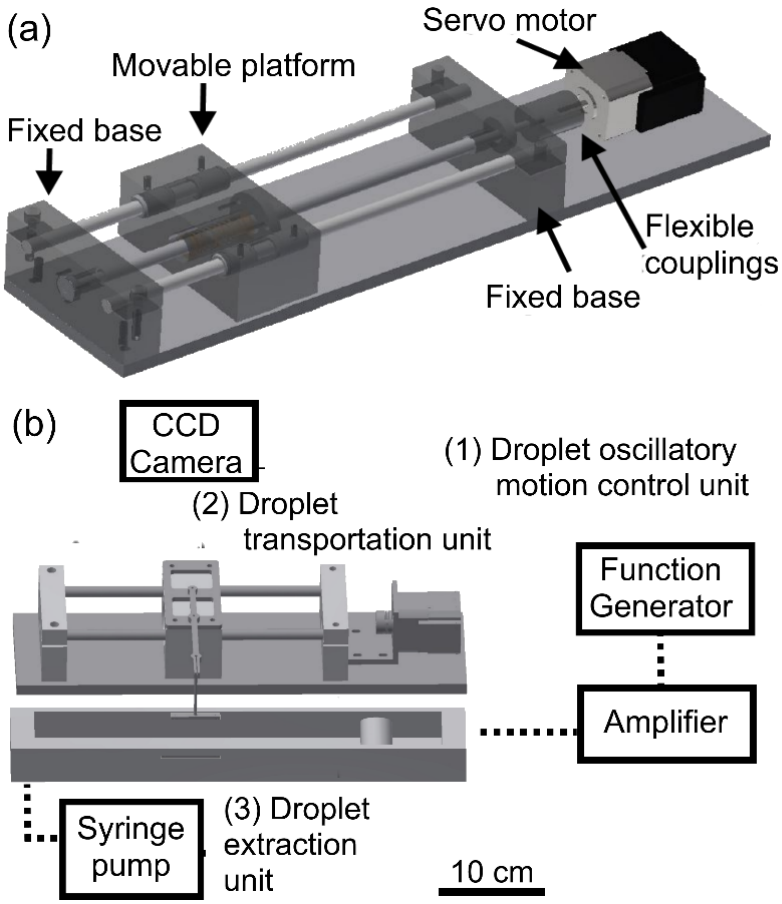

Figure 4.1 The linear motorized stage for droplet transportation. (b) Experimental setup to study the droplet-based microfluidic unit operations of transportation and extraction.

The operation of the oscillatory droplet unit was already mentioned in the previous chapter (Section 3.4). The droplet transportation unit consisted of the electrical tweezer mounted on the linear motorized stage. The linear motorized stage was fabricated in-house using the machine shop facility. The structural body of the stage was fabricated by machining the Aluminum metal. The linear stage was powered by the servo motor (Model: QCI-17-3-E-01, Quicksilver Controls, Inc., CA, USA). The software of servo motor (Quick control) was used to control the linear motion. The electrical tweezer was mounted on the movable platform to demonstrate transportation, and it was characterized at various speeds.

The droplet extraction unit consisted of a syringe pump, a capillary glass tube and acrylic chamber filled with bi-layer oil. The capillary glass was positioned at the interface of bi-layer oil medium. The syringe pump pushed the water through the glass capillary at the interface of bi-layer oil medium. Finally, electrical tweezer was used to detach the droplet from the tip of the glass capillary tube. The syringe pump was only used to dispense water for droplet extraction experiments. While for all other experiments pipette was used to dispense the water droplets at the interface of the bi-layer of oil.

4.1.2 Droplet transportation

The electrical tweezer was used to transport the droplet in bi-layer dielectric medium. First, the droplet (0.3 µL) was dispensed at the interface of bi-layer oil medium between the electrodes (4 mm apart). The electric potential of 480 Volts (V_{Peak}/d = 120 V/mm) was applied at the frequency of 3 Hz. Then the electrical tweezer moved mechanically along the Y-axis at a defined speed. The droplet transportation is shown in sequential images format (Figure 4.2).

The sequence of images shows two kinds of motion. The droplet back and forth motions with the tweezer due to the electric field. Secondly, the droplet is also transported in the y-direction with the electrical tweezer.

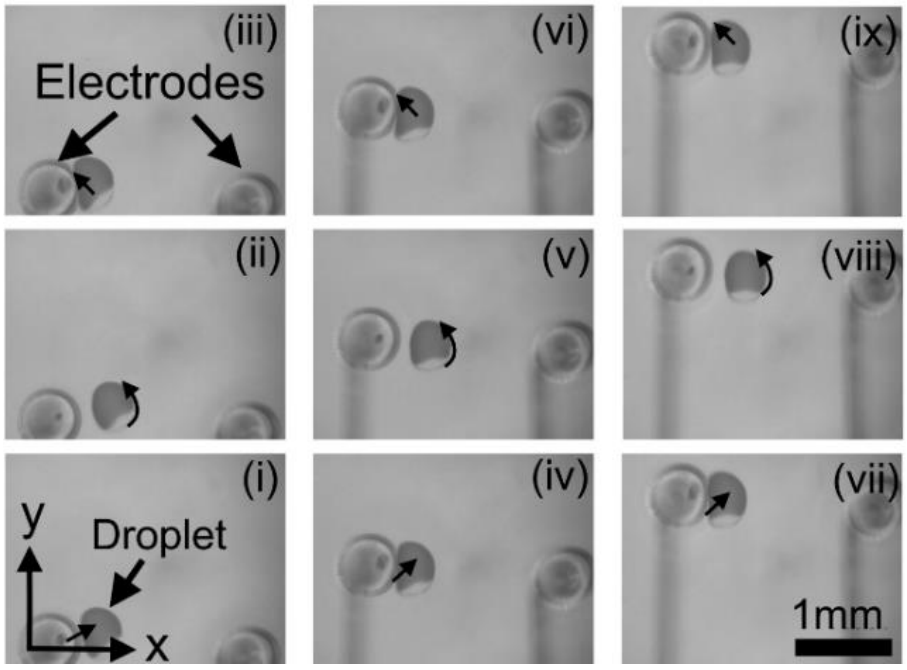

Figure 4.2 The sequential images illustrate the droplet (0.3 µL) transportation by the electrical tweezer (Electrodes 4 mm apart) under the 480 Volts (V_{Peak}/d = 120 V/mm) at 3 Hz. Meanwhile, the droplet also performed the oscillatory motion with the high voltage electrode.

Initially, the droplet contacted the high voltage electrode and acquired a charge from it (At t = 0s). Afterwards, the charged droplet initiated oscillatory motion and completed the trip by contacting again with the high voltage electrode (At t = 0.33s). The electrical tweezer was moved at speed ~3 mm/s in the y-direction. Consequently, the oscillating droplet followed the electrical tweezer during its forward motion (t = 0.33 to 9.03s). The electrophoretic force between the droplet and high voltage electrode kept the droplet in the vicinity of the electrode during the transportation.

4.1.2.1 Characterization of the droplet transportation

The droplet transportation was experimentally characterized by studying the effect the frequency of applied potential on the droplet transportation speed while maintaining the same applied electric potential.

The droplet transportation was characterized by using the 5 µL volume of water (Typical volume used in microfluidic operations) placed at the interface of bi-layer oil medium between the electrodes (10 mm apart). The electric potential of 2000 Volts (V_{Peak}/d = 200 V/mm) for various frequencies (5 to 1000 Hz). The droplet response was analyzed and characterized during droplet transportation for the distance ~20 cm at various speeds (Up to 25 mm/s), and results are shown in Figure 4.3

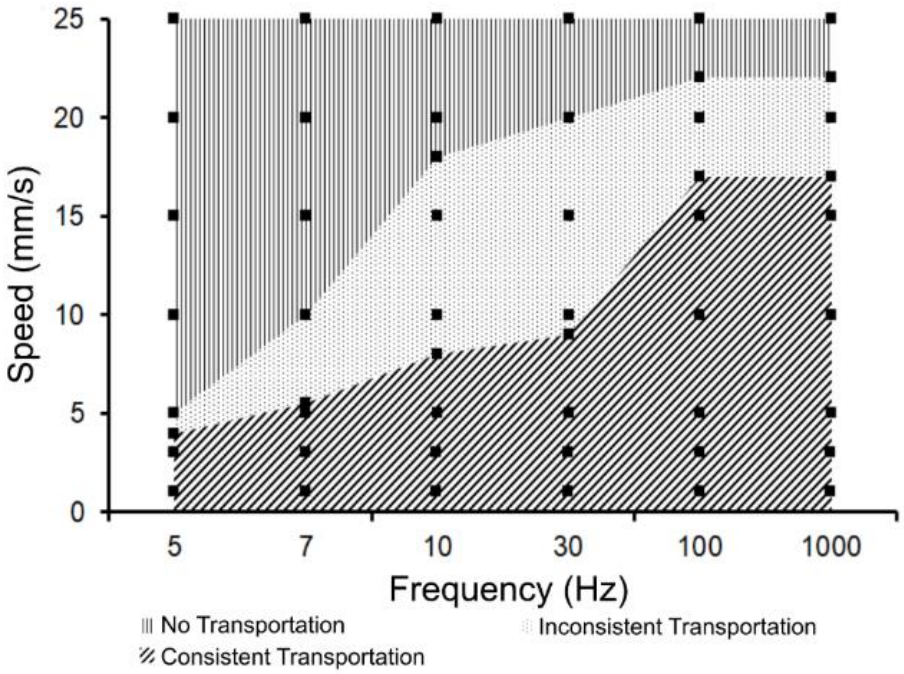

Figure 4.3 Characterization of the droplet (5 µL) transportation with the electrical tweezer under the applied potential of 2000 Volts (V_{Peak}/d = 200 V/mm) at various frequencies (5 to 1000) was categorized into three zones. a) No transportation. b) Inconsistent transportation. c) Consistent transportation.

At low speeds (Speed < 4 mm/sec), the droplet was found to move along with the electrode consistently for all frequency even in the oscillating regime without the contact of the electrical tweezer. As the speed of the tweezer motion was increased, a higher frequency was required to ensure consistent transportation. For instance, at a speed of 15 mm/s, an applied frequency of 100 Hz was needed to hold the droplet in the tweezer grip as it was being transported. A low frequency of 30 Hz resulted in the inconsistent

transportation where the droplet was sometimes attached to the tweezer and was transported while in other instances it was not. At low frequencies such as 7 Hz, the droplet was consistently left behind as the tweezer was moved.

The maximum speed with which the tweezers was moved while still consistently transporting the droplet was found to be ~15 mm/s. Beyond 22 mm/s the droplet was almost always left behind even at high frequencies beyond 1000 Hz. The behaviour of the droplet can be understood by analyzing the forces that act on it. During the transportation, droplet experienced both attractive and resistive forces. Electrophoretic forces of attraction served to keep the droplet oscillating between the electrodes and transported it along with the tweezer while the inertia, as well as the drag force on the droplet, forced it to remain behind. When the electrophoretic force was significantly larger than the inertia and the drag force, the droplet tends to be consistently transported with the tweezer. When the frequency was low, the distance that the droplet travelled away from the electrode (High electric field region) was higher, and therefore the likely hood that it may be left behind by inertia was greater.

On the other hand, at high frequencies, the distance travelled was shorter, the electrophoretic force encountered was higher and therefore the droplet was retained. At high speeds, the drag force became substantial and overcame the electrophoretic force thereby dislodging the droplet from the high field region close to the electrode. In summary, the electrical tweezer successfully transported the droplets. Under the same applied potential, higher frequencies were required to hold the droplets as the speed of motion of the tweezer increased.

4.1.3 Droplet extraction

Electrical tweezer was also used to demonstrate extraction of a defined volume of droplets from a reservoir, which is one of the critical droplet-based microfluidic operations.

Experiments were conducted to perform the droplet extraction using acrylic chamber fitted with the glass capillary (Micro-Hematocrit capillary tube, Inner diameter = 1.1-1.2 mm, Fisher Scientific, MA, USA) and filled with the bi-layer oil medium. The outlet of the glass capillary which served at the reservoir was positioned at the interface of the bi-layer oil medium. The inlet of the glass capillary was connected to the syringe pump (KD scientific 200) through flexible Tygon tubing. The syringe pushed the water at the flow rate of 1μL⁄min. The electrical tweezer (Electrodes ~10 mm apart) was used for these experiments.

The droplet extraction was performed for the various applied potential of 0 to 6000 Volts (V_{Peak}/d = 0 to 600 V/mm) at 5 Hz. The tweezer was brought near the emerging droplet at the glass capillary tip, and then, the tweezer was moved forward at ~1 mm/s (Away from the capillary) to extract the droplet. The droplet extraction in the image format is shown in Figure 4.4.

First, the control experiments were performed in the absence of electrical tweezer and results are shown in Figure 4.4a. It can be observed, the emerging droplet at the tip of the glass capillary did not detach on their own in the absence of the electrical tweezer. Then, the second kind of control experiment was conducted with the tweezer but in the absence of the applied electric potential. The sequential images (Figure 4.4b) demonstrate that the tweezer alone (No applied electric potential; V = 0 Volts) was unable to detach the emerging droplet from the capillary tip even when it physically contacted the droplet. Finally, the droplet was extracted from the capillary tip using the electrical tweezer under the applied potential of 2000 Volts (V_{Peak}/d = 200 V/mm) at 5 Hz. It can be seen (Figure 4.4c) that the droplet was easily extracted from the tip of the capillary. The sequence of events for extraction was as follows. First, the droplet size gradually increased as more liquid was pumped into it and it became polarized under the electric field. Then, the droplet was attracted toward the high voltage electrode.

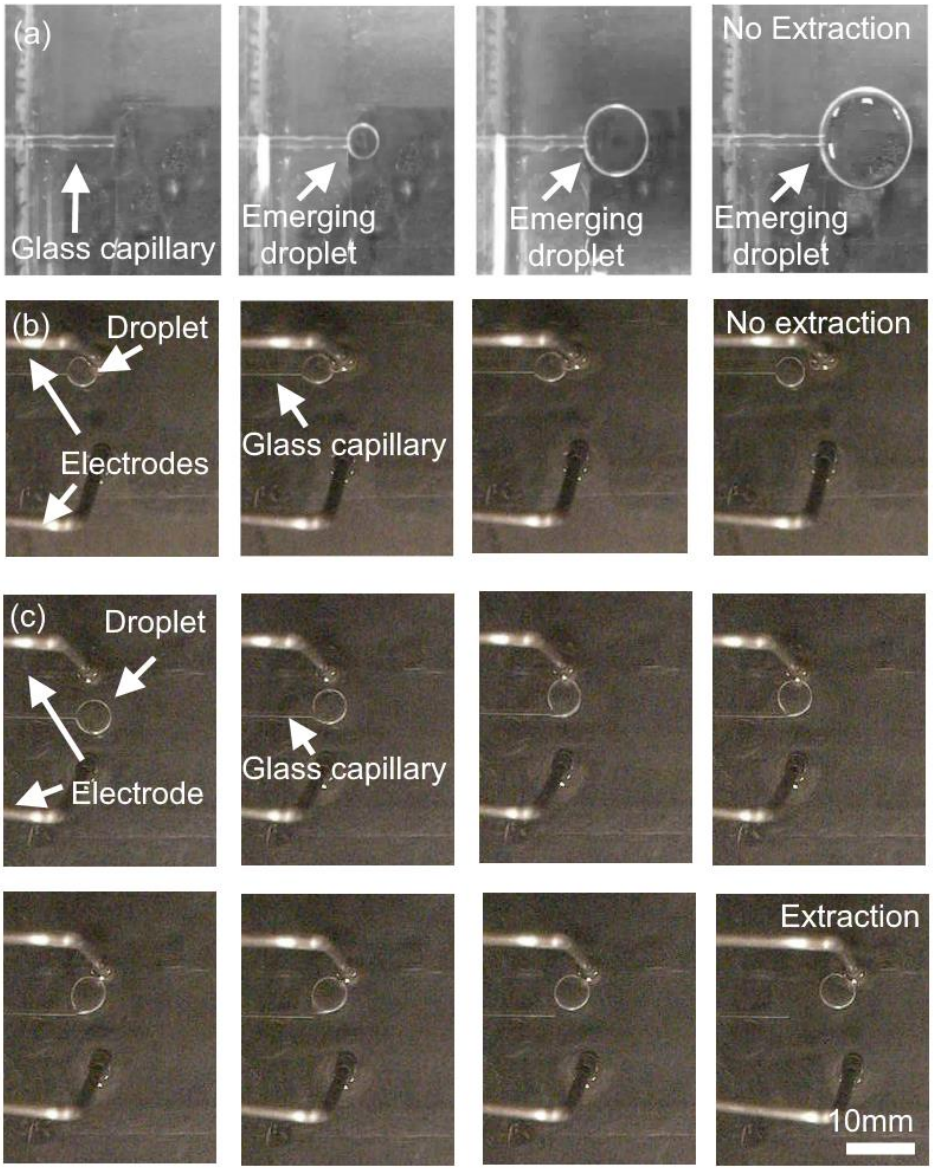

Figure 4.4 Electrical tweezer application for the droplet extraction from the capillary glass tip. (a) No-extraction of the droplet in the absence of electrical tweezer. (b) No-extraction of the droplet by the electrical tweezer (Electrodes 10 mm apart) under the absence of applied electric potential. (c) Droplet extraction by electrical tweezer (Electrodes 10 mm apart) under the applied potential of 2000 Volts (V_{Peak}/d = 200 V/mm) at 5 Hz.

The surface of the droplet attached to the capillary stretches and was pulled towards the electrode. Then, droplet contacted and acquired a charge from the high voltage

electrode. Next, the droplet was removed from the tip of the glass capillary and followed the electrical tweezer during its forward motion.

4.1.3.1 Characterization of the droplet extraction

The effect of the applied potential on the extracted droplet volume was studied, and results are shown in Figure 4.5.

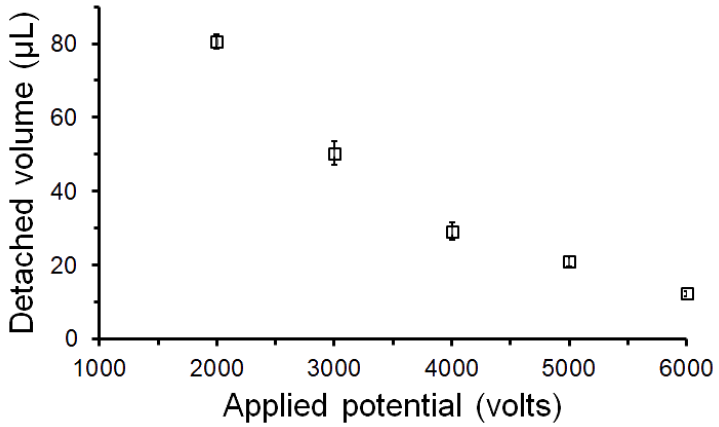

Figure 4.5 Electrical tweezer (Electrodes 10 mm apart) used for droplet extraction: The effect of applied potential ranges from 1000 to 6000 Volts (V_{Peak}/d = 100 to 600 V/mm) at 5 Hz on the extracted droplet volume.

It was found that the extracted droplet volume was dependent on the applied electric field strength between the electrodes of the electrical tweezer. The droplets of smaller volume could be extracted only with the higher applied potential. For instance, when the applied potential was increased from 2000 Volts (V_{Peak}/d = 200 V/mm) to 6000 Volts (V_{Peak}/d = 600 V/mm) at 5 Hz, the extracted droplet volume reduced from 80 µL to 12 µL.

The reason for this effect is as follows. The electrophoretic force of attraction (Fe=qE), between emerging droplet and high voltage electrode, increases with the increase in applied potential. The electric field was increased with the increase in applied potential. The surface tension forces keep emerging droplet attached with the tip of the capillary tube. The droplet was detached in a situation when electrophoretic forces of attraction between the droplet and electrical tweezer overcome the surface tension forces. The use of the

electric field to extract droplets provides an analog tunability to the volume that can be extracted. Thus, a precise volume of a liquid can be extracted by simply controlling the applied electric potential. This phenomenon is in contrast with the droplet extraction using the digital microfluidics. Digital microfluidics systems can extract fixed volumes from the reservoir.

The capability to extract a defined volume can potentially be used to aliquot reagents and water to be combined in different ratios to produce varying concentrations. To conclude, the electrical tweezer was used to detach the droplet from the reservoirs.

4.1.4 Droplet merging

Merging of droplets is crucial to mix chemicals in microfluidics. Electrical tweezer (Electrodes 4 mm apart) was used to demonstrate the merging of two droplets (0.3 µL). These droplets were dispensed in the bi-layer oil medium, ~5 cm apart from each other. The sinusoidal potential of 560 Volts (V_{Peak}/d = 140 V/mm) at the frequency of 2 Hz was applied to the tweezer which was then moved to bring them near the droplets. The droplet merging process was video graphed and shown in the images sequence format (Figure 4.6).

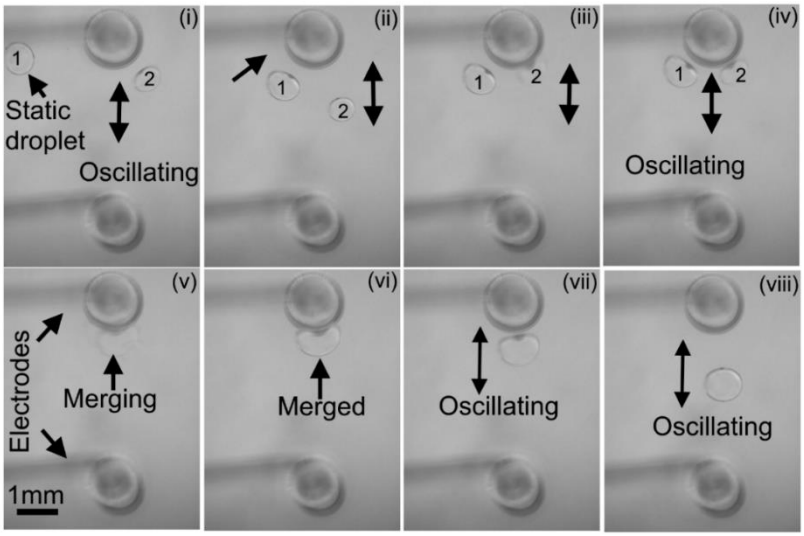

Figure 4.6 Merging of two droplets (0.3 µL) is demonstrated using electrical tweezer (Electrodes 4 mm apart) under the applied potential of 560 Volts (V_{Peak}/d = 140 V/mm) at 2 Hz.

It can be observed that the droplet 2, which is the closest to the electrode (Figure 4.6 (i)), was initially polarized and comes in contact with the electrode. It acquires a charge from the high voltage electrode and subsequently, undergoes oscillatory motion with it. Then, the electrical tweezer was moved so that the droplet 2 was brought closer to the droplet 1 (Figure 4.6 (ii)). Upon approach, droplet 1 also became polarized and consequently, attracted to the high voltage electrode (Figure 4.6 (iii)). The electrophoretic force of attraction between the high voltage electrode and polarized droplet attracts the droplet which makes contact, acquiring a charge. Upon charge acquisition, the droplet 1 also undergoes oscillatory motion. Subsequently, both oscillating droplet fused together after 2-3 oscillation (Figure 4.6 (iv)) with the high voltage electrode (Figure 4.6 (v & vi)). Then, the merged droplet started oscillatory motion with the high voltage electrode (Figure 4.6 (vii & viii)). The time required for droplet merging mainly depends upon the position of approaching and static droplet. The droplet merged within a couple of oscillations with the high voltage electrode. The droplets may acquire different charges while contacting with the high voltage electrode. The oppositely charged droplets attracted each other and subsequently merged as they come closer during the oscillatory motion. These droplets merging experiments demonstrated that not only can the individual droplets be transported, but they can also be merged into a single droplet. The electrical tweezer used to merge the droplets that are an essential step in microfluidic operations.

4.2 Loop-mediated isothermal amplification (LAMP) of nucleic acid by electrical tweezer

The sequential steps are required to perform common biochemical assays namely nucleic acid amplification. The electrical tweezer was used to perform various subsequent steps such as droplet transportation and merging to perform LAMP assays. These droplets consisted of LAMP reagents, and DNA template and dispensed in the low-temperature zone of the bi-layer oil chamber. The electrical tweezer transported the droplet of LAMP reagents and merged it with the droplet of DNA template. Then, the merged droplet was transported and immobilized in the amplification zone. Finally, the treated samples were

extracted, and end-point fluoresce intensity was measured using the commercial fluorescence device (ESEQuant).

4.2.1 Experimental setup for amplification of LAMP assays

The experimental setup required to perform nucleic acid amplification (LAMP) by electrical tweezers is shown in Figure 4.7a. It consisted of three components: (1) electrical tweezer system; (2) temperature controlling unit; and (3) fluorescence measurement unit.

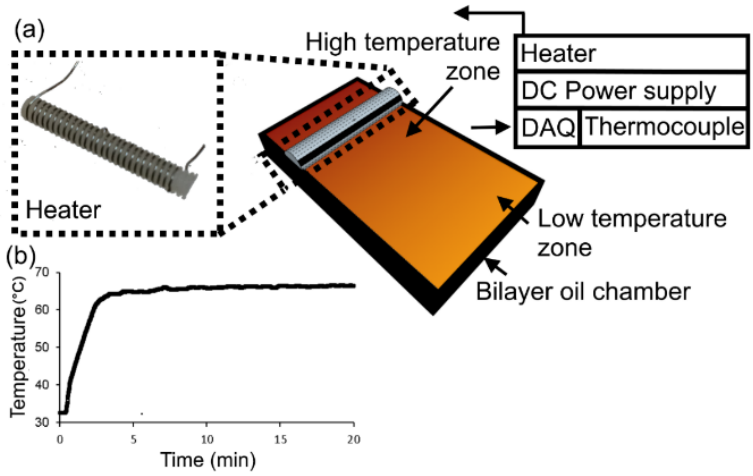

Figure 4.7 (a) Experimental setup to perform DNA amplification by loop-mediated isothermal amplification using the electrical tweezer. (b) The temperature of the amplification zone in the bi-layer chamber.

The electrical tweezer system used was similar to those reported in the previous chapter. The temperature controlling system consisted of three components: a heat generation unit; data acquisition unit; and controlling software. The direct current (DC) power supply (GPS-1850D, Good Will Instrument Co., Ltd., Taiwan) was used to generate heat by connecting to the wire heater. The resistive wire heater was fabricated in-house by tightly winding the nickel-chromium resistive wire (NI80, Omega Engineering, Inc., CT, USA) around screw threads. The wire heater was placed at one end of the bi-layer oil chamber. The T-type thermocouple (TMQSS-020G-12, OMEGA Engineering, Inc., TX, USA) connected with the DAQ (NI-6001, OMEGA Engineering, Inc., TX, USA) through

signal conditioner **(**Omega-CCT) to monitor the temperature. The closed feedback loop was formed by connecting the power supply to the computer through DAQ. Lab VIEW (V 14.0.0, National Instruments, Austin, TX, USA) with the PID kit was used to control the amplification temperature. The amplification temperature was maintained ~65°C for 30 min (Figure 4.7b). In this study, the commercial fluorescence device (ESEQuant TS95, Qiagen, Hilden, Germany) was used for two purposes: end-point fluorescence intensity measurement of LAMP assays treated by the electrical tweezer and amplification of LAMP assays.

4.2.2 Loop-mediated isothermal amplification (LAMP) assays

LAMP assays used to detect the Shiga toxin gene eae virulence factor gene of *E. coli (Escherichia coli)* 0157 consisted of sets of 5 or 6 primers for the specified gene. Reagents were provided by our collaborators (Dr. Mahoney's group) and were purchased as research use only (RUO) reagents from Canadian Molecular Developments (Division of Pro-Lab Diagnostics, Richmond Hill, ON, Canada). The LAMP amplification mixture (25 µL) consisted of three components: Optigene master mix (15 µL); primer mix (5 µL); and DNA template or ddH_2O (5 µL). Optigene master mix (ISO-0001 Isothermal Master Mix, Optigene, Horsham, U.K) contained MgSO4, dNTPs, and ds-DNA binding dye. The primer mixes for the targeted gene consisted of primer mix: forward outer (F3) and backward outer (B3) primers at 0.2 µM, forward inner (FIP) and backward inner (BIP) primers at 0.8 µM, and forward loop (LF) and backward loop (LB) primers at 0.4 µM. For positive reactions, DNA template (5 µL) was used to make the final concentration of 10^8 DNA/reaction. In the case of negative control, DNA template was replaced with the ddH_2O.

4.2.3 Amplification of LAMP assays using electrical tweezer

The electrical tweezer used the sequential droplet-based unit operations to perform the LAMP assays. The electrical tweezer with the electrodes 10 mm apart were used in this study. The electric potential of 1200 Volts (V_{Peak}/d = 120 V/mm) at 10 Hz was applied, and

two types of droplets were used. First, the droplets of the reaction mixture (20 µL): Optigene isothermal master mix (15 µL) and primer mix (5 µL). Second, the droplet of 5 µL consisted of either DNA template or ddH_2O (5 µL). The pipette was used to dispense them in the bi-layer oil medium ~5 cm apart. The electrical tweezer transported the droplet of the reaction mixture (20 µL) and merged with the droplet of DNA template or ddH_2O (5 µL). Then, the merged droplet (25 µL) was transported and immobilized in the amplification zone (~65°C) for 30 min. Finally, the droplet was extracted via pipette and loaded in the commercial fluorescence device (ESEQuant). The results of LAMP assays those were treated with the electrical tweezer and commercial fluorescence device (ESEQuant) are shown in Figure 4.8.

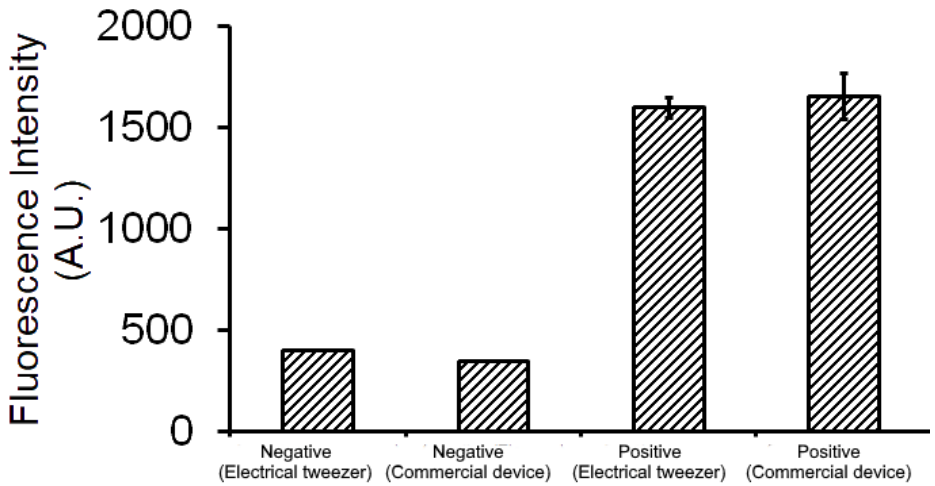

Figure 4.8 Electrical tweezer (Electrodes 10 mm apart) was used with the applied potential of 1200 Volts (V_{Peak}/d = 120 V/mm) at 10 Hz used for the droplet transportation and merging operation to perform DNA amplification. End-point samples fluorescence intensities (positive and negative) treated with an electrical tweezer and commercial fluorescence device. [Commercial fluorescence device (ESEQuant) measured the intensity originally in mV].

Initially, the negative control reaction was performed in the bi-layer oil chamber using the electrical tweezer. The end-point fluorescence intensities of a negative sample treated with the electrical tweezer (400 A.U.) was compared with the sample that was treated in the commercial fluorescence device (350 A.U.). The end-point fluorescence

intensities of both negative samples were in the same order of magnitude and subsequently, demonstrates the absence of contamination.

Furthermore, the fluorescence intensity levels of negative samples established the baseline to determine the successful amplification of positive LAMP assays. Then, the positive assays were performed in triplicates using the electrical tweezer. The end-point fluorescence intensity was 1600 ± 50 A.U. that is ~4 times higher than the intensity of the baseline. The amplification of LAMP assays treated with the electrical tweezer was further verified by comparing with the samples treated with the commercial fluorescence device (ESEQuant). The end-point fluorescence intensity of triplicates positive samples treated in commercial fluorescence device (ESEQuant) was 1653 ± 114 A.U. The end-point fluorescence intensity of positive samples treated with both types of devices are similar. Consequently, shows the successful amplification of LAMP assays using an electrical tweezer.

In conclusion, electrical tweezer used the droplet-based microfluidic operations of transportation and merging to demonstrate the successful isothermal amplification using LAMP assays. Currently, the probes of electrical tweezer are cleaned after a single use to avoid the cross-over contamination. Alternatively, probes could be replaced after each time use as they are low-cost. Nonetheless, the electrical conditions that will promote self-cleaning or prevent cross-contamination can be explored in the future. The self-cleaning phenomenon will make the probes reusable over longer durations of time. Electrical tweezer is suitable for systems with low through, but its applicability can be enhanced using the multiple electrical tweezers in parallel. This approach is expected to be of broad applicability in other biochemical assays such as immunoassays, and cell-based assays as well as in small-organism-based assays.

4.3 Summary

In this chapter, the application of the electrical tweezer has been discussed. Initially, the droplet-based microfluidic operations such as transportation, extraction, and merging

are shown. The droplet (5 µL) transportation was characterized for the range of frequency 5-1000 Hz. The electric potential of 2000 Volts (V_{Peak}/d = 200V/mm) was applied. The droplet was transported up to the speed of ~22 mm/s. Then, electrical tweezer was used to extract the water droplets from the water reservoir. Droplets of volumes ~12-80 µL were extracted by applying the voltage 1000-6000 Volts (V_{Peak}/d = 100-600 V/mm). Next, electrical tweezer was used to demonstrate the droplet merging. Two droplets were transported and merged by applying the optimized operational conditions.

Then, electrical tweezer was used to handle the loop-mediated isothermal amplification (LAMP) assays. Two droplets containing the various reagents required to perform the amplification reaction were transported and merged. Next, the DNA was amplified by transporting and immobilizing the merged droplet at ~ 65˚C.

Chapter: 5 A low-cost heater integrated microfluidic device to perform integrated sample processing and detection of bacteria

This chapter describes the integrated microfluidic device that has been developed to detect the bacteria samples. A low-cost electrical resistive wire heater has been integrated on the microfluidic device to create localized heating zones. The direct current (DC) power supply was used to maintain temperature zones for lysis of bacteria and the amplification of DNA. Moreover, dc power supply was used to transport DNA electrophoretically. Consequently, the use of pumps and washing steps were avoided. The operational steps mainly included the thermal lysis of bacteria, electrophoretic transportation of DNA, and DNA amplification by using the loop-mediated isothermal amplification (LAMP) assays. Finally, the DNA amplification was monitored by the in-situ measurement of real-time fluorescence intensity.

First, the conceptual design and working principle of the microfluidic device is explained. Then, the materials and methods used are explained. The operation of the microfluidic device is described in the three steps, (1) operation of individual components that include the on-chip lysis, transportation, and amplification modules, (2) working of two integrated components, on-chip lysis and transportation, on-chip transportation and amplification and finally, and (3) on-chip integrated operation of all three components.

5.1 Conceptual device design

The conceptual design of an integrated microfluidic device is shown in Figure 5.1. The device consists of five components: a cylindrical-shaped lysis chamber, a cylindrical-shaped amplification chamber, a connecting channel, two embedded wire heaters, and two metal electrodes.

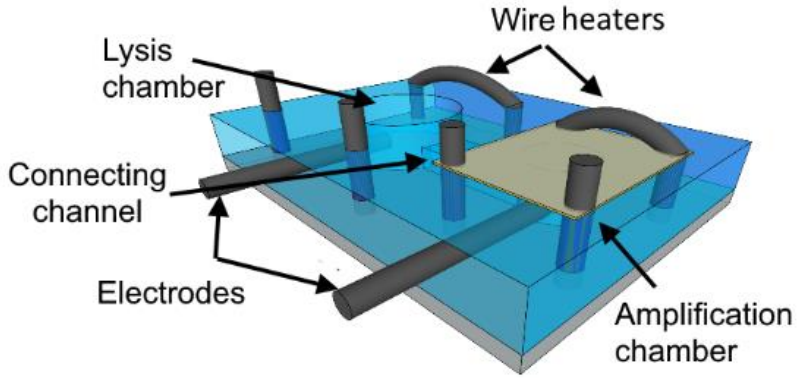

Figure 5.1 Schematic view of an integrated microfluidic device.

The two cylindrical reservoirs named as lysis chamber and amplification chamber were placed apart from each other and connected by a connecting channel. The lysis chamber was designed with the dimensions of 6.5 mm (Diameter) and 3 mm (Height) to hold a sample volume of 100 µL. The lysis chamber was designed to handle the two different types of fluids. These fluids included the sample (Bacterial solution) of 70 µL and the paraffin oil (30 µL). The paraffin oil was poured on top to avoid sample loss at higher temperature due to evaporation. The sample volume of 70 µL was selected to have sufficient bacteria cells available for detection in the lower concentration sample.

The amplification chamber had a dimension of 2.5 mm (Diameter) and 3 mm (Height). The chamber was designed to hold the reaction mixture volume of ~15 µL. The typical reaction volume of 25 µL of LAMP assays was used in the conventional amplification devices. While in this microfluidic device there was a sample loss during the sample loading process. Therefore, to keep the sample volume used under the 25 µL for the microfluidic device, the amplification chamber was designed to handle the smaller volume of ~15 µL.

The connecting channel was designed with the dimension of 50 µm (height) × 80 µm (width) × 8 mm (length) to handle to volume of a few nanoliters. First, the length of the connecting channel was selected to position the amplification chamber sufficiently

away from the lysis chamber. The elevated temperature of the lysis chamber could have adverse effects on the LAMP assay. It was experimentally determined that the LAMP assays failed to amplify when exposed to the temperature higher than 70˚C (Mention in section 5.1.2). The optimum length of 8 mm of connecting channel was selected. The measured temperature of the amplification chamber was ~40˚C (Mention in section 5.1.3) when the lysis chamber was exposed to the temperature of ~92˚C. Second, the connecting channel with the height of 50 µm was fabricated to stop the oil from entering to the connecting channel. Device operation can fail if the oil which is placed on top of the sample subsequently inadvertently enters in the connecting channel. The presence of oil in the connecting channel could prevent the application of an electric field across it and consequently stop the electrophoretic transportation of DNA.

The resistive wire (Nickel Chromium Alloy wire, 0.25 mm diameter) were embedded in the PDMS around both chambers (Mentioned in section 5.2.1). These resistive wires worked as heaters to maintain the appropriate temperatures for the cell lysis and DNA amplification. The heaters were embedded in a symmetrical four-wire configuration around both chambers as shown in Figure 5.1. The four-wire configuration of heaters was selected considering the two parameters, time to reach the setpoint and ease in fabrication. A higher number of inserted wires would deliver a higher flux of heat and help to achieve the setpoint quicker. However, the fabrication complexity will consequently increase. Four wires were an optimal choice to ensure that the setpoint is achieved at a reasonable timeframe with minimal complexity of the fabrication process. Metal electrodes (Platinum wire, 0.0508 mm diameter) were also inserted into both chambers and were used to apply an electric potential across the connecting channel to transport the DNA from lysis chamber to the amplification chamber.

5.1.1 Device Operation

The operation of the device was performed in four steps. First, the sample (bacteria) was thermally lysed in the lysis chamber. Then, the electric potential was applied between

the chambers. DNA was transported electrophoretically from lysis chamber to the amplification chamber. Finally, amplification of LAMP assays was detected by in-situ monitoring of fluorescence intensity in a real-time format.

Initially, the cells (bacteria) membrane was ruptured by exposing cells to the elevated temperature of ~ 92°C for 5 min. While the sample was heated, the covering layer of paraffin oil (lower density) protected the sample loss due to the evaporation. Afterwards, DNA was transported from lysis chamber to the amplification chamber by applying the electric potential (10 Volts) to the electrodes (Pt). Then, the transported DNA was amplified in the amplification chamber at ~65°C. Finally, the in-situ DNA amplification of LAMP assays was monitored by measuring the real-time fluorescence intensity.

5.1.2 Effect of temperature on LAMP assays

LAMP enzymes are temperature sensitive and may not work efficiently at elevated temperatures. Since the microfluidic device has elevated temperature zone for thermal lysis, therefore, it was essential to test the effect of temperature on the LAMP assays. For this experiment, seven reactions of LAMP assays were prepared with the volume of 25 µL use for each reaction. Each reaction mixture consisted of master mix (15 µL), primer mix (5 µL), and DNA template (5 µL). The DNA template with the concentration of 10^7 DNA molecules / 5 µL was used. The reaction mixtures were amplified at various temperatures in the commercial fluorescence device (ESEQuant). The end-point fluorescence intensities of different LAMP assays those were amplified at various temperatures are shown in Figure 5.2.

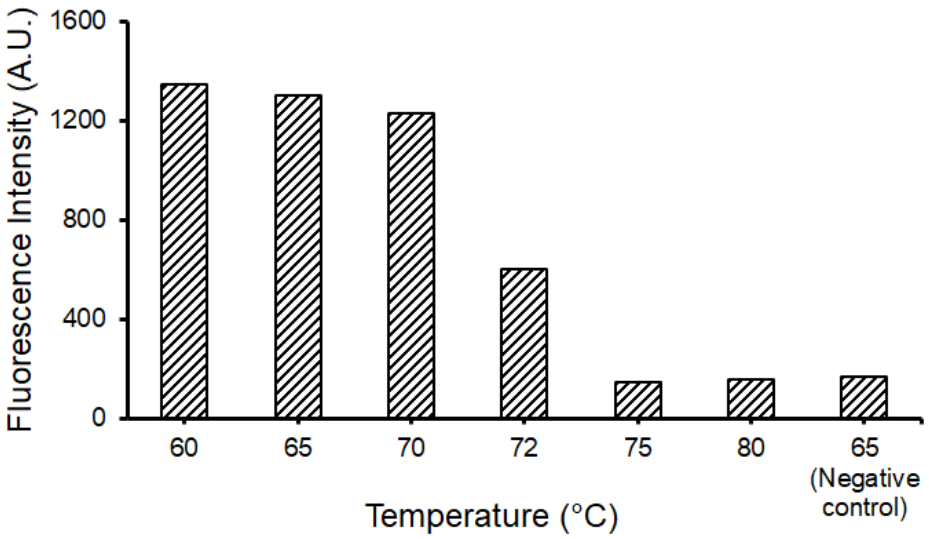

Figure 5.2 Effect of temperature on the LAMP assays. [Commercial fluorescence device (ESEQuant) measured the intensity originally in mV].

LAMP samples were successfully amplified when treated at the temperatures of 60, 65, and 70°C. The end-point fluorescence intensity was ~1300 A.U. The end-point fluorescence intensity of LAMP assays was reduced to half (~600 A.U.) when amplified at the temperature of 72°C. The LAMP assays failed to amplify when exposed to the higher temperatures of 75 and 80°C. The end-point fluorescence intensities (~100 A.U.) of these samples were similar to the end-point fluorescence intensity (~100 A.U.) of the negative control reaction. The negative control sample was amplified at 65°C. In conclusion, the distance between the chambers (lysis and amplification) should be selected carefully. Therefore, the temperature in the amplification chamber should be lower than 70˚C when the temperature of 92˚C was maintained in the lysis chamber.

5.1.3 Temperature measurement of amplification chamber in the microfluidic integrated device

The temperature of the amplification chamber was measured for the selected length of the connecting channel (8 mm) while the elevated temperature was maintained in the

lysis chamber. Results of the temperature measured in the amplification chamber are shown in Figure 5.3.

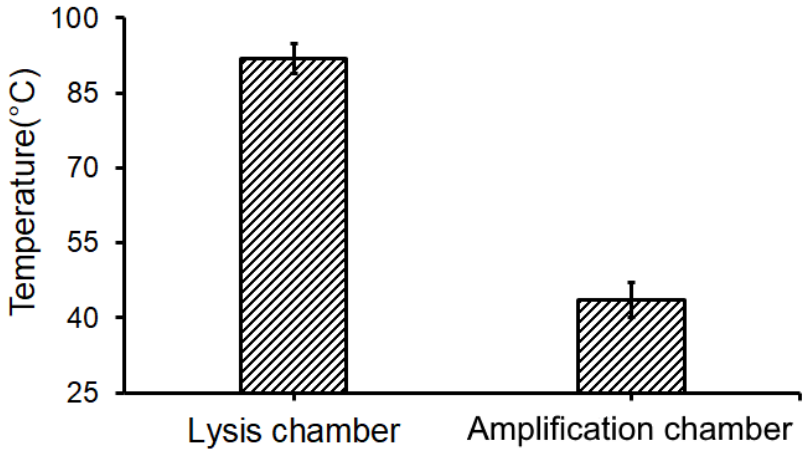

Figure 5.3 Temperature measurement of the amplification chamber due to the elevated temperature of the lysis chamber (~92°C).

Six devices were tested whose lysis chambers were maintained at an elevated temperature of 92˚C ± 4. Meanwhile, the measured temperatures in the amplification chamber were 43˚C ± 5. The average temperature value of the six devices was plotted. The standard deviation shows the variation in the average temperature of six devices. In conclusion, the distance of 8 mm between the chambers (lysis and amplification) was sufficient to keep the temperature of the amplification chamber in the safe limit. This design was used to perform the operations of a microfluidic device. Although, the distance could be further decreased that could enhance the difficulty of the heater fabrication process.

5.2 Materials and methods

5.2.1 Fabrication of device

The fabrication process of a microfluidic device is shown in Figure 5.4. The device was fabricated in four steps: (1) fabrication of master mold, (2) fabrication of connecting

channel and chambers, (3) device bonding and assembly, and (4) embedding of wire heaters and electrodes.

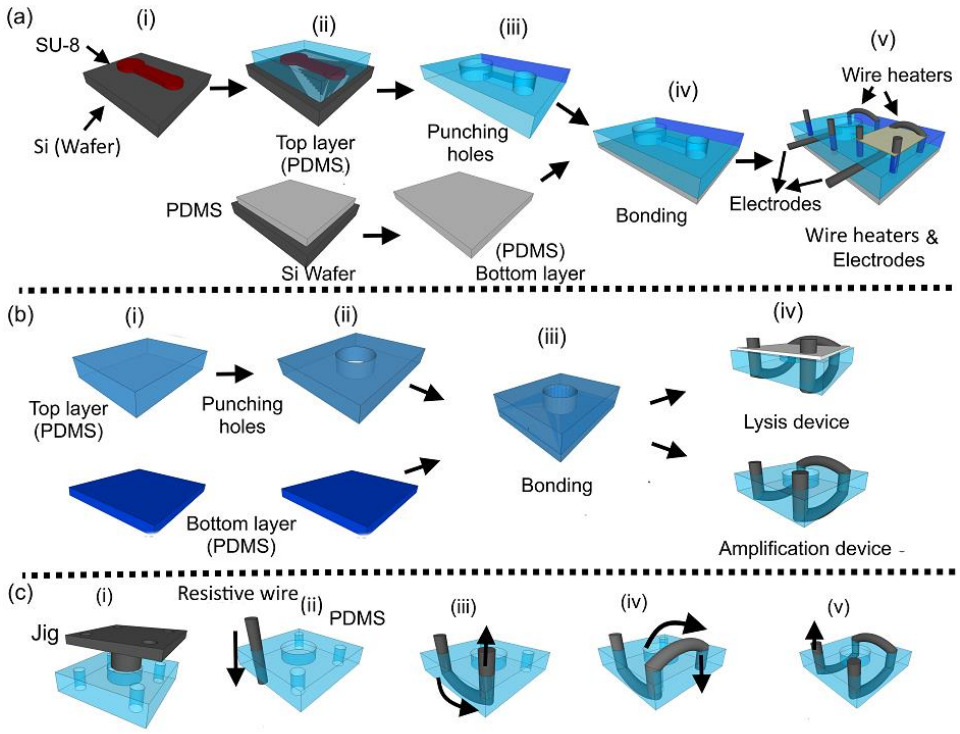

Figure 5.4 (a) The fabrication process of a microfluidic device. (b) The fabrication process of individual components (Lysis and Amplification). (c) Integration of wire heaters in the microfluidic device.

First, master mold (SU-8) was fabricated using the standard photolithography process (Mentioned in Appendix C) as shown in Figure 5.4a (i). Polydimethylsiloxane (PDMS, Sylgard 184 kit, Dow Corning Corporation, Midland, MI, USA) was used to fabricate the microfluidic device. Soft lithography technique was used to fabricate the connecting channel. The prepolymer mixture was prepared in the volumetric ratio of 10:1 (Base: Curing agent). Then, the mixture was degasified under the vacuum pressure to remove the air bubbles. Prepolymer mixture was poured on the master mold to prepare the top layer (Thick layer ~3 mm). And it was poured on the flat silicon wafer to make the bottom layer (Thin layer ~1.5mm) as shown in Figure 5.4a (ii). Finally, silicon wafers were placed on the hot plate at 75°C for ~ 2 h for curing.

Two pieces were cut and peeled from the silicon wafers. Then, punchers were used to punching the holes in the top layer (Thick layer) for lysis chamber (Diameter: 6.5 mm) and amplification chamber (Diameter: 2.5 mm) as shown in Figure 5.4a (iii). Two layers (top and bottom) were bonded together using the microcontact printing technique (Mentioned in Appendix C) as shown in Figure 5.4a (iv). Finally, the wire heaters (NI80-010, OMEGA Engineering, Inc., TX, USA) and electrodes (Platinum wire, 0.0508 mm dia, Alfa Aesar, MA, USA) were inserted in the device. The schematics of the microfluidic device is shown in Figure 5.4a (v).

The fabrication of individual components (lysis and amplification) of a microfluidic device is shown in Figure 5.4b. Prepolymer mixture (Base/Curing agent:10/1) was poured on the plain substrate (Silicon wafer). Two layers of PDMS were cut and peeled from the substrate to form the top and bottom layers as shown in Figure 5.4b (i). Then, holes for lysis or amplification chambers were punched in the top layer (Figure 5.4b (ii)).

Then, microcontact printing technique was used to bond two layers of a microfluidic device (Mentioned in Appendix C) as shown in Figure 5.4b (iii). Then, resistive wires those constituted the heating elements for both chambers (lysis and amplification) were manually embedded in the microfluidic device (Figure 5.4b (iv)). Paraffin oil (Caledon Laboratories Ltd, Georgetown, ON, Canada) was used to cover the sample in the lysis chamber. While, tape (Microseal B Adhesive Seals, Bio-Rad Laboratories, Inc., CA, USA) was used to seal the amplification chamber.

The integration of wire heaters in the microfluidic device is shown in Figure 5.4c. Vertical holes were punched in a symmetrical format around both chambers using the needle (23 G, Precision glide needle, BD, NJ, USA) and a guiding pattern mold (Figure 5.4c (i)). Next, the resistive wire was threaded through the fabricated heaters sequentially like a stitching operation as shown in Figure 5.4c (ii-v). Then, the gaps around the wire heaters and electrodes were sealed by wicking the prepolymer PDMS between the wires and the elastomer. Finally, the device was placed on the hot plate at 120° C for 1 h to cure.

The blade cutting machine (Cricut maker, *www.cricut.com*, Provo Craft & Novelty, Inc., UT, USA) was used to cut the pattern on the tape like the wiring pattern on the top surface of the amplification chamber. Amplification chamber was sealed by passing the tape through wires and pasting on the PDMS surface.

5.2.2 Bacterial sample preparation

The bacterial culture was prepared from a glycerol stock of Shiga Toxin *E. coli* (STEC) EAE gene fragment cloned into the pGEM-T easy vector. Then, 2-3 µL of the glycerol stock was added to 5 mL of LB broth +100mg/mL ampicillin. The bacteria were grown (37°C) in the shaking incubator overnight (~16 h). Then, bacterial cells were spun at 10 000 rpm for 5 minutes. The cell pellet was washed with 1 mL of 1×PBS (Bioshop Canada Inc., Burlington, ON, Canada) 3 times. Finally, 10-fold serial dilutions of the bacterial cells were prepared for testing.

5.2.3 LAMP assays

The bacterial culture was prepared from a glycerol stock of Shiga Toxin *E. coli* (STEC) EAE gene fragment cloned into the pGEM-T easy vector. Then, 2-3 µL of the glycerol stock was added to 5 mL of LB broth +100mg/mL ampicillin. The bacteria were grown (37°C) in the shaking incubator overnight (~16 h). Then, bacterial cells were spun at 10 000 rpm for 5 minutes. The cell pellet was washed with 1 mL of 1×PBS (Bioshop Canada Inc., Burlington, ON, Canada) 3 times. Finally, 10-fold serial dilutions of the bacterial cells were prepared for testing.

5.2.4 Sample loading

Sample loading is a crucial step in the operation of a microfluidic device. The sequential steps of sample loading in the microfluidic device are shown in Figure 5.5. First, the pipette was used to load the LAMP assays in the amplification chamber. Then, the tape was used to seal the amplification chamber. Then, gentle pressure was applied on the top

of the tape to push the LAMP reaction mixture through the connecting channel to the entrance of the lysis chamber. Next, the small volume (~5 µL) of 1×PBS was dispensed at the intersection of lysis chamber and connecting channel. This added phosphate buffer entered and filled the cavity generated in the connecting channel after the removal of pressure from the tape ensuring that no air bubbles were formed. Finally, the sample (bacteria solution) was loaded (70 µL) in the lysis chamber and covered by the small volume (30 µL) of paraffin oil.

Sample loading process in the individual components of microfluidic devices (lysis and amplification) consisted of two simple steps. First, the pipette was used to dispense the sample in the chambers (lysis or amplification) of the microfluidic device. Then, paraffin oil was dispensed to cover the lysis chamber. And the tape was used to seal the amplification chamber of a microfluidic device.

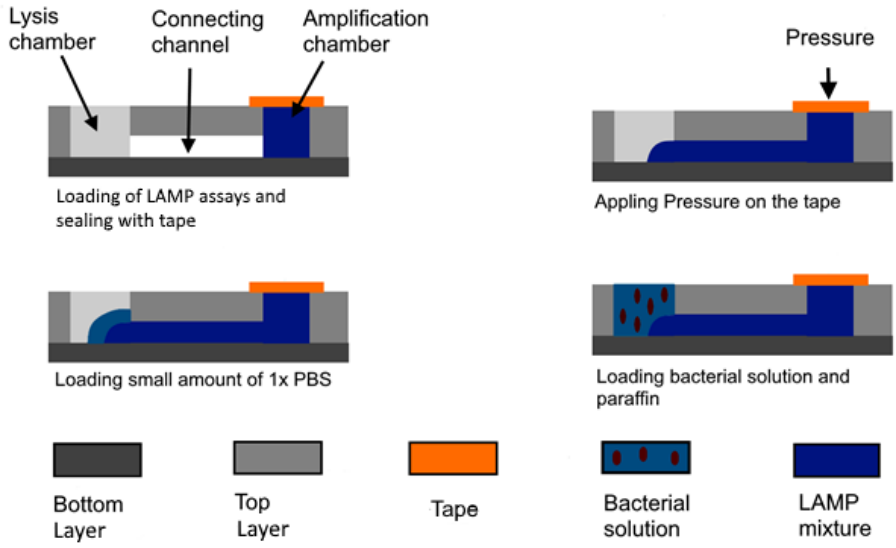

Figure 5.5 Sample loading process in the microfluidic device.

5.2.5 Experimental setup

The experimental setup for the integrated microfluidic device to detect the bacteria *(E. coli)* is shown in Figure 5.6. The experimental setup consisted of three units: (1)

Temperature controlling unit, (2) Optical fluorescence detection unit, and (3) DNA transportation unit.

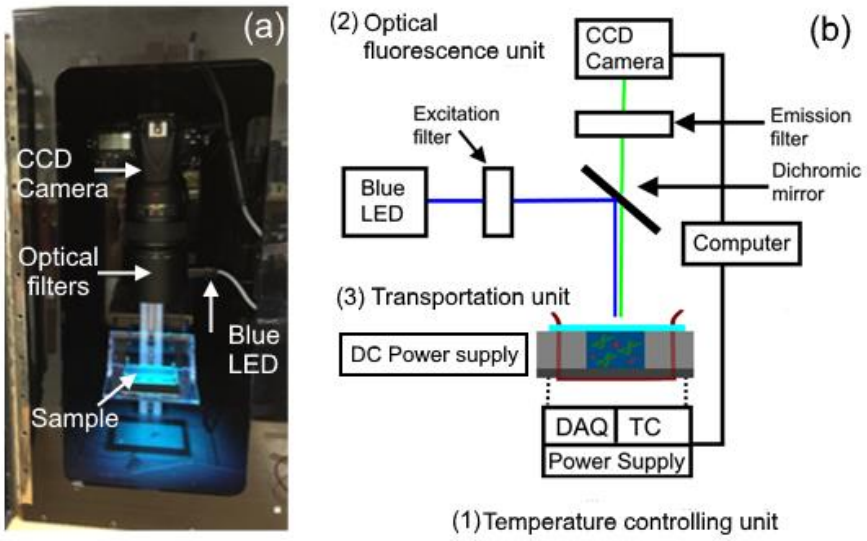

Figure 5.6 Experimental setup for the operation of a microfluidic device. (a) Image of the optical fluorescence detection system. (b) Schematics of experimental setup with the temperature control, optical fluorescence detection, and DNA transportation units.

5.2.5.1 Temperature controlling unit

The temperature was controlled by two methods: (1) with a feedback system and (2) without a feedback system. LabVIEW (V 14.0.0, National Instruments, Austin, TX, USA) with PID kit was used to control the temperature. The T-type thermocouple (5SC-TT-T-36-36, OMEGA Engineering, Inc., Houston, TX, USA) was used to measure the temperature and was connected to the computer through a signal conditioner (Omega-CCT) and DAQ (NI-6008, OMEGA Engineering, Inc., Houston, TX, USA). While, the direct current (DC) power supply (GPS-1850D, Good Will Instrument Co., Ltd., Taiwan) was connected to the wires heaters those were integrated into the microfluidic device. In the case with no feed system, DC power supply (GPS-1850D, Good Will Instrument Co., Ltd., Taiwan) was directly connected to the wire heater.

5.2.5.2 Optical fluorescence detection unit

The DNA amplification was detected by two methods: real-time and end-point fluorescence measurement. The real-time fluorescence measurement system was built in-house and consisted of five components: charged couple device (CCD) camera, LED light source, bandpass filter, emission filter, and a dichroic mirror. The blue LED (83-298, 470 nm, Edmund optics, NJ, USA) was used as excitation light source. The light was passed through the excitation filter 492 nm (Edmund optics, NJ, USA). The dichroic mirror 506 nm (Edmund optics, NJ, USA) was placed at 45 degrees to the incident light and diverted the light towards the LAMP sample. The reflected light from the sample was passed through the emission filter 525 nm (Edmund optics, NJ, USA) and finally, was recorded by the CCD camera (Nokia D810, Tokyo, Japan). End-point fluorescence intensity of the samples was measured using the commercial fluorescence device (ESEQuant TS95, Qiagen, Hilden, Germany).

5.2.5.3 Transportation unit

The source meter (237, Keithley Instruments Company, Cleveland, OH, USA) was used with the voltage source mode. The DC voltage was applied between the lysis chamber and amplification chamber for the DNA transportation.

5.2.5.4 Image analysis

Primarily, the images were recorded (Interval 20 s) in the raw format. Then, these recorded images were converted to the 16-bit format using the Nikon ViewNX-I software (Ver. 1.0.0, Nikon Corporation, Tokyo, Japan). Afterwards, converted images were analyzed by the ImageJ (https://imagej.nih.gov/ij/). Then, each image was split into multichannel (Red, Green, and Blue) and only images from the green channels were used for further analysis. First, the background was removed by considering the rolling ball radius. Then, the average intensity of the amplification chamber was measured for all the

processed sequential images. Finally, the real-time fluorescence intensity was plotted with respect to time.

5.3 Operation of individual components

5.3.1 On-chip lysis of bacteria cells

On-chip thermal lysis of bacteria cells was performed in the individual microfluidic device. The schematics of a microfluidic device is shown in Figure 5.7. The sample volume of 70 µL was loaded in the lysis chamber. The sample consisted of bacterial cells suspended in 1×PBS with the concentration of 10^8 CFU/mL. Paraffin oil (30 µL) was dispensed on top of the sample to avoid the sample loss at elevated temperature due to evaporation.

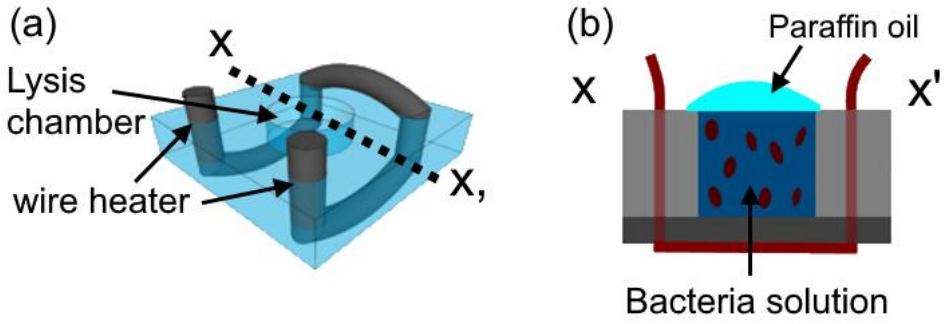

Figure 5.7 A microfluidic device for on-chip lysis of bacteria. (a) Schematics of a microfluidic device. (b) A cross-sectional view of a microfluidic device.

The temperature controlling system was used to maintain the temperature in the lysis chamber. Figure 5.8 shows that the temperature of ~92°C was maintained in the lysis chamber for 5 min. The temperature achieved was highly repeatable with the variation of ± 1˚C between five devices. The time required to reach the set point was 5.6 ± 0.3 min for the five tested devices.

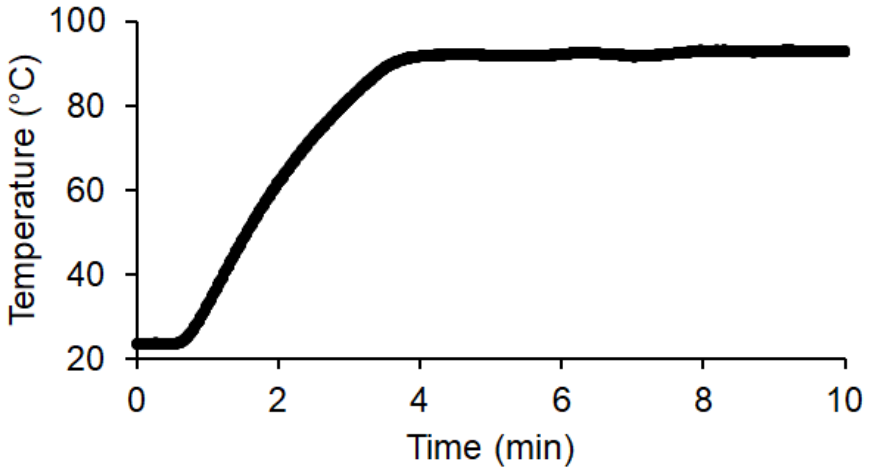

Figure 5.8 Temperature response of lysis chamber of a microfluidic device for on-chip thermal lysis of bacteria using the temperature controlling system.

On-chip bacteria lysis was performed in the three different devices. The lysate of bacteria cells was extracted from the microfluidic device for off-chip amplification. Then, lysate of bacteria cells (5 µL) was added with the 20 µL of the mixture (Primer mixture:5 µL and Master mix: 15 µL) to prepare the 25 µL reaction mixture for positive of LAMP assays. Two kinds of negative control experiments were performed. First, the lysate of bacteria cells was replaced with the unlysed bacteria cells (5 µL) of concentration 10^8 CFU/mL. Second, phosphate buffer (5 µL) with the concentration of 1× was added in the reaction mixture. Finally, the reaction mixtures were loaded in the commercial fluorescence device (ESEQuant). Subsequently, the real-time amplification reactions were performed at 65°C. The results of real-time amplification the LAMP assays are shown in Figure 5.9.

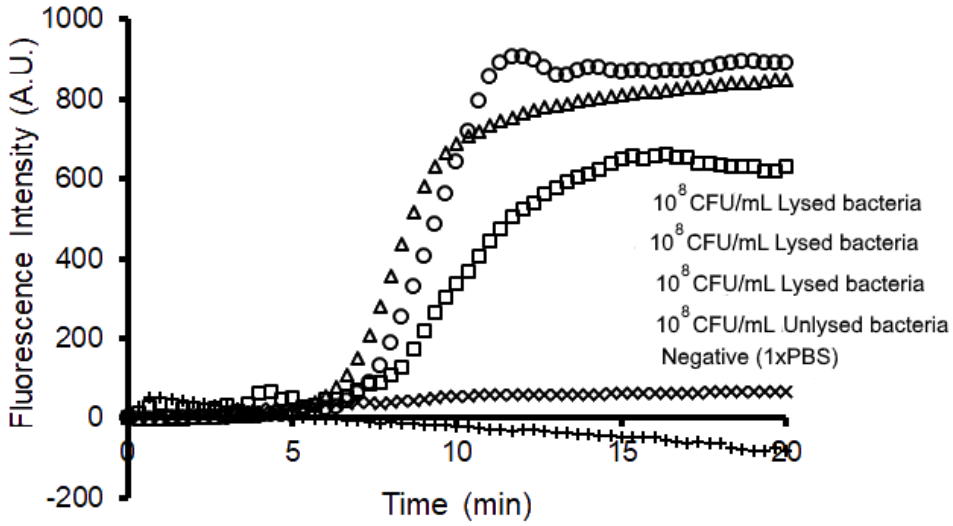

Figure 5.9 Off-chip real-time amplification curves for the bacteria samples collected from the microfluidic device for on-chip lysis. [Commercial fluorescence device (ESEQuant) measured the intensity originally in mV].

These reactions were performed with the lysate of bacteria cells, unlysed bacteria cells, and phosphate buffer. The fluorescence intensity values were plotted after normalizing them by subtracting the mean value of the intensity of the first three time points. The standard s-shaped amplification curves demonstrate that all the samples with the lysed bacterial cells were amplified. The negative control reaction with the unlysed bacterial cells did not amplify showing that the lysis step was crucial for the assay. The bacteria samples with high concentrations used for these experiments subsequent, the slight reduction in the fluorescence intensity possibly because of quenching effect. Finally, the second negative control reactions with the phosphate buffer demonstrate the absence of any contamination. These amplified results show that the bacteria cells were successfully lysed on-chip in the microfluidic device.

5.3.2 On-chip DNA transportation

On-chip transportation of DNA was demonstrated using the individual transportation component of a microfluidic device as shown in Figure 5.10.

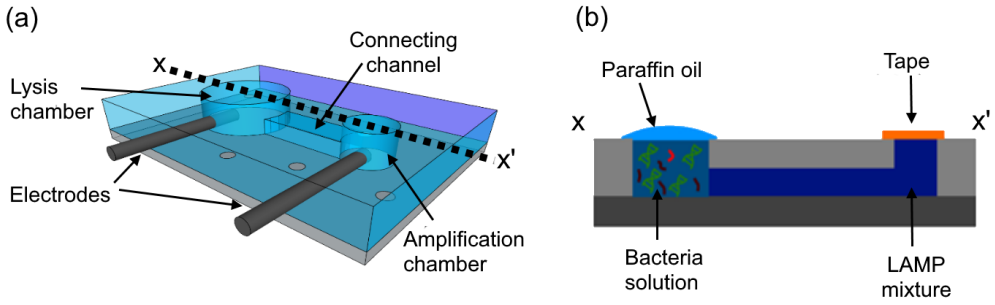

Figure 5.10 A microfluidic device for the on-chip transportation of DNA. (a) Schematics of a microfluidic device. (b) A cross-sectional view of a microfluidic device.

Initially, the operational parameters of time (min) and voltage (Volts) were determined for DNA transportation. The determination of the right condition to transport of DNA from the lysis chamber to the amplification chamber through the connecting channel is critical for the operation of the device. After determination of the transportation conditions, DNA transportation was tested for various sample concentrations.

5.3.2.1 Transportation time determination

The estimation of time required to transport DNA from the lysis chamber to the amplification chamber is critical for the successful operation of a microfluidic device. Both amplification chamber and connecting channel were filled with the 1×PBS (~15 µL). Then, the tape was used to seal the amplification chamber. The bacterial solution was prepared in 1×PBS with the concentration of 10^7 CFU/mL. These cells were lysed off-chip in the commercial fluorescence device (ESEQuant) at 92°C for 5 min. The lysed bacterial solution (70 µL) was stained with fluorescence dye PicoGreen (Concentration 0.5×). The paraffin oil (30 µL) was poured on top of lysate.

The electric potential of 10 Volts was applied between the lysis and amplification chamber through the embedded electrodes. The current of ~10 µA was recorded during these experiments. LumaScope (LS-500, Bioimager) fluorescence microscope with a 20× objective lens was used to record fluorescence images. The images were captured at the

intersection of connecting channel and amplification chamber. The presence of DNA at the entrance of the amplification chamber is shown in Figure 5.11.

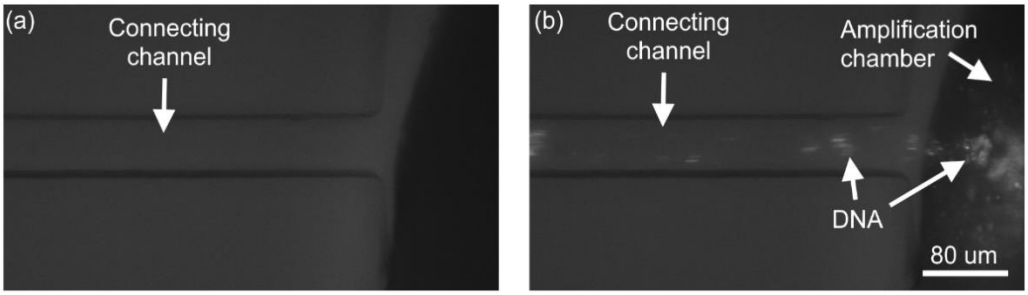

Figure 5.11 On-chip DNA transportation from lysis chamber to the amplification chamber under the applied potential of 10 Volts. (a) At t = 0 min, absence of DNA in the connecting channel. (b) At t = 3 min, DNA was present at the intersection of connecting channel and amplification chamber.

The electrophoretic force of attraction pulls the DNA molecules from the lysis chamber to the amplification chamber through the connecting channel. At t = 0 min, the section of the connecting channel close to the amplification chamber does not show any DNA molecules present. While, at t = 3min the DNA can be seen in that section, indicating that the electrophoretic force transported the DNA to the entrance of the amplification chamber. Subsequently, the DNA molecules entered the amplification chamber. Thus, extra time of t = 10 min was selected to ensure the sufficient quantity of DNA is successfully transportation at even low concentrations.

5.3.2.2 Applied potential optimization for on-chip DNA transportation

The optimization of the applied potential is an essential parameter for the successful operation of a microfluidic device. As the higher applied potential could damage the LAMP reagents while the lower applied potential could fail to transport DNA or transportation of DNA could be time-consuming.

First, the negative reaction mixture of LAMP assays of 25 µL volume was prepared. Subsequently, both connecting channel and amplification chamber were filled with the negative reaction mixture of LAMP assays (~15 µL). Then, the tape was used to seal the amplification chamber. Afterwards, the 1×PBS (70 µL) was loaded in the lysis chamber, and paraffin oil (30 µL) was poured on top of it. Then, the various electric potentials (V = 100, 50, 20, 10, 0 Volts) were applied for 10 min to the multiple samples. For each applied potential these tests were performed in triplicate. Negative samples of LAMP assays were collected from the microfluidic device after they were exposed to the electric potential. Then, the volume of 5 µL of the DNA template (Concentration: 10^7/5 µL) was added to the each collected sample. Then, collected samples were amplified off-chip in the commercial fluorescence device (ESEQuant). The results of amplification reactions are presented in Figure 5.12.

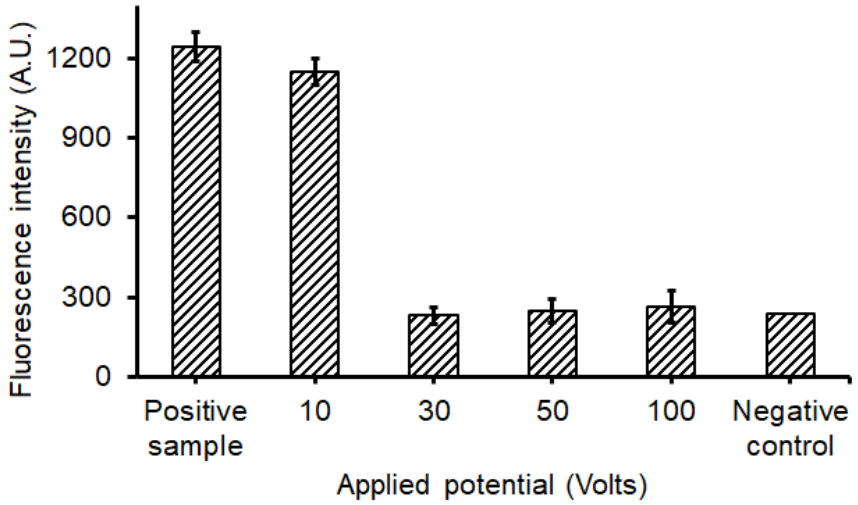

Figure 5.12 Effect of applied electric potential on the LAMP assays. [Commercial fluorescence device (ESEQuant) measured the intensity originally in mV].

The end-point fluorescence intensity of samples those were exposed to the electric potential was compared with the unexposed samples. End-point fluorescence intensities of samples those were exposed to the higher electric potential of 100, 50, and 30 Volts were similar to the negative samples (~250 A.U.). These results indicated that the

operation of a microfluidic device would be compromised if the LAMP assays were to be exposed to the higher electric potential. The end-point fluorescence intensity of the samples those were exposed to the lower electric potential of 10 Volts was similar to the end-point fluorescence intensity of unexposed samples (~1200 A.U.). Thus, the electric potential of 10 Volts was selected as the electric potential for DNA transportation.

5.3.2.2.1 Transportation of DNA using LAMP assays

Transportation of DNA from the lysis chamber to the amplification chamber was performed using the optimized parameters. Off-chip amplification of the LAMP assay confirmed transportation of DNA. Initially, the negative reaction mixture (25 µL) was prepared and subsequently, both the amplification chamber and connecting channel were filled with the negative reaction mixture (~15 µL). The tape was used to seal the amplification chamber.

The bacterial cells solution in 1×PBS of various concentrations (10^7 to 10^2 CFU/mL) were used to test DNA transportation. First, bacteria cells were lysed off-chip in the commercial fluorescence device (ESEQuant) at 92°C for 5 min. Then, the lysate of bacterial cells (70 µL) was loaded in the lysis chamber. Afterwards, the paraffin oil (30 µL) was poured on top of the bacterial lysate solution in the lysis chamber. The electric potential of 10 Volts was applied for t = 10 min. Finally, samples were collected from the amplification chamber using the pipette. These collected samples were amplified off-chip using the commercial fluorescence device (ESEQuant) at 65°C. DNA transportation for each concentration was performed in triplicate. For negative reactions, the lysate of bacteria cells was replaced with the 1×PBS. Results of amplification reactions of LAMP assays those were collected from the amplification chamber after the transportation of DNA are shown in Figure 5.13.

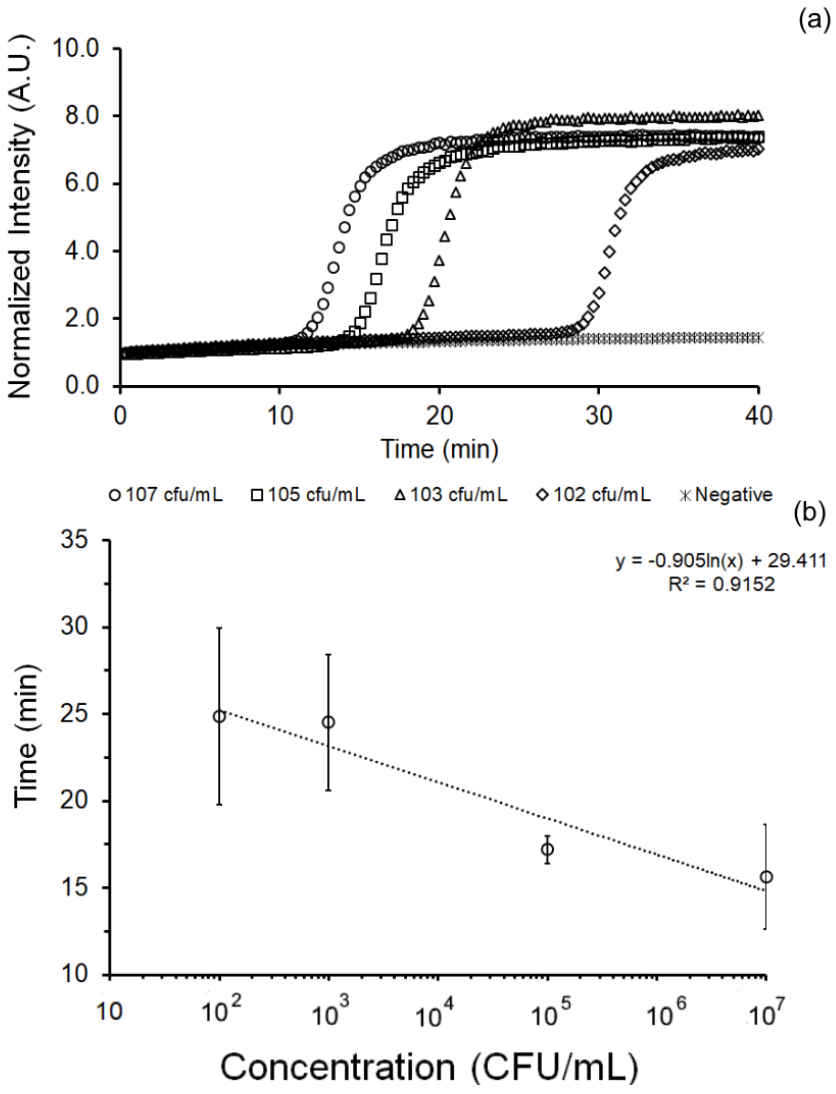

Figure 5.13 On-chip transportation of DNA in the microfluidic device. (a) Off-chip real-time amplification curves of LAMP assays for DNA transported from lysis chamber and collected from the amplification chamber. (b) Quantitative analysis of amplification reactions of LAMP assays. [Commercial fluorescence device (ESEQuant) measured the intensity originally in mV].

Standard s-shaped DNA amplification curves demonstrate that the DNA was successfully transported from the lysis chamber to the amplification chamber. The samples with high concentration of lysate of bacteria cells amplified earlier than the samples with the lower concentration. Subsequently, could be due to the lesser number of DNA molecules that are transported to the amplification chamber in case of the samples

of lower concentration. Negative control reaction shows no amplification as expected to indicate the absence of any contamination.

The quantitative analysis was performed and concentration of lysate of bacteria cells was plotted against the threshold time for DNA amplification. The threshold time for the positive reactions was chosen as the time at which the fluorescence intensity of the reactions reached the intensity level of 50% above the intensity of negative control reactions. The threshold time increased with the decrease in concentration (10^7 to 10^2 CFU/mL) of lysate bacteria cells.

The quantitative analysis was performed, and concentration of lysate of bacteria cells was plotted against the threshold time for DNA amplification. The threshold time for the positive reactions was chosen as the time at which the fluorescence intensity of the reactions reached the intensity level of 50% above the intensity of negative control reactions. The threshold time increased with the decrease in concentration (10^7 to 10^2 CFU/mL) of lysate bacteria cells.

5.3.3 On-chip DNA amplification

On-chip DNA amplification was performed in the microfluidic device. The schematics of the device is shown in Figure 5.14.

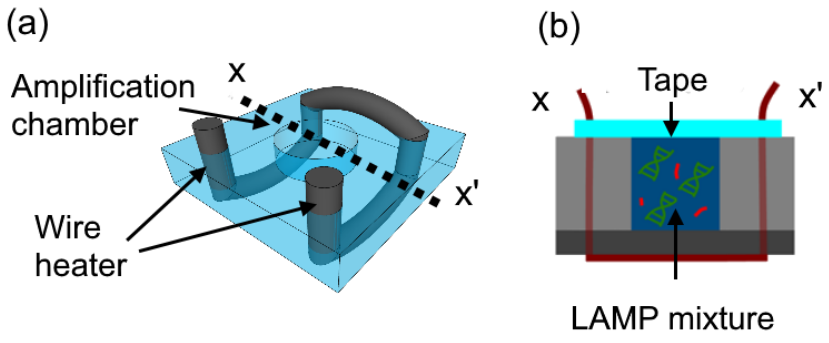

Figure 5.14 Microfluidic device for on-chip DNA amplification. (a) Schematics of a microfluidic amplification device. (b) Cross-sectional view of a microfluidic amplification device.

The LAMP reaction mixture was loaded in the amplification chamber using the pipette. Then, the microfluidic amplification device was sealed with the tape. The LAMP reaction mixture of 25 µL volume was prepared (Master mix 14.62 µL, Primer mix 5 µL, Eva green 0.38 µL, DNA template 5 µL). The volume of ~ 5 µL of the reaction mixture was loaded in the amplification device. For negative reactions, the DNA template was replaced with the ddH_2O. The amplification reactions for each concentration was performed in triplicate.

5.3.3.1 Temperature control of a microfluidic amplification device

The temperature of the amplification chamber was maintained using the two methods, using the feedback system and without the feedback system. The transient temperature response of the amplification chamber without using the feedback system is shown in Figure 5.15. It showed that various steady-state temperatures could be obtained by controlling the input power. The steady-state temperature of 30-70˚C was achieved with the increase in the input power from 0.23 to 1.08W. In many cases, it is required a longer time of 20 min to reach the steady state temperature. This mode of operation can be used when the time for analysis is not an issue and cost of the device, and its instrumentation is critical.

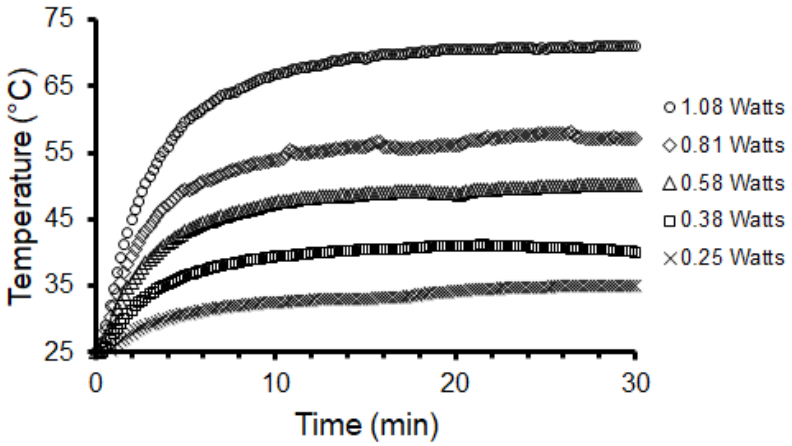

Figure 5.15 Temperature response of the amplification chamber of a microfluidic device for on-chip DNA amplification without using the temperature controlling system.

As an alternate strategy, the amplification temperature (~65°C) was maintained in the microfluidic device using a feedback system. The temperature response is shown in Figure 5.16.

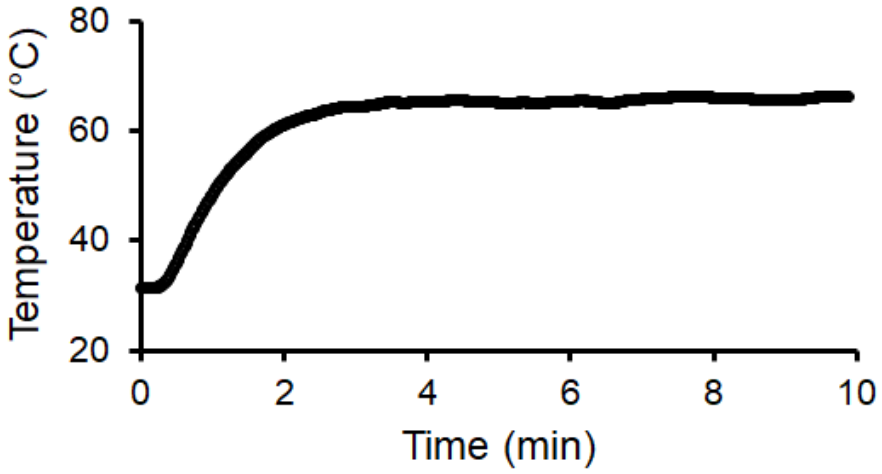

Figure 5.16 Temperature response of the amplification chamber of a microfluidic device for on-chip DNA amplification using the temperature controlling system.

The amplification temperature of ~65˚C was maintained in the amplification chamber. Five devices were tested, and the amplification temperature was maintained with the variation of ± 1˚C. The time required to reach the set point was 3.5 ± 0.3 min for the tested devices. The thermal response was ~4 times faster when the temperature controller was used.

5.3.3.2 Detection of LAMP assays

DNA amplification of LAMP assays was detected using the two approaches. Initially, the off-chip end-point fluorescence intensity of amplified samples was measured. Then, on-chip real-time amplification of LAMP assays was detected by in-situ measuring the fluorescence intensity.

5.3.3.2.1 End-point detection of LAMP assays

The positive samples of LAMP assays (25 µL) of various concentrations (10^8-10^3 DNA/reaction) were loaded in the microfluidic device. The devices with the chamber size of ~30 µL were used for this set of experiments. For negative control, DNA template was replaced with the ddH_2O. Then, the device was sealed with the tape. The temperature of the amplification chamber was maintained at ~65°C for 30 min. Then, the amplified samples were extracted from the microfluidic device, and off-chip end-point fluorescence intensity was measured using the commercial fluorescence device (ESEQuant). The amplification results are shown in Figure 5.17.

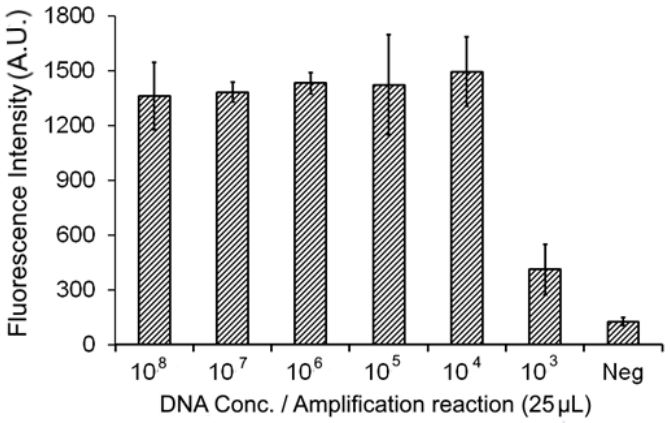

Figure 5.17 Off-chip end-point detection of LAMP assays in the commercial fluorescence device (ESEQuant). [Commercial fluorescence device (ESEQuant) measured the intensity originally in mV].

The triplicates of amplification reactions were performed for each concentration. Subsequently, the average value of end-point fluorescence intensity for each concentration was plotted. The standard deviation represents the variation in the end-point fluorescence intensity of three reactions of each concentration. End-point fluorescence intensities of positive samples (10^8 to 10^4 DNA molecules/reaction) was ~ 7 folds higher compared to the negative controls subsequently, demonstrate the successful DNA amplification. The end-point fluorescence intensity of the sample of lowest concentration (10^3 DNA molecules/reaction) was ~ 2-fold higher compared to the negative control. All the samples

were amplified for 30 min in the microfluidic device. As a result, the low concentration reaction did not reach the saturation point and consequently shows the lower level of fluorescence intensity.

5.3.3.2.2 Real-time detection of LAMP assays

Real-time amplification reactions of LAMP assays were performed in the microfluidic device during the second phase of testing. The master mix (14.62 µL), primer mix (5 µL), Eva green 0.5× (0.38 µL) and, DNA template (5 µL) were added to make the LAMP reaction mixture (25 µL). For negative control reactions, DNA template was replaced with the ddH_2O. The volume of ~15 µL was loaded in the amplification chamber for each concentration ($6x10^1$ to $6x10^6$ DNA molecules/reaction). The tape was used to seal the amplification chamber. The amplification reaction for each concentration was performed at ~65°C in triplicate. The CCD camera-based fluorescence imaging system was used to record the real-time sequential images during the amplification reactions.

First, real-time DNA amplification of LAMP assays is presented in the sequential images format as shown in Figure 5.18. LAMP amplification mixture (~15 µL) with the DNA concentration $6x10^6$ DNA molecules/reaction was amplified at ~65°C. The fluorescence intensity was at the baseline intensity level at the start of the reaction (At t = 0 min). The fluorescence intensity started to increase at t = 10 min. Afterwards, the fluorescence intensity was increased rapidly and subsequently, reached the maximum fluorescence intensity level at t = 17.3 min.

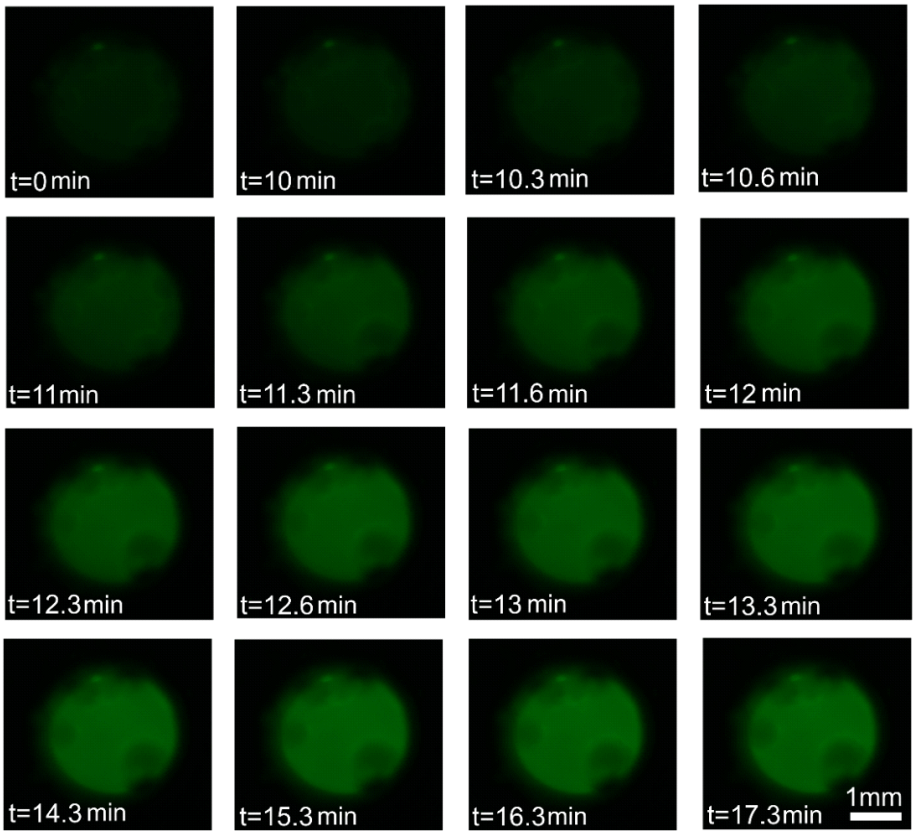

Figure 5.18 Sequential images demonstrate the on-chip real-time amplification (~65°C) of LAMP assays.

Standard s-shaped amplification curves for LAMP assays were plotted in Figure 5.19a.

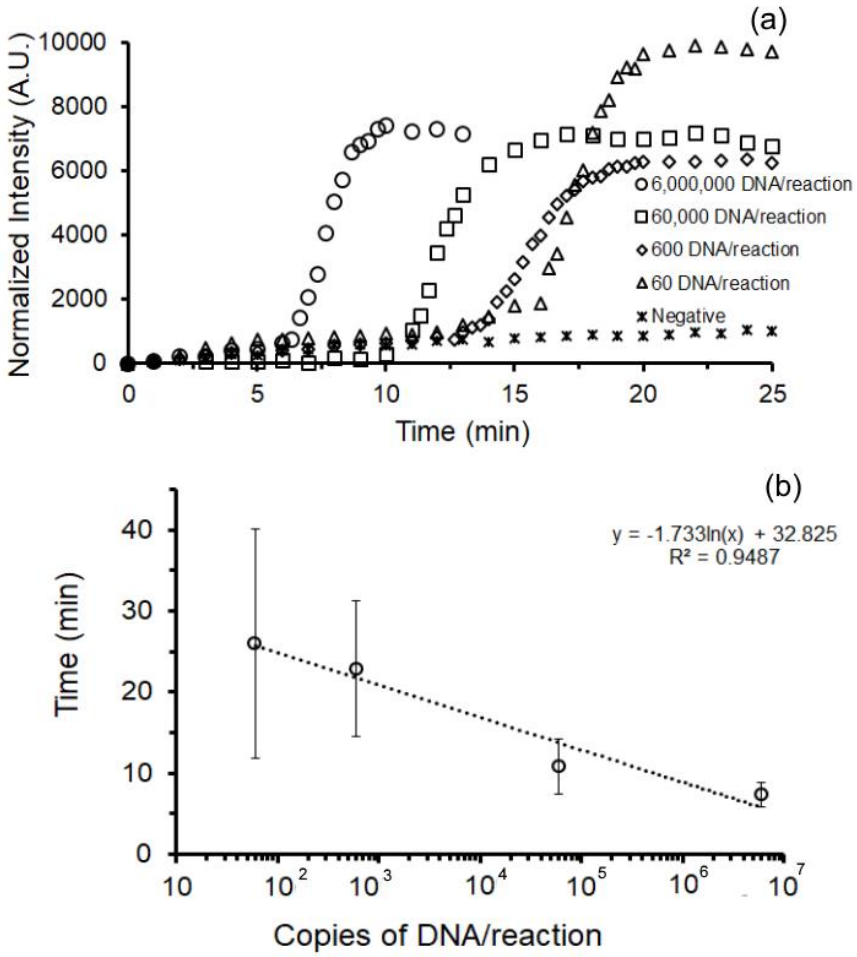

Figure 5.19 On-chip real-time detection of LAMP assays. (a) Real-time amplification curves for LAMP assays. (b) Quantitative analysis of LAMP assays.

S-shaped amplification curves for the samples of various DNA concentrations were plotted in Figure 5.19a. The fluorescence intensity was normalized and plotted as a function of time. The rapid increase in the fluorescence intensity demonstrates the DNA amplification. For quantitative analysis, the threshold time was plotted as a function of sample concentration (DNA copies/reaction) as shown in Figure 5.19b. The threshold time for the positive reactions was chosen as the time at which the fluorescence intensity of each reaction reached the intensity level of 50% above the intensity of the negative control reaction.

The threshold time for the amplification increased with the decrease in sample concentration. The threshold time was decreased from the from 26 ± 14 to 7.3 ± 1.5 min, as the DNA copies were increased from 60 to 6,000,000 DNA copies/reaction (Reaction volume ~15 µL). The samples with low concentrations show high variation in the threshold time required to amplify DNA possibly because of two reasons. First, sequential pipetting steps were involved in preparing the samples of low concentrations that subsequently increased the variation in initial concentrations of samples. Secondly, this variation in the initial concentrations propagate with the amplification reaction and consequently brought high variation in the threshold amplification time. Thus, DNA was amplified using the LAMP assays in a microfluidic device.

5.4 Operation of a microfluidic device with the integrated coupled components

The operation of a microfluidic device with the two integrated components was tested in the second phase of experiments. First, the microfluidic component of bacteria lysis was integrated with the component for DNA transportation. Then, the microfluidic device for the DNA transportation was integrated with the component for DNA amplification.

5.4.1 On-chip bacteria lysis and DNA transportation

On-chip bacteria cells were lysed, and subsequently, DNA was transported in the integrated microfluidic device. The schematics of a microfluidic device is shown in Figure 5.20.

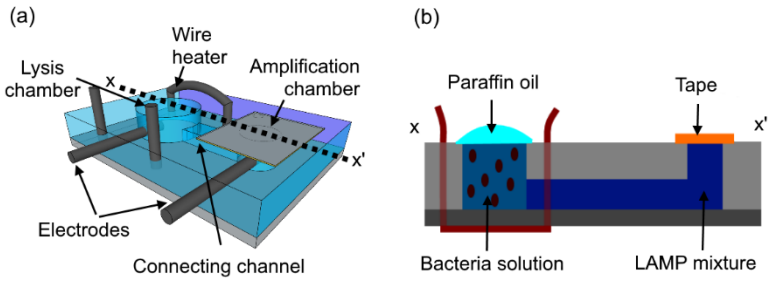

Figure 5.20 Microfluidic device with the integrated components of bacteria lysis and DNA transportation. (a) Schematics of a microfluidic device. (b) A cross-sectional view of a microfluidic device.

Initially, the negative reaction mixture of LAMP assay (25 µL) was prepared. Then, both connecting channel and the amplification chambers were filled with the ~15 µL of the negative reaction mixture. The tape was used to seal the amplification chamber. Then, the bacteria cells suspended in 1×PBS with the concentration of 10^7CFU/mL (70 µL) was loaded in the lysis chamber and subsequently, paraffin oil (30 µL) was poured on the top in the lysis chamber. The bacterial solution was replaced with the 1×PBS (70 µL) for the negative control.

Thermal lysis of bacterial cells was performed in the lysis chamber by maintaining the temperature of ~92°C for 5 min. Then, the electric potential of 10 Volts was applied between the lysis and amplification chambers for 10 min. Afterwards, the LAMP reaction mixture was collected from the amplification chamber. Finally, LAMP assays were amplified off-chip in the commercial fluorescence device (ESEQuant). The results of amplification reactions are presented in Figure 5.21.

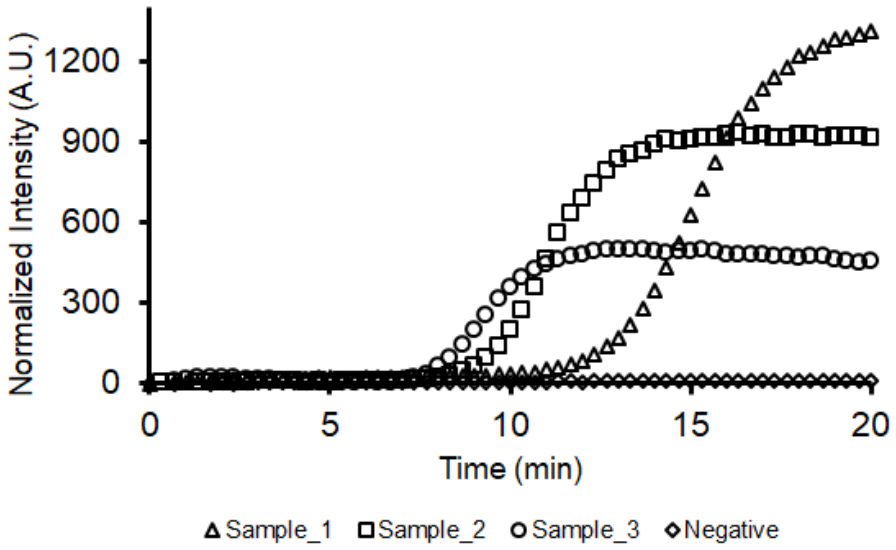

Figure 5.21 Off-chip real-time amplification curves of LAMP assays for the samples collected from the amplification chamber. Thermal lysis was performed at 92°C for 5 min and DNA transportation for 10 min under the applied potential of 10 Volts. [Commercial fluorescence device (ESEQuant) measured the intensity originally in mV].

The standard s-shape amplification curves for LAMP assays were plotted for the samples treated in the three different devices. The amplification curves were normalized by subtracting the mean value of the first three fluorescence intensities from the values of the specific amplification curve. The rapid increase in fluorescence intensity with time demonstrates the amplification of DNA. The amplification curves show that the bacteria cells were lysed in the lysis chamber and subsequently, DNA was transported to the amplification chamber. The negative control reaction indicates the absence of contamination. In conclusion, the microfluidic device successfully lysed the bacteria and transported the DNA under the optimized operational conditions.

5.4.2 On-chip DNA transportation and amplification

On-chip operations of DNA transportation and amplification were also performed in the integrated format. Two operations were integrated to demonstrate the successful

operation of this segment of the devices. The schematics of a microfluidic device with the integrated components of DNA transportation and amplification is shown in Figure 5.22.

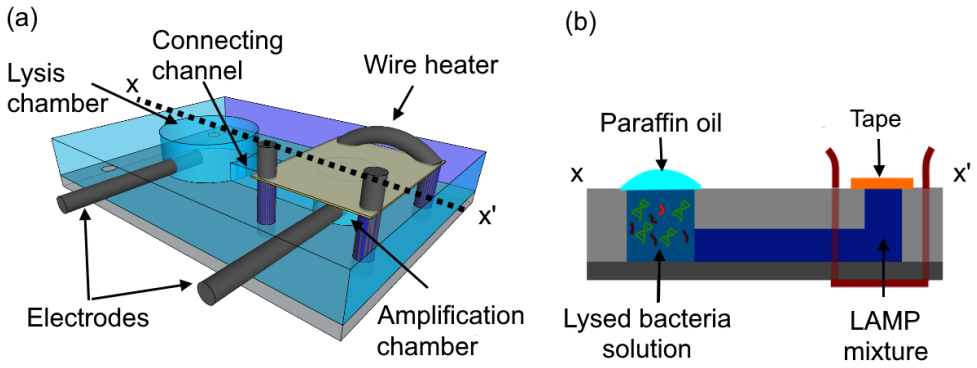

Figure 5.22 Microfluidic device with the integrated components of DNA transportation and amplification. (a) Schematics of a microfluidic device. (b) A cross-sectional view of a microfluidic device.

Negative control of LAMP assays of the volume of 25 µL was prepared. Then, the volume of ~15 µL was filled in the amplification chamber and connecting channel. Afterwards, the amplification chamber was sealed with the tape. The bacteria cells solution was prepared in 1×PBS with the concentration 10^7 CFU/mL. The sample was loaded in the commercial fluorescence device (ESEQuant). The bacteria cells were lysed off-chip at 92°C for 5 min. Subsequently, the bacterial lysate (70 µL) was loaded in the lysis chamber of the microfluidic device. Then, the lysis chamber was covered with the paraffin oil (30 µL). Bacterial lysate was replaced with the 1×PBS (70 µL) for negative control.

Initially, the electric potential of 10 Volts was applied between the lysis and amplification chambers for 10 min. Consequently, the amplification chamber was exposed to the temperature of ~65°C for 30 min. Finally, the samples were collected from the amplification chamber, and end-point fluorescence intensities were measured off-chip in the commercial fluorescence device (ESEQuant). The results of end-point fluorescence intensities of amplified samples are shown in Figure 5.23.

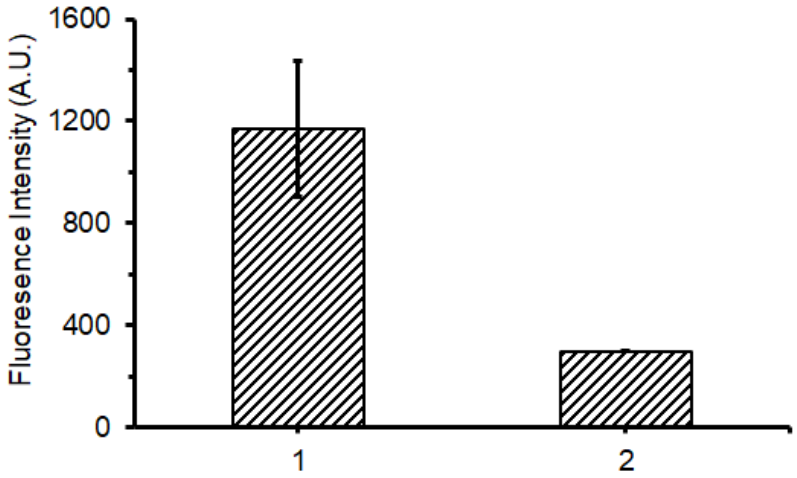

Figure 5.23 Off-chip end-point detection of LAMP assays collected from the amplification chamber for the DNA transported from the lysis chamber. [Commercial fluorescence device (ESEQuant) measured the intensity originally in mV].

The average value of end-point fluorescence intensities of three samples those were treated in the three different microfluidic devices was plotted. The standard deviation demonstrates the variation in the end-point fluorescence intensities. The end-point fluorescence intensities of positive samples (~1150 A.U.) was ~ 4-fold higher compared to the negative control (~ 300 A.U.). In conclusion, the DNA was successfully transported and amplified in the microfluidic device.

5.5 Operation of an integrated microfluidic device

Microfluidic device with the operation of all three components in the integrated format is presented. The schematic of a microfluidic device is shown in Figure 5.24.

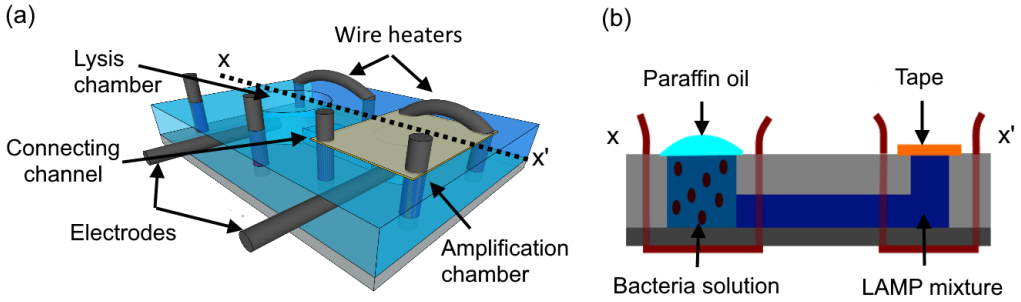

Figure 5.24 Microfluidic device with the three integrated components of bacteria lysis, DNA transportation, and amplification. (a) Schematics of a microfluidic device. b) A cross-sectional view of a microfluidic device.

The negative reaction mixtures (~15 µL) of LAMP assays were loaded in the connecting channel and amplification chamber. Then, the tape was used to seal the amplification chamber. The bacterial solutions of various concentrations (10^7,10^5,10^3,10^2 CFU/mL) were prepared in 1xPBS. The bacterial solution was loaded in the lysis chamber (70 µL) and covered with the paraffin oil (30 µL). Initially, bacteria cells were thermally lysed in the lysis chamber at 92°C for 5 min. Then, the electric potential of 10 Volts was applied to transport DNA from the lysis chamber to the amplification chamber. Finally, DNA was amplified in the amplification chamber at ~65°C. Two approaches were followed to detect the amplified DNA, off-chip end-point or on-chip real-time fluorescence intensity measurement. The commercial fluorescence device (ESEQuant) was used to measure the off-chip end-point fluorescence intensity while a CCD camera-based imaging system was used to measure the on-chip real-time fluorescence intensity.

First, the complete operation of the device was demonstrated by end-point fluorescence intensity measurement of LAMP assays in off-chip format. The bacterial sample (70 µL) was loaded in the lysis chamber of the device with the sample concentration of 10^7 CFU/mL. Bacteria samples were replaced with the 1×PBS for negative control. Repeatability of experiments was verified by testing the bacterial samples in 5 different devices. The amplification results of transported DNA are shown in Figure 5.24.

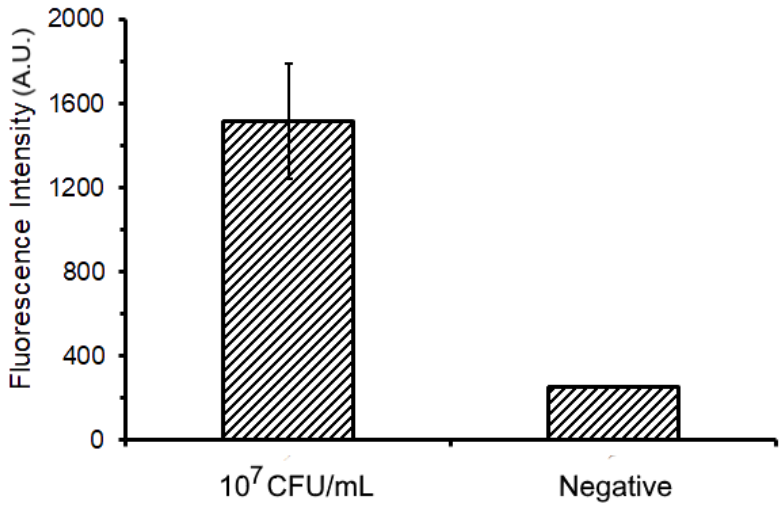

Figure 5.25 Off-chip end-point detection of LAMP assays to demonstrate the integrated operation three components of a microfluidic device. [Commercial fluorescence device (ESEQuant) measured the intensity originally in mV].

End-point fluorescence intensity of LAMP assays (~1500 A.U.) for the transported DNA from lysis chamber to the amplification chamber was ~6-fold higher than the negative control (250 A.U.). The higher end-point fluorescence intensity of positive samples shows that the bacteria was successfully lysed. Subsequently, DNA was transported from the lysis chamber to the amplification chamber. And finally, the transported DNA amplified in the amplification chamber.

Second, complete operation of a microfluidic device is demonstrated by measuring the in-situ fluorescence intensity in the real-time format. The s-shaped amplification curves show the amplification results in Figure 5.26a. The fluorescence intensity values were normalized (0-1) to compare the results of samples with various concentrations. The amplification time was increased with the decrease in sample concentrations. For quantitative analysis, the sample concentration was plotted against the threshold time (Figure 5.26b). Threshold time was defined as the time at which the fluorescence intensity was increased 50% higher than the baseline intensity. The samples with low concentrations show high variation in the threshold time required to amplify DNA possibly because of two reasons. First, sequential pipetting steps were involved in

preparing the samples of low concentrations that subsequently increased the variation in initial concentrations of samples. Secondly, during bacterial lysis and DNA transportation process there is a possibility of sample loss. Samples with low concentrations were affected more be in comparison to samples with high concentrations. This variation in the in the transported DNA propagated with amplification reactions and consequently caused high variations in threshold amplification time of samples with low concentrations.

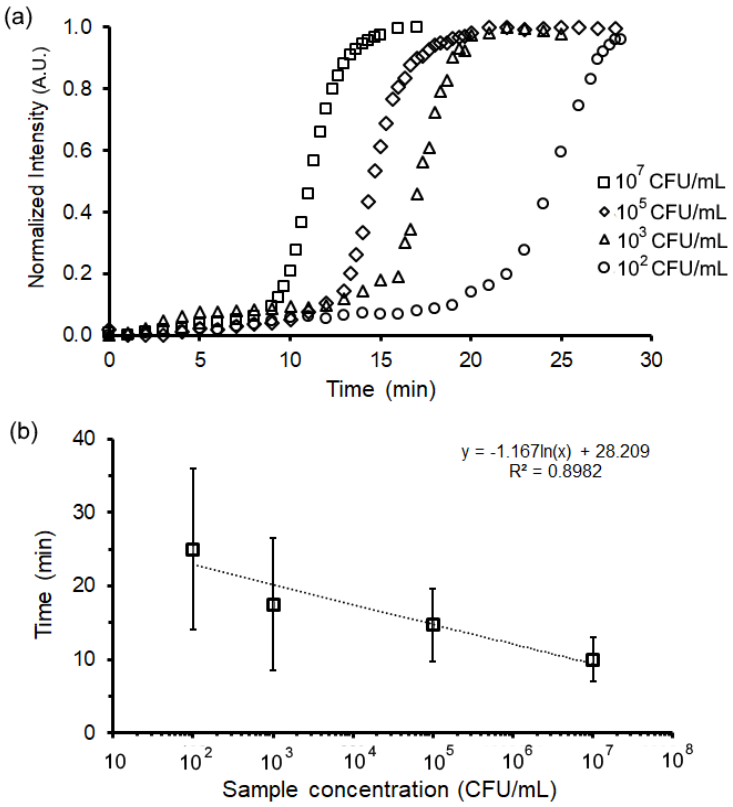

Figure 5.26 On-chip real-time detection of LAMP assays to demonstrate the integrated operation of three components of a microfluidic device. (a) On-chip real-time amplification curves of LAMP assays for the DNA transported to the amplification chamber after bacteria cells were lysed in the lysis chamber. (b) Quantitative analysis of amplification reactions of LAMP assays.

5.6 Summary

In this chapter, the design of a microfluidic device including device operation and characterization of operational parameters were explained. Then, fabrication of the device using the silicon master mold, PDMS, and integration of wire heaters was illustrated. Afterwards, methods those were used to prepare the bacterial samples and LAMP assays were demonstrated, followed by the sample loading technique. Finally, the operation of the device was explained in three steps, the operation of individual components, the operation of the two integrated components and the operation of a microfluidic device with the three integrated components.

Chapter: 6 Conclusion and future work

6.1 Conclusion

The pathogenic microorganism can contaminate water or food even at low concentration. These contaminated foods or water can be fatal for a human being. Early detection of such samples is essential for healthy human life. According to the World Health Organization (WHO), millions of people are affected by foodborne or waterborne diseases each year. Conventional culture-based detection methods are time-consuming, labour intensive and not suitable for on-site testing. Recently, nucleic acid-based detected methods have been developed. These methods are rapid, sensitive and quantitively detect the pathogens. Mainly, two approaches of polymerase chain reaction (PCR) and isothermal amplification methods were used to detect the pathogens. Microfluidic technology has been successfully used to develop the amplification-based device. Microfluidic technology offers several advantages such as using smaller volumes, rapid heating and cooling time, low cost and portability. Consequently, microfluidic-based devices are suitable for the rapid detection of pathogens in food or water sample. In conclusion, mainly two different approaches were used to develop the microfluidic-based devices for DNA amplification using the loop-mediated isothermal amplification (LAMP) assays.

6.1.1 Design and fundamentals of electrical tweezer and its applications

- A simple electromechanical probe (tweezers) has been developed that can manipulate a small aqueous droplet in a bi-layer oil phase. The tweezer consists of two needles positioned close to each other and used polarization of the aqueous droplet in an applied electrical field to confine the droplet between the needles with minimal solid contact.

- The oscillatory motion of droplet was studied under the influence of applied electric potential (AC). The oscillatory droplet motion was studied and characterized for applied electric potential and frequency. It was found that droplet oscillates with the high voltage electrode corresponding to the applied electric potential and frequency.

- Mechanical motion of the tweezer was used to perform various droplet-based operations such as transportation, extraction, and merging. First, the transportation of water droplet (5 µL) was characterized. Subsequently, the droplet was transported up to the speed of ~25mm/s. Second, electrical tweezer was used to extract the aqueous droplets (~12-80 µL) from the reservoir. Finally, electrical tweezer was used to merge the discrete droplets under the optimized operational conditions.

- Electrical tweezer was used to handle the biochemical assays. This application was demonstrated by performing the isothermal DNA amplification of LAMP assays. Initially, the droplets consisting of various components those were required to perform amplification assays, were transported and merged. Then, the merged droplet was transported and immobilized in the elevated temperature zone (~65˚C). Finally, off-chip end-point fluorescence intensity was measured to confirm the DNA amplification.

6.1.2 A low-cost heater integrated microfluidic device to perform integrated sample processing and detection of bacteria

- A low-cost microfluidic device has been developed which uses the electrical methods for on-chip sample preparation and isothermal DNA amplification. Various sequential operations such as lysis, transportation, and amplification were performed to detect the bacterial samples. The bacterial samples with the concentration up to 100 CFU/mL were detected in less than an hour.

- A low-cost fabrication method has been presented to integrate on-chip customized heating elements. Subsequently, these heating elements were used to create localized heating zones to perform operations such as lysis and amplification.

6.2 Future work

6.2.1 Future work suggestions for electrical tweezer

- Preliminary experiments show that the fundamental operation and applications of an electrical tweezer for low throughput applications. In the next phase, the electrical tweezer-based system can be upgraded and modified with various exciting features such as enhance in the portability, performing the operations in the integrated format for high throughput application. The schematics of such system is demonstrated in Figure 6.1.

- Multi electrical tweezers can be incorporated such that they can be operated simultaneously in the oil filled chamber. The throughput of the system can be enhanced by performing the various operations in a parallel format.
- A portable system can be developed by replacing the paraffin oil with the coconut oil. The coconut oil is in the solid state at the room temperature. So, the top, solid layer can serve as the cover, and bi-layer oil chamber can be transported easily.

- Pressure-driven flow system was used for droplet extraction. The portability of an electrical tweezer system can be enhanced by developing the system without the use of syringe pumps. Mainly two approaches can be used to develop such a system. First, the elevated water reservoir can be built and connected to the bi-layer oil medium. Subsequently, water will flow in the by layer oil chamber due to gravity. Then, electrical tweezer can be used to extract water droplets. Second, water-filled glass capillary tube can be attached to the bi-layer oil chamber in the horizontal format. Then, electrical force using the electrical tweezer can be applied to pull the water droplets from the capillary tube.

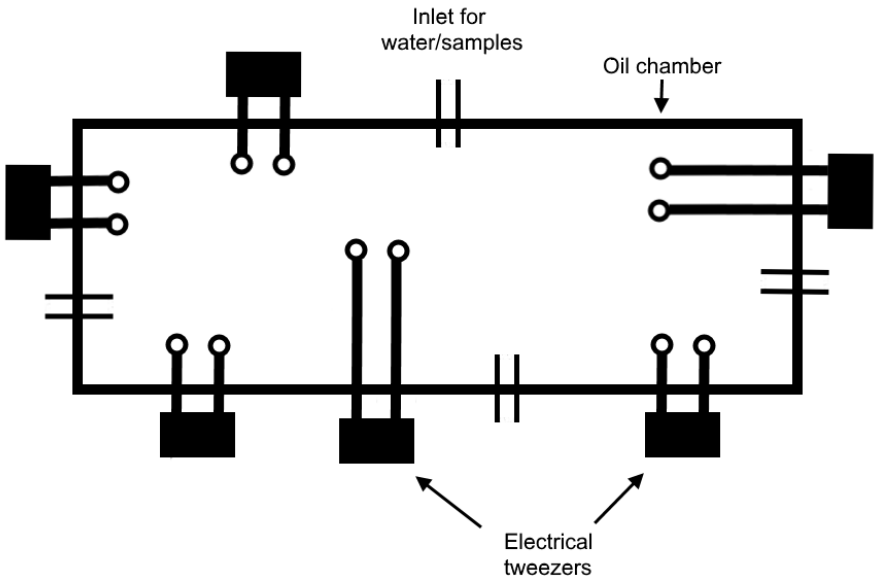

Figure 6.1 Schematics of an electrical tweezer system for high through the application.

6.2.2 Future work suggestions for microfluidic integrated device

- A low-cost fabrication method has been developed for on-chip integration of customized heating element. This current fabrication method is based on the manual embedding of the wires of the heating element, which make this process time consuming, labour intensive and lack of precision. This manual fabrication method is useful for the development of prototypes. Nevertheless, this fabrication method can be modified and upgraded for the scale-up manufacturing. The manual fabrication can be replaced by inserting the metallic wire using the CNC controlled sewing machine. For instance, such machines can precisely and rapidly embed the heating wires in the microfluidic device.

- Microfluidic device operation can be tested for the various bacterial and viral samples to show the diverse applicability of the device. Then, the microfluidic device can be used for the testing of clinical samples.

- The complete sample-to-answer based microfluidic device can be established in the next development phase. The integration of elution component with the current device can make it a complete sample-to-answer device. The swab is the main operational component for elution module. The swab is a low-cost device that can be used to collect various specimens such as the secretions from the throat, nose, buccal cavity, vagina, wound, and a small volume of blood. Then, this swab can be directly loaded in elution component of the microfluidic device. In the elution component, the pathogenic microorganisms can be extracted from the swab. Subsequently, the cells of microorganisms can be transported to lysis components. After cell lysis, the sequential operations can be performed in the microfluidic device (As mentioned in chapter 5) for the detection of pathogens.

Appendix A: Droplet oscillatory motion with the high voltage electrode

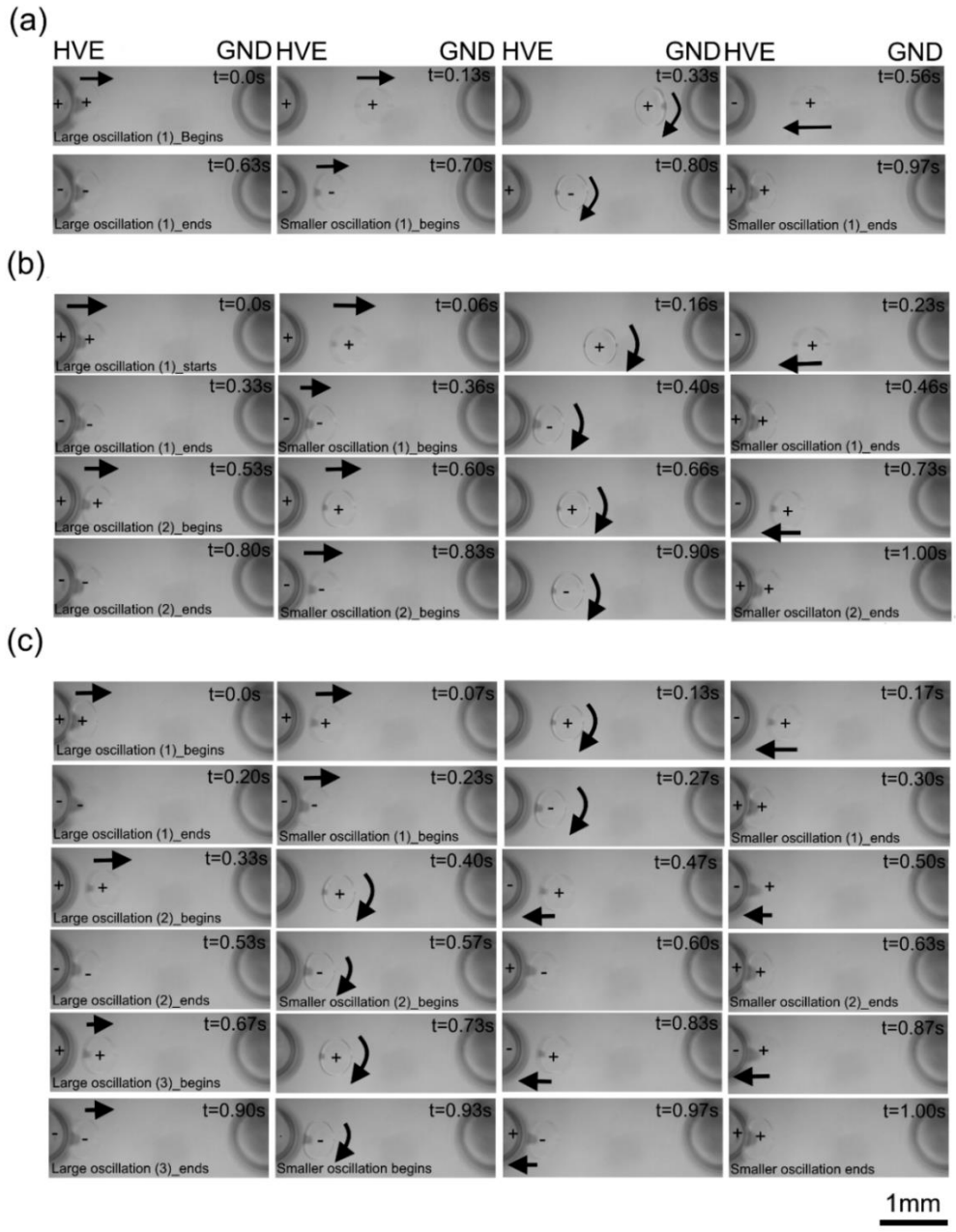

Figure A. 1 Droplet (0.3 µL) oscillatory motion with the high voltage electrode under the applied electric potential of V = 560 Volts (V_{Peak}/d = 140 V/mm) for the range of frequencies: (a) 1 Hz; (b) 2 Hz; and (c) 3 Hz.

Appendix B: Numerical simulation of electrical field between the electrodes

A two-dimensional numerical simulation was performed to understand the phenomenon of the smaller droplet oscillatory trip with the high voltage electrode. The electrostatics module in COMSOL Multiphysics 5.1 (COMSOL Inc., MA, USA) was used to plot the electric field distribution between the electrodes of the electrical tweezers. Initially, the 2D model was built in the COMSOL and shown in the (a). Then, the material properties of relative permittivity (ε_r): for paraffin oil ($\varepsilon_r = 2.2$) and stainless steel was used.

The following parameters were set for simulation.

1) Assumption
   a) A uniform temperature for the whole setup (293.15K)
   b) Charge conservation
2) Initial value V= 0 Volts (Applied to all the domains)
3) Boundary conditions

   Ground boundary condition was set for one electrode while the source electrode (high voltage electrode) condition was set for the second electrode. The boundary of oil medium was set with the zero charges ($n.D = 0$) because of the insulating properties of the oil medium. The following set of equations were used to perform the numerical simulation.

$$E = -\nabla V$$

$$\nabla . D = \rho_v$$

$$D = \varepsilon_o \varepsilon_r E$$

Where E is the electric field strength, V is the applied electric potential between the electrodes of the electrical tweezers, D is the electric displacement field, ε_o is the

permittivity of vacuum ($\varepsilon_o \approx 8.85 \times 10^{-12}\, F/m$). ε_r is the relative permittivity of the medium, ρ_v indicated the volume charge density of free charges in the material.

The mesh selection was one of the important steps to perform the numerical simulation. Initially, the mesh independency analysis was performed to check the accuracy of simulation results. The four different mesh sizes were tested (60, 120, 240 and 1200 µm) for the triangular mesh. The electric field (V/mm) was plotted on the central line along the x-axis joining the two electrodes. The central line was cut between the points (1.15, 2.5) to the point (4.85, 2.5). Therefore, the length of the line was 3.7 mm. The electric field distribution between electrodes is shown in Figure B.1.

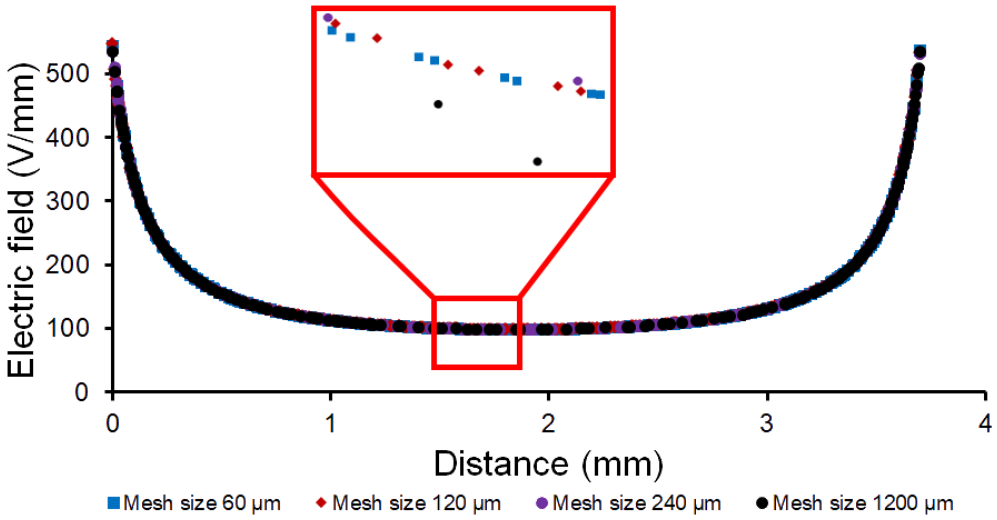

Figure B.1Mesh independency analysis. The electric field distribution along the central line (X-axis) between the electrodes of a tweezer.

It can be seen from Figure B.1that the mesh is converging with the decrease in decrease in the mesh size. The results were different when the mesh size of 1200 µm was used. However, the results are considered similar when the mesh sizes of 60, 120 and 240 µm were used. The element size parameters were selected: Maximum element size 120 µm; minimum element size 0.45 µm; Maximum element growth rate 1.2; curvature factor 0.25 and; resolution of narrow region 1.

In COMSOL a 2D cut line was plotted connected the high voltage electrode and ground electrode through center line. The electric field strength along the line was plotted for both positive and negative polarity (Figure B. 2).

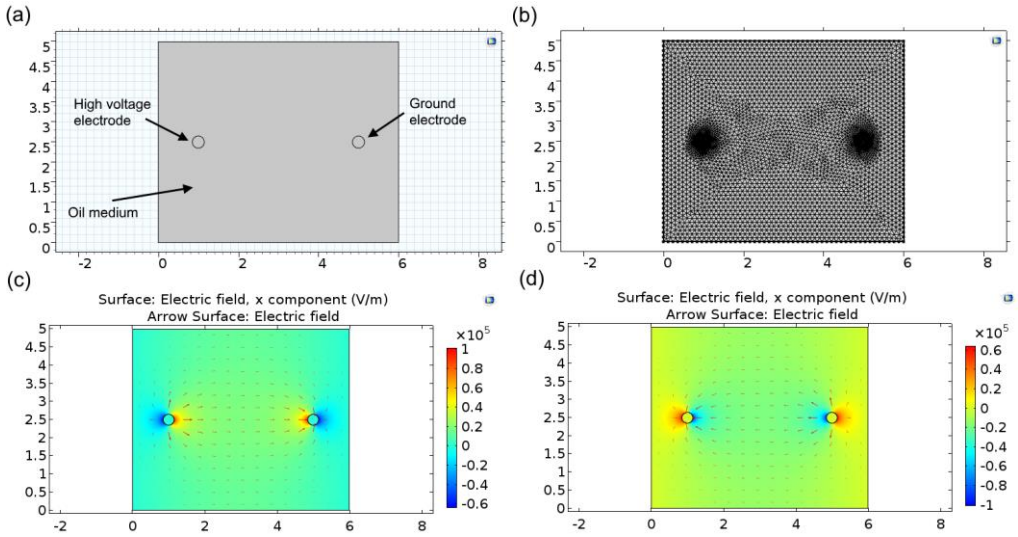

Figure B. 2 Schematic of numerical simulation. (a) 2-D geometry of the model. (b) Setting up the triangular mesh to the model. (c) Simulation results: electric field lines for a positive cycle of applied AC sinusoidal potential to the high voltage electrode. (d) Simulation results; electric field lines of applied AC sinusoidal potential to the high voltage electrode.

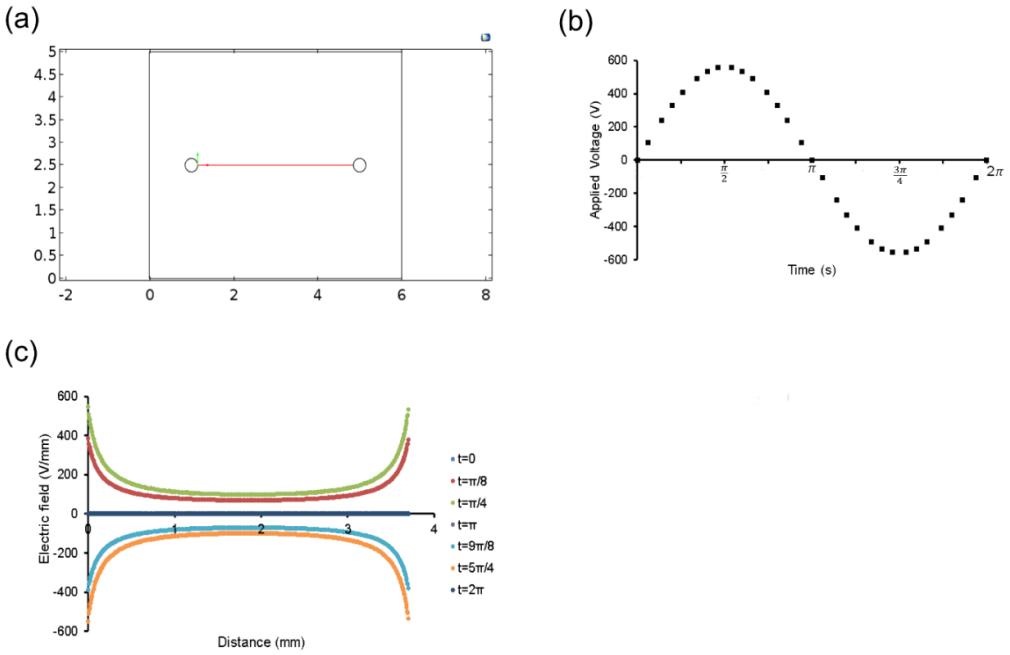

Figure B. 3 Numerical simulation of electric field potentials between the electrodes of electric tweezers. (a) A two-dimensional cut line was plotted to draw electric field between electrodes. (b) Applied sinusoidal electric potential to the electrodes. (c) Electric field strength between the electrodes for applied electric potential.

Appendix C: Microfabrication of master mold

- AutoCAD (Autodesk Inc., San Rafael, CA, USA) was used to design the mask.
- Silicon wafer (3") was put in the acetone for 1 minute.
- Silicon wafer (3") was put in the methanol for 1 minute
- Rinse the wafer with the DI water.
- Silicon wafer was treated with oxygen plasma at 50 watts for 1 min to remove residue on the top surface.
- Negative photoresist SU-8 (2075, MicroChem, Westborough, MA, USA) was poured on the silicon. The photoresist-covered ~1/3 of total wafer area.
- Silicon wafer was spun at 3500 rpm for 30 s.
- Silicon wafer was soft baked at 65˚C for 1 min and 17 s.
- Silicon wafer was baked at 95°C for 7 min 17 s.
- Silicon wafer and mask were loaded on the mask aligner.
- Silicon wafer was exposed to UV light (365 nm) with the power of 5.1 mW for 35s.
- The post-baking process was performed.
- Silicon wafer was baked on the hot plate at 65°C for 1 min 25 s.
- Silicon wafer was baked at 95°C for 6 min 25 s.
- Wafer was put in the SU-8 developer 10 min to remove unexposed photoresist.
- Silicon wafer was rinsed with Isopropyl Alcohol (IPA).
- Silicon wafer was rinsed with deionized water (DI).
- Silicon wafer was placed on a hot plate at 120°C for 1 h to increase the lifetime
- Microcontact printing
- The prepared prepolymer in the volumetric ratio of 1:3 (Base: Curing agent).
- Prepolymer was poured on the silicon wafer to cover the ~1/3 of the total area of a wafer.
- Silicon wafer was spun at 7000 rpm for 120 s.
- Top and bottom PDMS layers were stamped on the thin layer of a prepolymer.

- Stamped surfaces of PDMS were bonded together by contacting both surfaces.
- Bonded layers were placed at room temperature overnight ~16h for curing.
- The bonded device was placed on the hot plate at 75°C for 1 h.

References

[1] World Health Organization (WHO), “A global overview of national regulations and standards for drinking-water quality,” 2018.

[2] World Health Organization (WHO), “Water Sanitation & Hygiene,” *WHO*, 2015. [Online]. Available: http://www.who.int/water_sanitation_health/diseases-risks/diseases/diarrhoea/en/.

[3] World Health Organization (WHO), “Diarrhoeal disease: Key facts,” *WHO*, 2013. [Online]. Available: http://www.who.int/mediacentre/factsheets/fs330/en/.

[4] World Health Organization (WHO), “Emergencies preparedness , response,” *WHO*, 2014. [Online]. Available: http://www.who.int/csr/disease/meningococcal/en/.

[5] T. M. Arthur, J. M. Bosilevac, X. Nou, and M. Koohmaraie, “Evaluation of culture- and PCR-based detection methods for Escherichia coli O157:H7 in inoculated ground beef,” *J. Food Prot.*, vol. 68, no. 8, pp. 1566–1574, 2005.

[6] O. Lazcka, F. J. Del Campo, and F. X. Muñoz, “Pathogen detection: A perspective of traditional methods and biosensors,” *Biosens. Bioelectron.*, vol. 22, no. 7, pp. 1205–1217, 2007.

[7] G. T. Walker, M. S. Fraiser, J. L. Schram, M. C. Little, J. G. Nadeau, and D. P. Malinowski, “Strand displacement amplification--an isothermal, in vitro DNA amplification technique.,” *Nucleic Acids Res.*, vol. 20, no. 7, pp. 1691–6, Apr. 1992.

[8] M. Vincent, Y. Xu, and H. Kong, “Helicase-dependent isothermal DNA amplification.,” *EMBO Rep.*, vol. 5, no. 8, pp. 795–800, Aug. 2004.

[9] J. Compton, “Nucleic acid sequence-based amplification,” *Nature*, vol. 350, no. 6313, pp. 91–92, 1991.

[10] D. Liu, S. L. Daubendiek, M. A. Zillman, K. Ryan, and E. T. Kool, “Rolling circle DNA synthesis: Small circular oligonucleotides as afficient templates for DNA polymerases,” *J Am Chem Soc*, vol. 118, no. 7, pp. 1587–1594, 1996.

[11] J. Baner, M. Nilsson, M. Mendel-Hartvig, and U. Landegren, “Signal amplification of padlock probes by rolling circle replication,” *Nucleic Acids Res.*, vol. 26, no. 22, pp. 5073–5078, 1998.

[12] O. Piepenburg, C. H. Williams, D. L. Stemple, and N. A. Armes, “DNA detection using recombination proteins,” *PLoS Biol.*, vol. 4, no. 7, pp. 1115–1121, 2006.

[13] T. Notomi *et al.*, “Loop-mediated isothermal amplification of DNA.,” *Nucleic Acids Res.*, vol. 28, no. 12, p. E63, Jun. 2000.

[14] K. Mullis, F. Faloona, S. Scharf, R. Saiki, G. Horn, and H. Erlich, “Specific enzymatic amplification of DNA in vitro: The polymerase chain reaction,” *Cold Spring Harbor Symposia on Quantitative Biology*, vol. 51, no. 1. pp. 263–273, 1986.

[15] Y. Zhang and H. R. Jiang, “A review on continuous-flow microfluidic PCR in droplets: Advances, challenges and future,” *Analytica Chimica Acta*, vol. 914. pp. 7–16, 2016.

[16] B. Bruijns, A. van Asten, R. Tiggelaar, and H. Gardeniers, “Microfluidic devices for forensic DNA analysis: A review,” *Biosensors*, vol. 6, no. 3, pp. 1–35, 2016.

[17] C. D. Ahrberg, A. Manz, and B. G. Chung, “Polymerase chain reaction in microfluidic devices,” *Lab Chip*, vol. 16, no. 20, pp. 3866–3884, 2016.

[18] F. Ahmad and S. A. Hashsham, “Miniaturized nucleic acid amplification systems for rapid and point-of-care diagnostics: A review,” *Anal. Chim. Acta*, vol. 733, pp. 1–15, 2012.

[19] C. Zhang and D. Xing, “Miniaturized PCR chips for nucleic acid amplification and

analysis: Latest advances and future trends," *Nucleic Acids Res.*, vol. 35, no. 13, pp. 4223–4237, 2007.

[20] C. Zhang, J. Xu, W. Ma, and W. Zheng, "PCR microfluidic devices for DNA amplification," *Biotechnol. Adv.*, vol. 24, no. 3, pp. 243–284, 2006.

[21] L. J. Kricka and P. Wilding, "Microchip PCR.," *Anal. Bioanal. Chem.*, vol. 377, no. 5, pp. 820–5, Nov. 2003.

[22] I. Erill, S. Campoy, N. Erill, J. Barbé, and J. Aguiló, "Biochemical analysis and optimization of inhibition and adsorption phenomena in glass – silicon PCR-chips," *Sensors Actuators B*, vol. 96, pp. 685–692, 2003.

[23] Z. Q. Niu, W. Y. Chen, S. Y. Shao, X. Y. Jia, and W. P. Zhang, "DNA amplification on a PDMS–glass hybrid microchip," *J. Micromechanics Microengineering*, vol. 16, no. 2, pp. 425–433, 2006.

[24] J. Kim, D. Byun, M. G. Mauk, and H. H. Bau, "A disposable, self-contained PCR chip," *Lab Chip*, vol. 9, no. 4, pp. 606–612, 2009.

[25] X. Qiu, M. G. Mauk, D. Chen, C. Liu, and H. H. Bau, "A large volume, portable, real-time PCR reactor.," *Lab Chip*, vol. 10, pp. 3170–3177, 2010.

[26] N. Pak, D. C. Saunders, C. R. Phaneuf, and C. R. Forest, "Plug-and-play, infrared, laser-mediated PCR in a microfluidic chip," *Biomed. Microdevices*, vol. 14, no. 2, pp. 427–433, 2012.

[27] C. D. Ahrberg, B. R. Ilic, A. Manz, and P. Neužil, "Handheld real-time PCR device," *Lab Chip*, vol. 16, no. 3, pp. 586–592, 2016.

[28] X. Yu, D. Zhang, T. Li, L. Hao, and X. Li, "3-D microarrays biochip for DNA amplification in polydimethylsiloxane (PDMS) elastomer," *Sensors Actuators A*, vol. 108, pp. 103–107, 2003.

[29] Y. Matsubara, K. Kerman, M. Kobayashi, S. Yamamura, Y. Morita, and E. Tamiya, "Microchamber array based DNA quantification and specific sequence detection from a single copy via PCR in nanoliter volumes.," *Biosens. Bioelectron.*, vol. 20, no. 8, pp. 1482–90, Feb. 2005.

[30] H.-B. Liu, N. Ramalingam, Y. Jiang, C.-C. Dai, K. M. Hui, and H.-Q. Gong, "Rapid distribution of a liquid column into a matrix of nanoliter wells for parallel real-time quantitative PCR," *Sensors Actuators B Chem.*, vol. 135, no. 2, pp. 671–677, Jan. 2009.

[31] J.-H. Wang *et al.*, "A miniaturized quantitative polymerase chain reaction system for DNA amplification and detection," *Sensors Actuators B Chem.*, vol. 141, no. 1, pp. 329–337, Aug. 2009.

[32] L.-J. Chien *et al.*, "A micro circulating PCR chip using a suction-type membrane for fluidic transport.," *Biomed. Microdevices*, vol. 11, no. 2, pp. 359–67, Apr. 2009.

[33] E. K. Wheeler *et al.*, "Under-three minute PCR: Probing the limits of fast amplification," *Analyst*, vol. 136, no. 18, p. 3707, 2011.

[34] S. O. Sundberg *et al.*, "Microfluidic genotyping by rapid serial PCR and high-speed melting analysis," *Clin. Chem.*, vol. 60, no. 10, pp. 1306–1313, 2014.

[35] C. D. Ahberg, A. Manz, and P. Neuzil, "Single Fluorescence Channel-based Multiplex Detection of Avian Influenza Virus by Quantitative PCR with Intercalating Dye," *Sci. Rep.*, vol. 5, no. January, p. 11479, 2015.

[36] J. H. Son *et al.*, "Ultrafast photonic PCR," *Light Sci. Appl.*, vol. 4, no. 7, p. e280, 2015.

[37] C. D. Ahrberg, "Handheld devices for PCR," *Lab Chip*, vol. 16, pp. 586–592, 2016.

[38] Y. Lin, M. Huang, and K. Young, "A rapid micro-polymerase chain reaction system

for hepatitis C virus amplification," *Sensors Actuators B*, vol. 71, pp. 2–8, 2000.

[39] J. H. Daniel *et al.*, "Silicon microchambers for DNA amplification," *Sensors And Actuators*, vol. 71, 1998.

[40] A. S. S.Poser, T.Schulz, U.Dillner, V.Baier, J.M.Kohler, D.Schimkat, G.Mayer, "Chip elements for fast thermocycling," *Sensors Actuators A*, vol. 62, pp. 672–675, 1997.

[41] D. S. Yoon *et al.*, "Precise temperature control and rapid thermal cycling in a micromachined DNA polymerase chain reaction chip," *J. Micromechanics Microengineering*, vol. 12, no. 6, pp. 813–823, Nov. 2002.

[42] I. Erill, S. Campoy, N. Erill, J. Barbé, and J. Aguiló, "Biochemical analysis and optimization of inhibition and adsorption phenomena in glass-silicon PCR-chips," *Sensors Actuators, B Chem.*, vol. 96, pp. 685–692, 2003.

[43] A. Gulliksen *et al.*, "Real-time nucleic acid sequence-based amplification in nanoliter volumes.," *Anal. Chem.*, vol. 76, no. 1, pp. 9–14, Jan. 2004.

[44] Z. Q. Niu, W. Y. Chen, S. Y. Shao, X. Y. Jia, and W. P. Zhang, "DNA amplification on a PDMS–glass hybrid microchip," *J. Micromechanics Microengineering*, vol. 16, no. 2, pp. 425–433, Feb. 2006.

[45] P. Neuzil, J. Pipper, and T. M. Hsieh, "Disposable real-time microPCR device: lab-on-a-chip at a low cost.," *Mol. Biosyst.*, vol. 2, no. 6–7, pp. 292–298, 2006.

[46] F. Wang and M. a Burns, "Performance of nanoliter-sized droplet-based microfluidic PCR.," *Biomed. Microdevices*, pp. 1071–1080, May 2009.

[47] a Ranjitprakash, S. Adamia, V. Sieben, P. Pilarski, L. Pilarski, and C. Backhouse, "Small volume PCR in PDMS biochips with integrated fluid control and vapour barrier," *Sensors Actuators B Chem.*, vol. 113, no. 1, pp. 398–409, Jan. 2006.

[48] T. Pokfai, S. Mongpraneet, A. Wisitsoraat, and A. Tuantranont, "Portable Polymerease Chain Reaction System with Thermoelectric Cooling," *Heal. (San Fr.*, pp. 665–668, 2008.

[49] Y. S. Shin, K. Cho, S. H. Lim, and S. Chung, "PDMS-based micro PCR chip with Parylene coating," *J. Micromech.Microeng.*, vol. 13, pp. 768–774, 2003.

[50] R. P. Oda *et al.*, "Infrared-Mediated Thermocycling for Ultrafast Polymerase Chain Reaction Amplification of DNA," *Anal. Chem.*, vol. 70, no. 20, pp. 4361–4368, 1998.

[51] Y. Ouyang *et al.*, "A disposable laser print-cut-laminate polyester microchip for multiplexed PCR via infra-red-mediated thermal control," *Anal. Chim. Acta*, vol. 901, pp. 59–67, 2015.

[52] K. J. Shaw *et al.*, "Rapid PCR amplification using a microfluidic device with integrated microwave heating and air impingement cooling.," *Lab Chip*, vol. 10, no. 13, pp. 1725–8, Jul. 2010.

[53] N. a Friedman and D. R. Meldrum, "Capillary tube resistive thermal cycling.," *Anal. Chem.*, vol. 70, no. 14, pp. 2997–3002, Jul. 1998.

[54] J. a Lounsbury, B. L. Poe, M. Do, and J. P. Landers, "Laser-ablated poly(methyl methacrylate) microdevices for sub-microliter DNA amplification suitable for micro-total analysis systems," *J. Micromechanics Microengineering*, vol. 22, no. 8, p. 085006, Aug. 2012.

[55] J. H. Son *et al.*, "Ultrafast photonic PCR," *Light Sci. Appl.*, vol. 4, no. 7, 2015.

[56] A. M. S. and M. G. Roper, "Frequency-encoded laser-induced fluorescence for multiplexed detection in infrared-mediated quantitative PCR," *Analyst*, vol. 139, pp. 2695–2701, 2014.

[57] E. K. Wheeler *et al.*, "Under-three minute PCR: Probing the limits of fast amplification," *The Analyst*, vol. 136, no. 18. p. 3707, 2011.

[58] T. Houssin *et al.*, "Ultrafast, sensitive and large-volume on-chip real-time PCR for the molecular diagnosis of bacterial and viral infections," *Lab Chip*, vol. 16, no. 8, pp. 1401–1411, 2016.

[59] P. Neuzil, L. Novak, J. Pipper, S. Lee, L. F. P. Ng, and C. Zhang, "Rapid detection of viral RNA by a pocket-size real-time PCR system.," *Lab Chip*, vol. 10, no. 19, pp. 2632–4, Oct. 2010.

[60] N. Ramalingam *et al.*, "Real-time PCR-based microfluidic array chip for simultaneous detection of multiple waterborne pathogens," *Sensors Actuators, B Chem.*, vol. 145, no. 1, pp. 543–552, 2010.

[61] H. Nagai, Y. Murakami, Y. Morita, K. Yokoyama, and E. Tamiya, "Development of a microchamber array for picoliter PCR.," *Anal. Chem.*, vol. 73, no. 5, pp. 1043–7, Mar. 2001.

[62] J. S. Marcus, "Parallel Picoliter RT-PCR Assays Using Microfluidics," *Anal. Chem*, vol. 78, pp. 956–958, 2006.

[63] K. Qin, "A BSA coated NOA81 PCR chip for gene amplification," *Anal. Methods*, vol. 8, pp. 2584–2591, 2016.

[64] C. Consolandi, "Polymerase chain reaction of 2-kb cyanobacterial gene and human anti-α1-chymotrypsin gene from genomic DNA on the In-Check single-use microfabricated silicon chip," *Anal. Biochem.*, vol. 353, pp. 191–197, 2006.

[65] N. Ramalingam *et al.*, "Real-time PCR-based microfluidic array chip for simultaneous detection of multiple waterborne pathogens," *Sensors Actuators B Chem.*, vol. 145, no. 1, pp. 543–552, Mar. 2010.

[66] K. Sun, A. Yamaguchi, Y. Ishida, S. Matsuo, and H. Misawa, "A heater-integrated transparent microchannel chip for continuous-flow PCR," *Sensors Actuators B*, vol. 84, pp. 283–289, 2002.

[67] J. Kim, J. Lee, S. Seong, S. Cha, S. Lee, and T. Park, "Fabrication and characterization of a PDMS–glass hybrid continuous-flow PCR chip," *Biochem. Eng. J.*, vol. 29, no. 1–2, pp. 91–97, Apr. 2006.

[68] W. Wu and N. Y. Lee, "Three-dimensional on-chip continuous-flow polymerase chain reaction employing a single heater," *Anal. Bioanal. Chem.*, vol. 400, no. 7, pp. 2053–2060, 2011.

[69] D. Moschou *et al.*, "Sensors and Actuators B : Chemical integrated microheaters for rapid DNA amplification," *Sensors Actuators B. Chem.*, vol. 199, pp. 470–478, 2014.

[70] M. Ha and N. Lee, "Miniaturized polymerase chain reaction device for rapid identification of genetically modified organisms," *Food Control*, vol. 57, pp. 238–245, 2015.

[71] H. Tachibana, M. Saito, K. Tsuji, K. Yamanaka, L. Q. Hoa, and E. Tamiya, "Self-propelled continuous-flow PCR in capillary-driven microfluidic device: Microfluidic behavior and DNA amplification," *Sensors Actuators, B Chem.*, vol. 206, pp. 303–310, 2015.

[72] J. West *et al.*, "Application of magnetohydrodynamic actuation to continuous flow chemistry.," *Lab Chip*, vol. 2, no. 4, pp. 224–30, Nov. 2002.

[73] M. Hashimoto, P.-C. Chen, M. W. Mitchell, D. E. Nikitopoulos, S. a Soper, and M. C. Murphy, "Rapid PCR in a continuous flow device.," *Lab Chip*, vol. 4, no. 6, pp. 638–45, Dec. 2004.

[74] J. Chiou, P. Matsudaira, a Sonin, and D. Ehrlich, "A closed-cycle capillary

polymerase chain reaction machine.," *Anal. Chem.*, vol. 73, no. 9, pp. 2018–21, May 2001.

[75] L. Chen, J. West, P. Auroux, A. Manz, and P. Day, "Ultrasensitive PCR and Real-Time Detection from Human Genomic Samples Using a bidirectional flow microreactor," *Anal Chem*, vol. 79, no. 23, pp. 9185–9190, 2007.

[76] C. Zhang, H. Wang, and D. Xing, "Multichannel oscillatory-flow multiplex PCR microfluidics for high-throughput and fast detection of foodborne bacterial pathogens," *Biomed. Microdevices*, vol. 13, no. 5, pp. 885–897, 2011.

[77] S. Brunklaus *et al.*, "Fast nucleic acid amplification for integration in point-of-care applications," *Electrophoresis*, vol. 33, no. 21, pp. 3222–3228, 2012.

[78] C. Yu, W. Liang, I. Kuan, C. Wei, and W. Gu, "Fabrication and characterization of a flow-through PCR device with integrated chromium resistive heaters," *J. Chinese Inst. Chem. Eng.*, vol. 38, no. 3–4, pp. 333–339, May 2007.

[79] N. Crews, C. Wittwer, and B. Gale, "Continuous-flow thermal gradient PCR.," *Biomed. Microdevices*, vol. 10, no. 2, pp. 187–95, Apr. 2008.

[80] J. J. Chen, C. M. Shen, and Y. W. Ko, "Analytical study of a microfludic DNA amplification chip using water cooling effect," *Biomed. Microdevices*, vol. 15, no. 2, pp. 261–278, 2013.

[81] A. Harandi and T. Farquhar, "A microfluidic device providing continuous-flow polymerase chain reaction heating and cooling," *J. Micromechanics Microengineering*, vol. 24, no. 11, 2014.

[82] J. Wu *et al.*, "Research to Improve the Efficiency of Double Stereo PCR Microfluidic Chip by Passivating the Inner Surface of Steel Capillary with NOA61," *Cell Biochem. Biophys.*, vol. 72, no. 2, pp. 605–610, 2015.

[83] M. U. Kopp, A. J. De Mello, and A. Manz, “Chemical Amplification: Continuous-Flow PCR on a Chip,” *Science (80-.).*, vol. 280, no. 15, p. 1046, 1998.

[84] I. Schneegass and J. M. Köhler, “Flow-through polymerase chain reactions in chip thermocyclers,” *Rev. Mol. Biotechnol.*, vol. 82, no. 2, pp. 101–21, Dec. 2001.

[85] I. Schneegass, R. Brautigam, and J. M. Kohler, “Miniaturized flow-through PCR with different template types in a silicon chip thermocycler.,” *Lab Chip*, vol. 1, no. 1, pp. 42–9, Sep. 2001.

[86] C. Obeid, P, Theodore K, “Continuous-flow DNA and RNA amplification chip combined with laser-induced fluorescence detection,” *Anal. Chim. Acta*, vol. 494, pp. 1–9, Oct. 2003.

[87] P. J. Obeid, T. K. Christopoulos, H. J. Crabtree, and C. J. Backhouse, “Microfabricated device for DNA and RNA amplification by continuous-flow polymerase chain reaction and reverse transcription-polymerase chain reaction with cycle number selection.,” *Anal. Chem.*, vol. 75, no. 2, pp. 288–95, Jan. 2003.

[88] T. Fukuba, T. Yamamoto, T. Naganuma, and T. Fujii, “Microfabricated flow-through device for DNA amplification—towards in situ gene analysis,” *Chem. Eng. J.*, vol. 101, no. 1–3, pp. 151–156, Aug. 2004.

[89] S. Li *et al.*, “A Continuous-Flow Polymerase Chain Reaction Microchip With Regional Velocity Control.,” *J. microelectromechanical Syst.*, vol. 15, no. 1, pp. 223–236, Feb. 2006.

[90] T. Nakayama *et al.*, “Circumventing air bubbles in microfluidic systems and quantitative continuous-flow PCR applications.,” *Anal. Bioanal. Chem.*, vol. 386, no. 5, pp. 1327–33, Nov. 2006.

[91] M. Hashimoto, F. Barany, and S. A. Soper, “Serial processing of biological reactions using flow-through microfluidic devices : coupled PCR / LDR for the detection of

low-abundant DNA point mutations," *Analyst*, vol. 132, pp. 913–921, 2007.

[92] M. L. Ha and N. Y. Lee, "Miniaturized polymerase chain reaction device for rapid identification of genetically modified organisms," *Food Control*, vol. 57, pp. 238–245, 2015.

[93] D. Moschou *et al.*, "All-plastic, low-power, disposable, continuous-flow PCR chip with integrated microheaters for rapid DNA amplification," *Sensors Actuators, B Chem.*, vol. 199, pp. 470–478, 2014.

[94] N. C. Cady, S. Stelick, M. V Kunnavakkam, and C. A. Batt, "Real-time PCR detection of Listeria monocytogenes using an integrated microfluidics platform," *Sensors Actuators A*, vol. 107, pp. 332–341, 2005.

[95] H. Tachibana, M. Saito, K. Tsuji, K. Yamanaka, L. Q. Hoa, and E. Tamiya, "Self-propelled continuous-flow PCR in capillary-driven microfluidic device: Microfluidic behavior and DNA amplification," *Sensors Actuators, B Chem.*, vol. 206, pp. 303–310, 2015.

[96] J. West *et al.*, "Application of magnetohydrodynamic actuation to continuous flow chemistry," *Lab Chip*, vol. 2, pp. 224–230, 2002.

[97] H. Wang, J. Chen, L. Zhu, H. Shadpour, M. L. Hupert, and S. a Soper, "Continuous flow thermal cycler microchip for DNA cycle sequencing.," *Anal. Chem.*, vol. 78, no. 17, pp. 6223–31, Sep. 2006.

[98] J. R. Peham *et al.*, "Long target droplet polymerase chain reaction with a microfluidic device for high-throughput detection of pathogenic bacteria at clinical sensitivity," *Biomed. Microdevices*, vol. 13, no. 3, pp. 463–473, 2011.

[99] R. Snodgrass, A. Gardner, L. Jiang, C. Fu, E. Cesarman, and D. Erickson, "KS-detect validation of solar thermal PCR for the diagnosis of kaposi's sarcoma using pseudo-biopsy samples," *PLoS One*, vol. 11, no. 1, pp. 1–15, 2016.

[100] L. Chen, J. West, P.-A. Auroux, A. Manz, and P. J. R. Day, "Ultrasensitive PCR and real-time detection from human genomic samples using a bidirectional flow microreactor," *Anal. Chem.*, vol. 79, no. 23, pp. 9185–90, Dec. 2007.

[101] O. Frey, S. Bonneick, A. Hierlemann, and J. Lichtenberg, "Autonomous microfluidic multi-channel chip for real-time PCR with integrated liquid handling," *Biomed. Microdevices*, vol. 9, no. 5, pp. 711–718, 2007.

[102] M. Krishnan, V. M. Ugaz, and M. A. Burns, "PCR in a Rayleigh-Be'nard Convection Cell," *Science (80-.).*, vol. 298, no. 5594, p. 793, 2002.

[103] J. W. Allen, M. Kenward, and K. D. Dorfman, "Coupled flow and reaction during natural convection PCR," *Microfluid. Nanofluidics*, vol. 6, no. 1, pp. 121–130, 2009.

[104] W. P. Chou, P. H. Chen, M. Miao, L. S. Kuo, S. H. Yeh, and P. J. Chen, "Rapid DNA amplification in a capillary tube by natural convection with a single isothermal heater.," *Biotechniques*, vol. 50, no. 1, pp. 52–7, Jan. 2011.

[105] X. Qiu *et al.*, "Instrument-free point-of-care molecular diagnosis of H1N1 based on microfluidic convective PCR," *Sensors Actuators, B Chem.*, vol. 243, pp. 738–744, 2017.

[106] E. K. Wheeler *et al.*, "Convectively driven polymerase chain reaction thermal cycler," *Anal. Chem.*, vol. 76, no. 14, pp. 4011–4016, 2004.

[107] Z. Chen, S. Qian, W. R. Abrams, D. Malamud, and H. H. Bau, "Thermosiphon-based PCR reactor: experiment and modeling.," *Anal. Chem.*, vol. 76, no. 13, pp. 3707–15, Jul. 2004.

[108] M. Hennig and D. Braun, "Convective polymerase chain reaction around micro immersion heater," *Appl. Phys. Lett.*, vol. 87, no. 18, p. 183901, 2005.

[109] D. Braun, N. Goddard, and A. Libchaber, "Exponential DNA Replication by

Laminar Convection," *Phys. Rev. Lett.*, vol. 91, no. 15, pp. 1–4, Oct. 2003.

[110] D. Braun and A. Libchaber, "Thermal force approach to molecular evolution.," *Phys. Biol.*, vol. 1, no. 1–2, pp. P1-8, Jun. 2004.

[111] W.-P. Chou, C. Lee, Z.-J. Hsu, M.-H. Lai, L.-S. Kuo, and P.-H. Chen, "Development of Capillary Loop Convective Polymerase Chain Reaction Platform with Real-Time Fluorescence Detection," *inventions*, vol. 2, no. 3, pp. 1–8, 2017.

[112] B. Shu, C. Zhang, and D. Xing, "A sample-to-answer, real-time convective polymerase chain reaction system for point-of-care diagnostics," *Biosens. Bioelectron.*, vol. 97, no. March, pp. 360–368, 2017.

[113] A. G. Sciancalepore, A. Polini, E. Mele, S. Girardo, R. Cingolani, and D. Pisignano, "Rapid nested-PCR for tyrosinase gene detection on chip," *Biosens. Bioelectron.*, vol. 26, no. 5, pp. 2711–2715, 2011.

[114] S. Mohr *et al.*, "Numerical and experimental study of a droplet-based PCR chip," *Microfluid. Nanofluidics*, vol. 3, no. 5, pp. 611–621, 2007.

[115] and J. H. L. Margaret Macris Kiss, Lori Ortoleva-Donnelly, N. Reginald Beer, Jason Warner, Christopher G. Bailey, Bill W. Colston, Jonathon M. Rothberg, Darren R. Link and Raindance, "High-Throughput Quantitative Polymerase Chain Reaction in Picoliter Droplets High-Throughput Quantitative Polymerase Chain Reaction in Picoliter Droplets," *Anal. Chem*, vol. 80, no. 23, pp. 8975–8981, 2008.

[116] A. N. Reginald Beer, Elizabeth K. Wheeler, Lorenna Lee-Houghton, Nicholas Watkins, Shanavaz Nasarabadi, Nicole Hebert, Patrick Leung, Don W. Arnold, Christopher G. Bailey and B. W. C. Colston, "On-Chip Single-Copy Real-Time Reverse-Transcription PCR in Isolated Picoliter Droplets," *Anal. Chem*, vol. 80, no. 6, pp. 1854–1858, 2008.

[117] A. C. Hatch, T. Ray, K. Lintecum, and C. Youngbull, "Continuous flow real-time

PCR device using multi-channel fluorescence excitation and detection," *Lab Chip*, vol. 14, no. 3, pp. 562–568, 2014.

[118] Y. Schaerli *et al.*, "Continuous-Flow Polymerase Chain Reaction of Single-Copy DNA in Microfuidic Microdroplets," *Anal. Chem*, vol. 81, no. 1, pp. 302–306, 2009.

[119] M. Abdelgawad and A. R. Wheeler, "The digital revolution: A new paradigm for microfluidics," *Adv. Mater.*, vol. 21, pp. 920–925, 2009.

[120] M. Washizu and S. Member, "Electrostatic Actuation of Liquid Droplets for Microreactor Applications," *IEEE Trans. Ind. Appl.*, vol. 34, no. 4, pp. 732–737, 1998.

[121] J. Lee, H. Moon, J. Fowler, T. Schoellhammer, and C. J. Kim, "Electrowetting and electrowetting-on-dielectric for microscale liquid handling," *Sensors Actuators, A Phys.*, vol. 95, no. 2–3, pp. 259–268, 2002.

[122] Y. H. Chang, G. Bin Lee, F. C. Huang, Y. Y. Chen, and J. L. Lin, "Integrated polymerase chain reaction chips utilizing digital microfluidics," *Biomed. Microdevices*, vol. 8, no. 3, pp. 215–225, 2006.

[123] Z. Hua *et al.*, "Multiplexed real-time polymerase chain reaction on a digital microfluidic platform," *Anal Chem*, vol. 82, no. 6, pp. 2310–2316, 2010.

[124] D. J. You, P. L. Tran, H.-J. Kwon, D. Patel, and J.-Y. Yoon, "Very quick reverse transcription polymerase chain reaction for detecting 2009 H1N1 influenza A using wire-guide droplet manipulations," *Faraday Discuss.*, vol. 149, pp. 159–170, 2011.

[125] D. J. You and J. Y. Yoon, "Droplet centrifugation, droplet DNA extraction, and rapid droplet thermocycling for simpler and faster PCR assay using wire-guided manipulations," *J. Biol. Eng.*, vol. 6, pp. 1–10, 2012.

[126] S. V. Angus, S. Cho, D. K. Harshman, J. Y. Song, and J. Y. Yoon, "A portable,

shock-proof, surface-heated droplet PCR system for Escherichia coli detection," *Biosens. Bioelectron.*, vol. 74, pp. 360–368, 2015.

[127] P. J. Asiello and A. J. Baeumner, "Miniaturized isothermal nucleic acid amplification, a review," *Lab Chip*, vol. 11, no. 8, p. 1420, 2011.

[128] A. M. Foudeh, T. Fatanat Didar, T. Veres, and M. Tabrizian, "Microfluidic designs and techniques using lab-on-a-chip devices for pathogen detection for point-of-care diagnostics," *Lab Chip*, vol. 12, no. 18, p. 3249, 2012.

[129] C. C. Chang, C. C. Chen, S. C. Wei, H. H. Lu, Y. H. Liang, and C. W. Lin, "Diagnostic devices for isothermal nucleic acid amplification," *Sensors (Switzerland)*, vol. 12, no. 6, pp. 8319–8337, 2012.

[130] L. M. Zanoli and G. Spoto, "Isothermal amplification methods for the detection of nucleic acids in microfluidic devices," *Biosensors*, vol. 3, no. 1, pp. 18–43, 2013.

[131] C.-M. Chang, W.-H. Chang, C.-H. Wang, J.-H. Wang, J. D. Mai, and G.-B. Lee, "Nucleic acid amplification using microfluidic systems," *Lab Chip*, vol. 13, no. 7, p. 1225, 2013.

[132] M. Safavieh *et al.*, "Emerging Loop-Mediated Isothermal Amplification-Based Microchip and Microdevice Technologies for Nucleic Acid Detection," *ACS Biomater. Sci. Eng.*, vol. 2, no. 3, pp. 278–294, 2016.

[133] S. Y. Lee, C. N. Lee, H. Mark, D. R. Meldrum, and C. W. Lin, "Efficient, specific, compact hepatitis B diagnostic device: Optical detection of the hepatitis B virus by isothermal amplification," *Sensors Actuators, B Chem.*, vol. 127, no. 2, pp. 598–605, 2007.

[134] S. Y. Lee *et al.*, "Compact optical diagnostic device for isothermal nucleic acids amplification," *Sensors Actuators, B Chem.*, vol. 133, no. 2, pp. 493–501, 2008.

[135] T. L. Chuang, S. C. Wei, S. Y. Lee, and C. W. Lin, "A polycarbonate based surface plasmon resonance sensing cartridge for high sensitivity HBV loop-mediated isothermal amplification," *Biosens. Bioelectron.*, vol. 32, no. 1, pp. 89–95, 2012.

[136] C. Liu, M. G. Mauk, R. Hart, X. Qiu, and H. H. Bau, "A self-heating cartridge for molecular diagnostics," *Lab Chip*, vol. 11, no. 16, p. 2686, 2011.

[137] C. Liu, M. G. Mauk, and H. H. Bau, "A disposable, integrated loop-mediated isothermal amplification cassette with thermally actuated valves," *Microfluid. Nanofluidics*, vol. 11, no. 2, pp. 209–220, 2011.

[138] K. a. Curtis *et al.*, "Isothermal amplification using a chemical heating device for point-of-care detection of HIV-1," *PLoS One*, vol. 7, no. 2, pp. 1–6, 2012.

[139] C. Liu, M. G. Mauk, R. Hart, M. Bonizzoni, G. Yan, and H. H. Bau, "A low-cost microfluidic chip for rapid genotyping of malaria-transmitting mosquitoes," *PLoS One*, vol. 7, no. 8, pp. 1–7, 2012.

[140] L. Lam *et al.*, "Loop-mediated isothermal amplification of a single DNA molecule in polyacrylamide gel-based microchamber," *Biomed. Microdevices*, vol. 10, no. 4, pp. 539–546, 2008.

[141] X. Fang, Y. Liu, J. Kong, and X. Jiang, "Loop-mediated isothermal amplification integrated on microfluidic chips for point-of-care quantitative detection of pathogens," *Anal Chem*, vol. 82, no. 7, pp. 3002–3006, 2010.

[142] C. Duarte, E. Salm, B. Dorvel, B. Reddy, and R. Bashir, "On-chip parallel detection of foodborne pathogens using loop-mediated isothermal amplification," *Biomed. Microdevices*, vol. 15, no. 5, pp. 821–830, 2013.

[143] J. Luo *et al.*, "A real-time microfluidic multiplex electrochemical loop-mediated isothermal amplification chip for differentiating bacteria," *Biosens. Bioelectron.*, vol. 60, pp. 84–91, 2014.

[144] X. Fang, H. Chen, S. Yu, X. Jiang, and J. Kong, "Predicting viruses accurately by a multiplex microfluidic loop-mediated isothermal amplification chip," *Anal. Chem.*, vol. 83, no. 3, pp. 690–695, 2011.

[145] F. Ahmad, G. Seyrig, D. M. Tourlousse, R. D. Stedtfeld, J. M. Tiedje, and S. A. Hashsham, "A CCD-based fluorescence imaging system for real-time loop-mediated isothermal amplification-based rapid and sensitive detection of waterborne pathogens on microchips," *Biomed. Microdevices*, vol. 13, no. 5, pp. 929–937, 2011.

[146] D. M. Tourlousse, F. Ahmad, R. D. Stedtfeld, G. Seyrig, J. M. Tiedje, and S. a Hashsham, "A polymer microfluidic chip for quantitative detection of multiple water- and foodborne pathogens using real-time fluorogenic loop-mediated isothermal amplification.," *Biomed. Microdevices*, vol. 14, no. 4, pp. 769–78, 2012.

[147] X. Fang, H. Chen, L. Xu, X. Jiang, W. Wu, and J. Kong, "A portable and integrated nucleic acid amplification microfluidic chip for identifying bacteria," *Lab Chip*, vol. 12, no. 8, p. 1495, 2012.

[148] R. D. Stedtfeld *et al.*, "Gene-Z: a device for point of care genetic testing using a smartphone," *Lab Chip*, vol. 12, no. 8, p. 1454, 2012.

[149] T. Wang *et al.*, "Detect early stage lung cancer by a LAMP microfluidic chip system with a real-time fluorescent filter processor," *Sci. China Chem.*, vol. 55, no. 4, pp. 508–514, 2012.

[150] A. Gansen, A. M. Herrick, I. K. Dimov, L. P. Lee, and D. T. Chiu, "Digital LAMP in a sample self-digitization (SD) chip," *Lab Chip*, vol. 12, no. 12, p. 2247, 2012.

[151] D. P. Manage, L. Chui, and L. M. Pilarski, "Sub-microliter scale in-gel loop-mediated isothermal amplification (LAMP) for detection of Mycobacterium tuberculosis," *Microfluid. Nanofluidics*, vol. 14, no. 3–4, pp. 731–741, 2012.

[152] M. Safavieh, M. U. Ahmed, M. Tolba, and M. Zourob, "Microfluidic

electrochemical assay for rapid detection and quantification of Escherichia coli," *Biosens. Bioelectron.*, vol. 31, no. 1, pp. 523–528, 2012.

[153] K. Hsieh, A. S. Patterson, B. S. Ferguson, K. W. Plaxco, and H. T. Soh, "Rapid, sensitive, and quantitative detection of pathogenic DNA at the point of care through microfluidic electrochemical quantitative loop-mediated isothermal amplification," *Angew. Chemie - Int. Ed.*, vol. 51, no. 20, pp. 4896–4900, 2012.

[154] T. D. Rane, L. Chen, H. C. Zec, and T.-H. Wang, "Microfluidic continuous flow digital loop-mediated isothermal amplification (LAMP)," *Lab Chip*, vol. 15, no. 3, pp. 776–782, 2015.

[155] L. Wan *et al.*, "A digital microfluidic system for loop-mediated isothermal amplification and sequence specific pathogen detection," *Sci. Rep.*, vol. 7, no. 1, pp. 1–11, 2017.

[156] C. Liu *et al.*, "An isothermal amplification reactor with an integrated isolation membrane for point-of-care detection of infectious diseases," *Analyst*, vol. 136, no. 10, p. 2069, 2011.

[157] Q. Wu *et al.*, "Integrated glass microdevice for nucleic acid purification, loop-mediated isothermal amplification, and online detection," *Anal. Chem.*, vol. 83, no. 9, pp. 3336–3342, 2011.

[158] W. H. Chang *et al.*, "Rapid isolation and detection of aquaculture pathogens in an integrated microfluidic system using loop-mediated isothermal amplification," *Sensors Actuators, B Chem.*, vol. 180, pp. 96–106, 2013.

[159] M. Safavieh, M. U. Ahmed, E. Sokullu, A. Ng, L. Braescu, and M. Zourob, "A simple cassette as point-of-care diagnostic device for naked-eye colorimetric bacteria detection," *Analyst*, vol. 139, no. 2, pp. 482–487, 2014.

[160] C. H. Wang, K. Y. Lien, T. Y. Wang, T. Y. Chen, and G. Bin Lee, "An integrated

microfluidic loop-mediated-isothermal-amplification system for rapid sample pre-treatment and detection of viruses," *Biosens. Bioelectron.*, vol. 26, no. 5, pp. 2045–2052, 2011.

[161] C.-H. Wang, K.-Y. Lien, J.-J. Wu, and G.-B. Lee, "A magnetic bead-based assay for the rapid detection of methicillin-resistant Staphylococcus aureus by using a microfluidic system with integrated loop-mediated isothermal amplification.," *Lab Chip*, vol. 11, no. 8, pp. 1521–31, 2011.

[162] Y. Hataoka, L. Zhang, Y. Mori, N. Tomita, T. Notomi, and Y. Baba, "Analysis of Specific Gene by Integration of Isothermal Amplification and Electrophoresis on Poly (methyl methacrylate) Microchips," *Anal Chem*, vol. 76, no. 13, pp. 3689–3693, 2004.

[163] M. D. Borysiak, K. W. Kimura, and J. D. Posner, "NAIL: Nucleic Acid detection using Isotachophoresis and Loop-mediated isothermal amplification," *Lab Chip*, vol. 15, pp. 1697–1707, 2015.

[164] Y. Sun, T. L. Quyen, T. Q. Hung, W. H. Chin, A. Wolff, and D. D. Bang, "A lab-on-a-chip system with integrated sample preparation and loop-mediated isothermal amplification for rapid and quantitative detection of Salmonella spp. in food samples," *Lab Chip*, vol. 15, no. 8, pp. 1898–1904, 2015.

[165] F. Ahmad *et al.*, "Most probable number - loop mediated isothermal amplification (MPN-LAMP) for quantifying waterborne pathogens in < 25 min," *J. Microbiol. Methods*, vol. 132, pp. 27–33, 2017.

[166] J. YANG, "DESIGN & FABRICATION OF A MICROFLUIDIC DEVICE FOR CLINICAL OUTCOME PREDICTION OF SEVERE SEPSIS DESIGN & FABRICATION OF A MICROFLUIDIC DEVICE," McMaster University, 2014.

[167] R. Pethig, "Review Article—Dielectrophoresis: Status of the theory, technology,

and applications," *Biomicrofluidics*, vol. 4, no. 1, p. 022811, 2010.

[168] Y. M. Jung, H. C. Oh, and I. S. Kang, "Electrical charging of a conducting water droplet in a dielectric fluid on the electrode surface," *J. Colloid Interface Sci.*, vol. 322, pp. 617–623, 2008.

[169] J. Voldman, *BioMEMS and Biomedical Nanotechnology*. Boston, MA: Springer, 2007.

[170] D. Choi *et al.*, "Spontaneous electrical charging of droplets by conventional pipetting.," *Sci. Rep.*, vol. 3, p. 2037, Jan. 2013.